J. C. Rasser

Platinum-iridium reforming catalysts

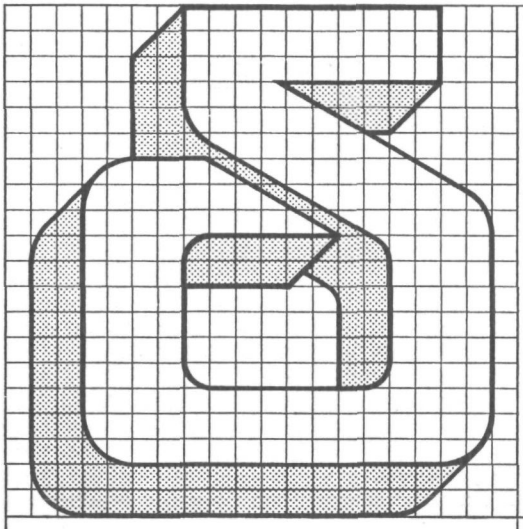

Delft University Press

Platinum-iridium reforming catalysts

Platinum-iridium reforming catalysts

TPD of hydrogen, selectivity and activity in heptane conversion

J. C. Rasser

with a foreword by
J. J. F. Scholten

Delft University Press/1977

Published and distributed by
Delft University Press
Mijnbouwplein 11
2628 RT Delft
The Netherlands

ISBN 90 6275 005 2

Foreword

Among researchworkers in catalysis it is common knowledge that there is still a large gap between what is known and predictable with respect to chemisorption and catalysis from fundamental studies, using metal films and monocrystal faces, and the actual behaviour of technical catalysts under realistic conditions. One of the reasons is that in applying the 'surface science approach' one mostly works with low dispersions of the catalytic materials, and at extremely low pressures, whereas in technical catalysis by preference high degrees of dispersion of the catalytic material and high pressures are used.

One of the consequences of this is that weakly bound adsorption states, which are formed at higher pressures, and which are very important from a catalytical point of view, are not detectable in the pure fundamental approach. Furthermore, the influence of edges and corners on the catalytic performance, which is very pronounced at high dispersion, and various types of carrier-effects like 'hydrogen spillover' and the dissolution of metal ions in the carrier, only comes to the fore if the catalysts are studied also in their technical form and under technical conditions.

Nowadays, very attractive research techniques are available, which may be applied to both fundamental and technical probes, viz. Temperature Programmed Desorption (TPD) and Electron-spectroscopic Analysis, and by using those techniques the problems raised above are more or less circumvented. Many workers, and also Dr. Rasser the author of the present book, applied these techniques very succesfully.

The complicated chemical events at the surface of heterogeneous catalysts can only be described satisfactorally if we know all variables which play a role, i.e., besides the texture of the catalysts we have to know the structure and the analytical composition of the catalyst surface.

Furthermore, we should be able to detect the various forms in which reactants and intermediates are adsorbed.

Especially in this last respect Rasser's book, which is at the same time his doctoral thesis, asks in my view for a more general attention. He clearly shows that well-resolved TPD spectra may be obtained by making use of an all-steel mercury- and grease-free apparatus, replacing the traditional ultra-high vacuum by an extremely purified inert carrier gas like helium.

Another important point is that in the chapters I and II the full theory is presented for analyzing TPD spectra, and for calculating the population, the heat of adsorption, the entropy of adsorption and the kinetic order of desorption of adsorbed species. For the first time the theory is extended for the important case of dissociative adsorption with freely occurring readsorption. By making use of the various tables and theoretical line shapes presented in these chapters, the reader will certainly be able to apply this knowledge to his own problems.

In the other chapters, Rasser describes the application of the TPD and AES (Auger electron-spectroscopy) techniques to a very important technical problem, viz. catalytic reforming over Pt/Ir-on-alumina catalysts, and he shows that, notwithstanding the great resemblance between Pt and Ir, at certain alloy compositions well-detectable differences in the hydrogen-TPD spectra occur. Also the presence of impurities in the surface, like carbon, often have a clear influence on the position of the desorption peaks.

I recommend this Delft University Press publication to all who see it as there task to follow the fundamental developments in catalysis, but at the same time want to apply this knowledge in technical catalysis.

J.J.F. Scholten

Delft, July 1977

CONTENTS

List of symbols

A	Arrhenius pre-exponential factor	s^{-1}
A^*	equilibrium pre-exponential factor	
A.1	first order desorption without readsorption	
A.2	second order desorption without readsorption	
B	parameters accounting for the tempe-	
b	rature dependence of $A(A^*):A(A^*)=BT^b$	
B.1	first order desorption with freely occurring readsorption	
B.2	second order desorption with freely occurring readsorption	
C	concentration of desorbing gas in the carrier gas	
C_M	concentration C at peak maximum	
C_n	normalized concentration, C/C_M	
E_d	activation energy of desorption	kJ $mole^{-1}$
E_M	normalized activation energy, E_d/RT_M	
E_M^*	normalized adsorption enthalpy, $\Delta H/RT_M$	
F	in TPD: carrier gas flow rate	$cm^3(NTP)s^{-1}$
	in conversion reaction: reactant flow	mole s^{-1}
ΔG	free enthalpy of mixing	kJ $mole^{-1}$
ΔH	enthalpy of adsorption	kJ $mole^{-1}$
$I_{(1)}$	integral, defined by equation (I.23)	
$I_{(2)}$	integral, defined by equation (I.15)	
K	desorption equilibrium constant, k_d/k_a	
k_a	adsorption rate constant	s^{-1}
k_d	desorption rate constant	s^{-1}
n(E)	density of states at energy E	
n_{ws}	electron density	$10^2 kg^{\frac{1}{2}} cm^{-5/2}$
P	partial pressure of the desorbing gas	Nm^{-2}
P_o	total pressure	Nm^{-2}

R	gas constant	8.314	J $mole^{-1}K^{-1}$
ΔS	entropy of adsorption		J $mole^{-1}K^{-1}$
S_a	atomatization selectivity		
S_c	cyclization selectivity		
S_h	hydrogenolysis selectivity		
S_i	isomerization selectivity		
S_{nd}	selectivity for non-destructive reactions		
t	time		s
T	temperature		K
T_c	critical temperature of a miscibility gap		K
T_M	temperature at peak maximum		K
T_n	normalized temperature		
V_m	max.amount of gas adsorbed (in cm^3 NTP) per cm^3 of the solid phase		
V_s	volume of solid phase in the catalyst bed		cm^3
W	weight of the catalyst		kg
ΔW	width of a desorption peak at half peak maximum, in T_n units		
x	in TPD: substitution parameter, $x=E_m(1-1/Tn)$ in alloys: composition parameter		

Greek symbols

β	heating rate	K s^{-1}
θ	fractional surface coverage	
θ_i	initial coverage	
θ_M	coverage at peak maximum	
ξ	conversion	
Ω	interaction parameter for bi-metallic allys	

General Introduction

After World War II, the growing need of high octane number petrol governed more and more the direction of search in the petrochemical industry.

Basis for petrol production is the C_6-C_{10} fraction of crude oil, the amount of which can be increased by hydrocracking of heavier fractions. This fraction mainly contains n-alkanes, having a very low octane number. Conversion into iso-, neo-, and cycloalkanes, and even aromatics, appeared to be necessary. As platinum-on-alumina turned out to be the best catalyst for this "reforming" process, the term "platforming" was introduced. Further improvement of the octane number is achieved by the addition of a radical inhibitor, like tetra-methyl-lead (t.m.l.), or tetra-ethyl-lead (t.e.l.) to petrol.

Now that the role of lead in pollution has been recognized, other ways of octane number improvement have been sought, one of them being the use of an alloy of Pt and another transition metal for the reforming process, rather than Pt alone.

Much attention has been given to the Pt-Ir system, mainly by the group of Sinfelt (1-4), but also by French investigators (5). Another French group introduced as a third constituent Nb (6), La (7), Tl or In (8), and Mn (9). Others tried metalloids as a third component, like Ge (10) and Bi (11). The importance of the Pt-Ir system in catalysis has also been emphasized by Russian scientists (12).

Without any exception, all patent letters claim an improvement of the activity, of the selectivity towards isomerization, and of the stability against coke formation and sintering, shown by the platinum catalyst on introduction of iridium. Since patent letters deal with practical applicability rather than with the theoretical aspects, a theoretical explanation of the described phenomenon is not given. More sophisticated scientific publications, however, show the understanding of the catalytic behaviour of the Pt-Ir system and related alloys to be rather poor (13-24).

The aim of our investigations, the results of which are presented in this thesis, was to elucidate the behaviour of the Pt-Ir system as a catalyst in reforming reactions. For this purpose, two ways of attack were chosen.

a) The physical properties of the binary system, like miscibility of the two metals, phase segregation, and enrichment of the surface in one of the two constituents, were investigated by X-ray diffraction techniques and Auger electron spectroscopy (AES) carried out on metal and alloy powders.
b) The chemical behaviour of the metal surface was examined by means of the adsorption and temperature programmed desorption (TPD) of hydrogen, and of the conversion of n-hexane and n-heptane on Pt-Ir deposited on γ-alumina.

In order to make full use of the obtained TPD-data, the current theory on this matter has been revised and extended in chapter I. In chapter II, the use of the derived theoretical equations in the interpretation of TPD-spectra is discussed in some detail.

Chapter III gives a review of the available literature on the Pt-Ir-system. Recent thermodynamic data have been used for a refinement of the phase diagram, and possible consequences for the catalytic behaviour are discussed.

In chapter IV, the results of the TPD-experiments are presented. The differences in hydrogen adsorption behaviour caused by differences in catalyst composition appear to be marginal. The effect on the catalytic behaviour is outlined.

Chapter V deals with the conversion of n-hexane and n-heptane. Special attention has been given to the isomerization selectivity, as compared with hydrogenolysis. This selectivity appears to depend on catalyst composition. This dependence is enhanced by selective poisoning with sulfur.

Chapter VI is devoted to a general discussion of the results obtained. An interpretation is given in terms of the electronic structure of both Pt and Ir, the thermodynamic properties of the binary system, and the probable composition of the catalyst surface under reaction conditions. Results of physical measurements (X-ray diffraction and AES) are incorporated. The insight thus obtained is used for a prediction of other possibly favourable bimetallic systems. The effect of a third constituent is briefly discussed.

References

1. U.S. Patent 3,953,368
Exxon Research & Engineering Co.

2. U.S. Patent 3,867,280
Exxon Research & Engineering Co.

3. U.S. Patent 3,839,194
Esso Research & Engineering Co.

4. British Patent 1,364,375
Esso Research & Engineering Co.

5. U.S. Patent 3,886,061
Cie française de Raffinage

6. British Patent 1,400,345
Sté française des Produits pour Catalyse

7. British Patent 1,390,625
Sté française des Produits pour Catalyse

8. British Patent 1,364,744
Sté française des Produits pour Catalyse

9. French Appl. 2,209,604
Sté française des Produits pour Catalyse

10. U.S. Patent 3,839,193
Universal Oil Products Co.

11. U.S. Patent 3,878,089
Universal Oil Products Co.

12. N.S. Kozlov, L. Ya Mostovaya, G.A. Zhizhanko
Neftekhimiya, 14 (1974) 591

13. Dowden, D.A., J. Chem. Soc., (1950) 242

14. Mc Kee, D.W., Norton, F.J., J. Catal., 4 (1965) 510

15. Bond, G.C., Webster, D.E., Plat.Met.Rev., 10 (1966) 10

16. Rienäcker, G., Proc. 4th Int.Congr.Catal., (Moscow, 1968) p. 537

17. Bond, G.C., Webster, D.E., Ann.N.Y. Acad.Sci., 158 (1969) 540

18. Dowden, D.A., in: "Chemisorption and Catalysis", E.P. Hepple, ed. Institute of Petroleum, London (1970) p. 1.

19. Moss, R.L., Plat. Met. Rev., 17, (1973) 137

20. Karpinski, Z., Clarke, J.K.A.,
J.Chem.Soc., Faraday Trans., I, 71, (1975) 893

21. Clarke, J.K.A., Chem.Rev., 75, (1975) 291

22. Sinfelt, J.H., Plat.Met.Rev., 20 (1976) 114

23. Brunelle, J.P., Montarnal, R.E., Sugier, A.A.,
Proc. 6th Int.Congr.Catal.,London(1976), paper B 24

24. Ramaswamy, A.V., Ratnasamy, P., Sivasanker, S.,
Proc. 6th Int.Congr.Catal.,London (1976), paper B 25

Chapter I

Theory of Temperature Programmed Desorption

I.1.1 General Introduction

Temperature Programmed Desorption (TPD) is a technique that studies desorption of a preadsorbed gas as a function of time, caused by a temperature rise of the sample to be examined. In general, this temperature rise is governed by a pre-chosen time-temperature schedule, e.g. linear or reciprocal. The quantity of the desorbing gas is monitored as a function of time, so that the rate of desorption as a function of temperature can be determined. A graph of the latter function is called the desorption spectrum or desorption trace. Since various adsorbate-solid surface bonds will dissociate at different temperatures, each one being characteristic for a certain type of adsorption, several desorption peaks can be observed in the desorption spectrum (fig. (I.1)). Multiple peak spectra may also arise from lateral interactions of the adsorbed molecules (1).

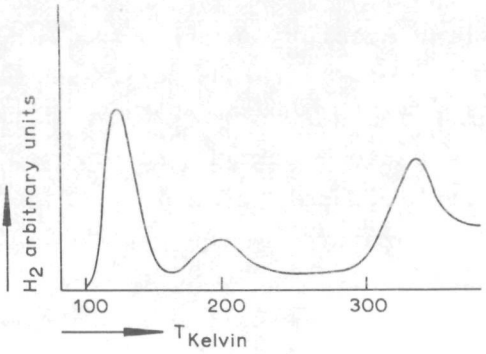

I.1 Part of the H_2/Pt - black TPD - spectrum

I.1.2 Flash desorption and Thermodesorption

In the field of TPD, two different methods may be distinguished. Here we adopt the nomenclature that is mostly encountered in literature, though other nomenclatures have also been used (2). Flash desorption is desorption by very fast heating of the sample (heating rate $>> 1\ Ks^{-1}$), whereas thermodesorption is desorption by slow heating in an inert gas stream (heating rate $\lesssim 1\ Ks^{-1}$).

Hybride methods can also be met in literature, c.f. desorption by slow heating in a vacuum system (3). Since the heating rate is decisive, we shall call this Thermodesorption. Desorption by fast heating in an inert gas stream, being hardly feasible without a serious temperature gradient, is not likely to be encountered in literature.

I.1.3 Theoretical Analysis

I.1.3.1 Flash desorption

So far, Flash desorption is the method most widely used, and many theoretical papers are devoted to it. The solid phase, generally a polycrystalline filament or ribbon, is raised in temperature by resistance heating, and the desorption is monitored by measuring the pressure changes by means of an ionisation gauge. In most cases, the system is pumped during the desorption experiment and, the pumping speed being much higher than the theoretical rate of re-adsorption, the desorption spectrum is believed to reflect the rate of desorption as a function of temperature (2-10).

The development of the method up to the early sixties is reviewed by Ehrlich (11). The theoretical analysis is extended by Redhead (8) and by Carter (13). So far, the analysis was restricted to homogeneous surfaces. Grant and Carter (14), and Erents, Grant and Carter (15) took heterogeneous surfaces into consideration. Their method was adopted and refined by others (4-6,12,13,15-17), especially by Yakerson et al. (17).

It was recognized by many authors that the best way of investigating the influence of various parameters on the desorption behaviour is model simulation of the desorption experiment by means of a computer (5,6,13,15,16,18), preferably using an analog computation procedure (5,6).

I.1.3.2 Thermodesorption

In the thermodesorption case, heating is slow, and readsorption cannot always be excluded. Cvetanovic and Amenomiya (16,19) derived equations for first order de-

sorption kinetics in a flow system for the two limiting cases: negligible adsorption on the one hand, and freely occurring readsorption on the other hand. They extended their analysis to a heterogeneous surface with a uniform site distribution (16).

Recently, the readsorption phenomenon has been treated by Edwards for partial occurring readsorption as a perturbation of the no-readsorption case (20). A recent review has been given by Smutek et al. (21).

I.2 The analysis presented in this thesis

The analysis by Cvetanovic et al. (16,19) turned out to be very valuable for our purpose. For a complete analysis of hydrogen desorption to be possible, second order desorption kinetics should be incorporated. So, we extended their approach to second order equations, both with and without readsorption. In the following sections we review their results, making some necessary corrections (22). Our extension to second order kinetics is given in section I.4.

In section I.5, the main equations are summarized. Section I.6 gives an analysis of the value of the flow rate, necessary for a complete suppression of the readsorption. In section I.7, the influence of the temperature on the pre-exponential factors is discussed. Section I.8 deals with the case of an energetically heterogeneous surface.

It should be emphasized here that by the assumption of the validity of the Langmuir equations for first and second order adsorption and desorption throughout section I.3 to I.5, it is implicitly assumed that all adsorbed molecules are held by the same strength of chemisorption bond, up to a fractional coverage $\theta = 1$. Though this assumption may not

hold for the whole desorption spectrum, it may be a valid approximation for one type of adsorption, associated with one desorption peak in the spectrum.
If we assume a heating schedule that is linear with time, the temperature T at time t is given by

$$T = T_0 + \beta t \qquad (I.1)$$

T_0 is the temperature at time zero (start of the desorption run), β is the heating rate coefficient. Preferably, t is given in seconds [s], T in Kelvin [K], so that the dimension of β should be [K/s].

I.3.1
First, we consider the case of desorption of first order in the adsorbate. Under the steady state conditions, neglecting any diffusion control, the net desorption rate of a sample, consisting of a single component, is given by the Langmuir equation:

$$-\frac{d\theta}{dt} = k_d\theta - k_a \cdot \frac{p}{p_o} (1 - \theta) \qquad (I.2)$$

where θ is the fractional surface coverage, k_d and k_a are the rate constants of desorption and of adsorption respectively, p is the partial pressure of the desorbing gas in the carrier gas, and p_o is the total pressure.

In the following analysis, it is assumed that throughout the desorption experiment, the partial pressure p is negligibly small as compared to the total pressure p_o. In other words, the phenomenon of desorption does not influence the total pressure p_o nor the gas flow rate F.
Thus

$$FC = V_s v_m k_d \theta - V_s v_m k_a C(1-\theta) \qquad (I.3)$$

F is the gas flow rate in [cm^3(NTP)/s], V_s is the volume of the solid phase in the catalyst bed in [cm^3], v_m is the amount of the sample adsorbed per unit volume of the solid phase when θ=1, in [cm^3/cm^3], and C is the concentration of the sample in the carrier gas, in [cm^3/cm^3] or in [pressure unit/pressure unit], which is the same if the gases behave ideally.

The fractional surface coverage θ is a function of the temperature T and of the time t.

$$\theta = \theta(T,t) \rightarrow \frac{d\theta}{dt} = \left(\frac{\partial\theta}{\partial T}\right)_t \cdot \left(\frac{\partial T}{\partial t}\right) + \left(\frac{\partial\theta}{\partial t}\right)_T$$

Now, following e.q. (I.1), and because of the last right hand term being zero (the experiment is started under equilibrium conditions, so that desorption only occurs as a consequence of temperature rise), we arrive at

$$\frac{d\theta}{dt} = \beta \cdot \frac{d\theta}{dT} \qquad (I.4)$$

Combining eqs. (I.2), (I.3), and (I.4), we get

$$C = \frac{V_s v_m k_d \theta}{F + V_s v_m k_a (1-\theta)} \qquad (I.5)$$

It is further assumed that we deal with a homogeneous surface; k_d is not a function of θ, and the temperature dependence of k_d is given by the Arrhenius equation

$$k_d = A \exp\left(-E_d/RT\right). \qquad (I.6)$$

Two limiting cases may be considered:

case A : Readsorption does not occur.
case B : Readsorption occurs freely.

I.3.2 Case A.1. First order desorption without readsorprion.

If no readsorption takes place, the last term at the right hand side of eq. (I.2) can be neglected. By doing this, eq. (I.5) is reduced to:

$$C = \frac{V_s v_m k_d \theta}{F} \qquad (I.7)$$

This result can also be obtained directly from eq.(I.5) by stating that

$$F >> V_s v_m k_a (1-\theta),$$

which means that the flow rate is some orders of magnitude higher than the rate of adsorption.

Eqs. (I.2), (I.3), and (I.4) can be combined to give

$$\frac{d\theta}{dT} = - \frac{\theta}{\beta} k_d = - \frac{\theta}{\beta} A \exp (- E_d/RT) \qquad (I.8)$$

At peak maximum, $\frac{dC}{dT} = 0$.

Since $C = C(\theta, k_d)$,

$$\frac{dC}{dT} = \left(\frac{\partial C}{\partial \theta} \right).\left(\frac{d\theta}{dT} \right) + \left(\frac{\partial C}{\partial k_d} \right). \left(\frac{dk_d}{dT} \right)$$

$$\text{or} \quad \frac{dC}{dT} = - C. \frac{A}{\beta} \exp (- E_d/RT) + C. \frac{Ed}{RT^2} , \qquad (I.9)$$

$$\text{and} \left(\frac{dC}{dT}\right)_{T=T_M} = 0,$$

$$(k_d)_M = \beta. \frac{E_d}{RT_M^2} = A \exp (- E_d/RT_M) \qquad (I.10)$$

The index M stands for "the value attained at peak maximum".

Eq. (I.10) can be rearranged to give

$$2 \ln(T_M) - \ln(\beta) = \frac{E_d}{RT_M} + \ln(\frac{E_d}{A}) \qquad (I.11)$$

This equation relates the temperature of the peak maximum, T_M, with the heating rate, β, for a fixed value of the desorption activation energy E_d.

In order to obtain an equation describing the shape of the theoretical desorption peak, eq. (I.8) has to be solved for θ, so that C can be evaluated from eq. (I.7) as a function of time (or temperature).
Eq. (I.10) can be solved for β; after substitution in eq. (I.9) we get

$$\frac{dC}{dT} = - C. \frac{E_d}{RT_M^2} \exp (\frac{E_d}{RT_M} - \frac{E_d}{RT}) + C. \frac{E_d}{RT^2} \qquad (I.12)$$

It appears to be convenient to normalize the temperature dependent parameters, and the temperature itself, with respect to their values at the peak maximum. So, we write: $T_n = T/T_M$, $C_n = C/C_M$, and $E_M = E_d/RT_M$. Hence:

$$- \frac{dC_n}{dT_n} = C_n E_M \{ \exp [E_M(1 - \frac{1}{T_n})] - \frac{1}{T_n^2} \} \qquad (I.13)$$

With the substitution $x = E_M (1 - 1/T_n)$ this changes into:

$$- \frac{dC_n}{d_x} = C_n \{ \frac{\exp(x)}{(1-x/E_M)^2} - 1 \} \qquad (I.14)$$

$$\ln(C_n) = x - I_{(2)} \qquad (I.15)$$

$$I_{(2)} = \int_0^x \frac{\exp(x)}{(1-x/E_M)^2}\, dx$$

The integral $I_{(2)}$ can be computed numerically. For a chosen value of E_M, C_n can be evaluated for different values of x(that is, for different values of T_n). In this way, normalized theoretical peak shapes can be computed.

I.3.3 Case B.1. First order desorption with freely occurring readsorption.

For this case, $F << V_s v_m k_a (1-\theta)$, and now, eq. (I.5) reduces to

$$C = K. \frac{\theta}{(1-\theta)} \qquad (I.16)$$

where $K = \frac{k_d}{k_a}$, the reciprocal value of the conventional equilibrium constant of adsorption, or

$$K = A^* \exp(-\Delta H/RT) = \exp(\Delta S/R) \exp(-\Delta H/RT) \qquad (I.17)$$

ΔS and ΔH being the entropy and the enthalpy of adsorption, respectively.

Proceeding in the same way as before, we derive

$$K_M = \frac{V_s v_m \beta}{F} (1-\theta_M)^2 \frac{\Delta H}{RT_M^2} = A^* \exp(-\Delta H/RT_M) \qquad (I.18)$$

$$\text{or } 2\ln(T_M) - \ln(\beta) = \frac{\Delta H}{RT_M} + \ln \frac{(1-\theta_M)^2 V_s v_m \Delta H}{FA^* R} \qquad (I.19)$$

In the same way in which we derived eq. (I.8), we get

$$- \frac{d\theta}{dT} = \frac{F}{V_s v_m \beta} \cdot \frac{\theta}{(1-\theta)} \cdot A^* \exp(-\Delta H/RT) \qquad (I.20)$$

The value of $(\frac{F}{V_s v_m \beta})$ is to be substituted from eq.(I.18). In doing so, θ_M, the coverage at peak maximum, is introduced into the equation which has to be solved for θ. First of all, it will be necessary to evaluate θ_M as a function of the initial coverage θ_i. Making the same substitutions as above, and writing $E^* = \Delta H/RT$ and $E_M^* = \Delta H/RT_M$, eq.(I.20) is transformed into:

$$- \frac{d\theta}{dT_n} = \frac{\theta}{(1-\theta)} \cdot \frac{F}{V_s v_m \beta} \cdot T_M \cdot A^* \exp(-E_m^*/T_n) \qquad (I.21)$$

and, on substituting the value of $(F/V_s v_m)$ from eq. (I.18), into

$$- \frac{d\theta}{dT_n} = \frac{\theta}{(1-\theta)} (1-\theta_M)^2 E_M^* \exp(E_M^*) \exp(-E_M^*/T_n) \qquad (I.22)$$

It should be noted that the latter substitution makes the equation independent of A*, that is, independent of the entropy of adsorption.
We wish to emphasize, that this is a consequence of the assumption that the entropy of adsorption is independent of temperature, which is, in general, not true. The consequences of the temperature dependence of A* will be discussed in section I.7.

Integration of equation (I.22) between the limits θ_i and and θ_M (the initial coverage and the coverage at peak maximum, respectively), and between the corresponding normalized temperature limits $T_n = T/T_M = 0$, and $T_n = T/T_M = 1$, gives

$$\frac{\ln\left(\frac{\theta_i}{\theta_M}\right) - (\theta_i - \theta_M)}{(1 - \theta_M)^2} = E_M^* \exp(E_M^*) I_{(1)}$$

$$I_{(1)} = \int_0^1 \exp(-E_M^*/T_n)\, dT_n \qquad \text{(I.23)}$$

After numerical evaluation of $I_{(1)}$, for different values of E_M^*, θ_M can be estimated for different values of θ_i and E_M^*.

With a knowledge of θ_M, e.g. (I.22) can be solved for θ as a function of E_M^*, θ_i, and T_n . The transformation $x = E_M^*(1-1/T_n)$ is again made, giving

$$-\frac{d\theta}{dx} = \frac{\theta}{(1-\theta)} (1 - \theta_M)^2 \frac{\exp(x)}{(1-x/E_M^*)^2} \qquad \text{(I.24)}$$

or

$$\ln(\theta) - \theta = \ln(\theta_M) - \theta_M - (1-\theta_M)^2 I_{(2)}$$

$$I_{(2)} = \int_0^x \frac{\exp(x)}{(1-x/E_M^*)^2}\, dx \qquad \text{(I.25)}$$

From eq.(I.16) we can derive (with $C_n = C/C_M$)

$$C_n = \frac{\theta}{(1-\theta)} \cdot \frac{(1-\theta_M)}{\theta_M} \exp(x) \qquad \text{(I.26)}$$

I.4. The desorption is second order in coverage.

The Langmuir equation now reads:

$$-\frac{d\theta}{dt} = k_d\theta^2 - k_a \frac{p}{p_o} (1 - \theta)^2 \qquad (I.27)$$

which leads to

$$C = \frac{V_s v_m k_d \theta^2}{F + V_s v_m k_a (1-\theta)^2} \qquad (I.28)$$

The same two limiting cases as before will be considered.

I.4.1. Case A.2 Second order desorption kinetics, without readsorption

For this case, eq. (I.28) reduces to

$$C = \frac{V_s v_m k_d \theta^2}{F} \qquad (I.29)$$

from which we derive

$$(k_d)_M = \frac{\beta}{2\theta_M} \cdot \frac{E_d}{RT_M^2} \qquad (I.30)$$

or

$$2 \ln (T_M) - \ln(\beta) = \frac{E_d}{RT_M} + \ln \left[\frac{E_d}{2\theta_M AR} \right] \qquad (I.31)$$

The expression for β contains θ_M, so that, as in case B.1 it is first of all necessary to solve for θ_M. Following the same procedure, we arrive at

$$2\,\theta_M\left(\frac{1}{\theta_M}-\frac{1}{\theta_i}\right)=E_M\exp(E_M)\,I_{(1)} \qquad (I.32)$$

$$I_{(1)}=\int_0^1 \exp(-E_M/T_n)\,dT_n$$

from which θ_M can be evaluated as a function of θ_i and E_M.

Still following the procedure as outlined in section I.3 for case B1, we obtain

$$\frac{1}{\theta}=\frac{1}{\theta_M}-\frac{1}{2\theta_M}\cdot I_{(2)} \qquad (I.33)$$

$$I_{(2)}=\int_0^x \frac{\exp(x)}{(1-x/E_M)^2}\,dx$$

and

$$C_n=\frac{\theta^2}{\theta_M^2}\exp(x) \qquad (I.34)$$

I.4.2 Case B.2 Second order description kinetics, with freely occurring readsorption

Now, eq. (I.28) is transformed into

$$C=K\,\frac{\theta^2}{(1-\theta)^2} \qquad (I.35)$$

leading to

$$2\ln(T_M)-\ln(\beta)=\frac{\Delta H}{RT_M}+\ln\left[\frac{(1-\theta_M)^3\,V_s v_m \Delta H}{2\theta_M F A^* R}\right] \qquad (I.36)$$

and to

$$\frac{2\theta_M}{(1-\theta_M)^3}\left[\frac{1}{\theta_M} - \frac{1}{\theta_i} + \ln\left(\frac{\theta_M}{\theta_i}\right)^2 - (\theta_M-\theta_i)\right] = E_M^* \exp(E_M^*)\, I_{(1)}$$

$$I_{(1)} = \int_0^1 \exp(-E_M^*/T_n)\, dT_n \qquad (I.37)$$

and to

$$\theta - \frac{1}{\theta} - 2\ln(\theta) = \theta_M - \frac{1}{\theta_M} - 2\ln(\theta_M) - \frac{(1-\theta_M)^3}{2\theta_M} \cdot I_{(2)} \qquad (I.38)$$

$$I_{(2)} = \int_0^x \frac{\exp(x)}{(1-x/E_M^*)^2}\, dx$$

and, finally, to

$$C_n = \frac{\theta^2}{(1-\theta)^2} \quad \frac{(1-\theta_M)^2}{\theta_M^2} \quad \exp(x) \qquad (I.39)$$

I.5 Summary

In the foregoing sections, equations were derived describing the two limiting cases of both first and second order desorption kinetics, the most important of them providing us with the following quantities:

1. The temperature at peak maximum, T_M, as a function of the heating rate, β, and the activation energy of desorption, E_d, (or the enthalpy of adsorption, ΔH).

2. The value of the coverage at peak maximum, θ_M, as a function of the initial coverage, θ_i, and the reduced activation energy of desorption, E_M (= E_d/RT_M), or the reduced enthalpy of adsorption, E_M^*(= $\Delta H/RT_M$).

3. The value of the coverage, θ, as a function of the normalized temperature, T_n (= T/T_M), and E_M or E_M^*.

4. The value of the normalized concentration, C_n (=C/C_M), of the desorbing gas in the carrier gas stream, as a function of θ,x (= $E_M(1-1/T_n)$ or = $E_M^*(1-1/T_n)$, and θ_M.

N.B. Since $C_n = C_n(\theta,x,\theta_M)$ and
$\theta = \theta(E_M,\theta_i,T_n)$, $x = x(E_M,T_n)$, $\theta_M = \theta_M(E_M,\theta_i)$
it follows that

$$C_n = C_n\,(\theta_i,\ E_M,\ T_n).$$

An exception is to be made for the simplest case, e.g. case A.1, for which separate equations for $\theta_M=\theta_M(E_M,\theta_i)$ and for $\theta = \theta(E_M,T_n)$ are not necessary.

The equations derived are summarized below. Also a new numeration is introduced, to be used for references throughout this thesis.

I.5.1 $T_M = T_M\,(\theta,\ E_d)$ or $T_M = T_M\,(\theta,\Delta H)$

$$2\ln(T_M) - \ln(\beta) = \frac{E_d}{RT_M} + \ln\left(\frac{E_d}{AR}\right) \qquad \text{(A.1.1)}$$

$$2\ln(T_M) - \ln(\beta) = \frac{\Delta H}{RT_M} + \ln\left[\frac{(1-\theta_M)^2\, V_s V_m \Delta H}{FA^*R}\right] \qquad \text{(B.1.1)}$$

$$2 \ln (T_M) - \ln(\beta) = \frac{E_d}{RT_M} + \ln[\frac{E_d}{2\theta_M^2 AR}] \qquad (A.2.1)$$

$$2 \ln (T_M) - \ln(\beta) = \frac{\Delta H}{RT_M} + \ln [\frac{(1-\theta_M)^3 V_s v_m \Delta H}{2\theta_M^2 FA^* R}] \qquad (B.2.1)$$

I.5.2 $\theta_M = \theta_M(E_M, \theta_i)$ or $\theta_M = \theta_M (E_M^*, \theta_i)$

$$\frac{\ln(\frac{\theta_i}{\theta_M}) - (\theta_i - \theta_M)}{(1-\theta_M)^2} = E_M^* \exp(E_M^*) I_{(1)} \qquad (B.1.2)$$

$$2 \theta_M (\frac{1}{\theta_M} - \frac{1}{\theta_i}) = E_M \exp(E_M) I_{(1)} \qquad (A.2.2)$$

$$\frac{2 \theta_M}{(1-\theta_M)^3} [(\frac{1}{\theta_M} - \frac{1}{\theta_i}) + \ln (\frac{\theta_M}{\theta_i})^2 - (\theta_M - \theta_i)] =$$

$$E_M^* \exp(E_M^*) I_{(1)} \qquad (B.2.2)$$

where $I_{(1)} = \int_0^1 \exp (-E_M/T_n) \, dT_n$

or $I_{(1)} = \int_0^1 \exp (-E_M^*/T_n) \, dT_n$, where appropriate.

I.5.3 $\theta = \theta(\theta_i, E_M, T_n)$ or $\theta = \theta(\theta_i, E_M^*, T_n)$

$$\ln(\theta) - \theta \simeq \ln(\theta_M) - \theta_M - (1-\theta_M)^2 . I_{(2)} \qquad (B.1.3)$$

$$\frac{1}{\theta} = \frac{1}{\theta_M} - \frac{1}{2\theta_M} . I_{(2)} \qquad (A.2.3)$$

$$\theta - \frac{1}{\theta} - 2\ln(\theta) = \theta_M - \frac{1}{\theta_M} - 2\ln(\theta_M) - \frac{(1-\theta_M)^3}{2\theta_M} I_{(2)} \qquad (B.2.3)$$

where $I_{(2)} = \int_0^x \frac{\exp(x)}{(1-x/E_M)}\, dx$.

E_M is to be replaced by E_M^*, when appropriate.

I.5.4 $C_n = C_n(\theta_i, E_M, T_n)$ or $C_n = C_n(\theta_i, E_M^*, T_n)$

$$\ln(C_n) = x - I_{(2)} \qquad (A.1.4)$$

$$C_n = \frac{\theta}{(1-\theta)} . \frac{(1-\theta_M)}{\theta_M} \exp(x) \qquad (B.1.4)$$

$$C_n = \frac{\theta^2}{\theta_M^2} \exp(x) \qquad (A.2.4)$$

$$C_n = \frac{\theta^2}{(1-\theta)^2} . \frac{(1-\theta_M)^2}{\theta_M^2} \exp(x) \qquad (B.2.4)$$

I.6 Comparison of the flow rate and the rate of readsorption.

In section I.3, equations were derived with the assumption that the rate of readsorption is negligibly small, as compared to the carrier gas flow rate. In sections I.4, I.3.3 and I.4.2, on the other hand, we assumed the rate of readsorption to be some orders of magnitude higher than the gas flow rate.

In this section, a rough estimate of the rate of adsorption is made, on which a criterion for a choice of one of the two limiting cases can be based.

At temperature T, the rate of adsorption is given by (18):

$$r_a = s.p. \ (2\pi mkT)^{-\frac{1}{2}}, \qquad (I.40)$$

where s is the sticking coefficient, p is the partial pressure of the adsorbing gas, m is the mass of a gas molecule, k is Boltzmann's constant.

At T = 300 K, we estimate for hydrogen

$r_a = s.p. \ \ 1.08 * 10^{23}$

For the adsorption of hydrogen on platinum, s has been estimated to be about 0.1 (23), so that

$r_a \gtrsim 10^{22}.p \ \ (\text{molecules} \ .s^{-1}. \ m^{-2})$

$r_a \gtrsim .017 \ p \ \ (\text{mole}. \ s^{-1}. \ m^{-2})$

$r_a \gtrsim 400 \ \ p \ \ (10^{-6} \ m^3 (\text{NTP}) \ s^{-1} \ m^{-2})$

Thus for $p \gtrsim 1 \ N \ m^{-2}$ ($p \gtrsim 10^{-3}$ atm.), the situation is met where $F << r_a$, F being in the order of 1 ml s^{-1}.

In the same way it can be derived that the criterion for the inverse case, $F >> r_a$ during the whole desorption experiment, would be $F \geq 4.10^5$ ml s^{-1}, a condition that is hardly feasible in a conventional flow apparatus.

It appears therefore that, in thermodesorption using a flow system, one generally deals with case B, the readsorption case. Nevertheless, the equations derived for case A have more than just a theoretical meaning. First, adsorption might be a strongly activated process (s very low, e.g. N_2 on iron). Then, the flow rate requirements are less severe. Secondly, working in U.H.V. with high pumping rates and low rates of desorption, readsorption is often negligible, and case A equations are applicable. Further, one might imagine that desorption of a state i is accompanied by readsorption in state ii. Indications for such a situation to occur are to be found in recent TPD work by Konvalinka and Scholten (24) on the desorption of hydrogen from Pd. Here the description of "type C" hydrogen is first order in coverage, and the half value peak width points to readsorption in a state which is irreversibly adsorbed at that temperature.

I.7 Temperature dependence of the pre-exponential factor

I.7.1 Temperature dependence

Hitherto, it was assumed that the pre-exponential factors in eqs. (I.6) and (I.17) are temperature independent.

In eq. (I.6), the pre-exponential A stands for (25):

$$A = \kappa . \frac{kT}{h} . \exp (\Delta S_d^{\dagger}/R) \qquad (I.41)$$

where $\Delta S_d^{\dagger}$ is the activation entropy of desorption, k is Boltzmann's constant, h is Planck's constant, R is the gas constant, T is the temperature, and κ is the transmission

coefficient.

Mostly, A is set equal to kT/h, or even chosen to be 10^{13} s^{-1}, which is the value of kT/h for T = 300K(3,8,9)

In general, the desorption activation entropy does not equal zero. For example, the adsorbed state might be immobile, but the transition state is likely to be mobile. The value of $\Delta S_d^{\dagger}$ depends on the difference in mobility between the initial state (the adsorbed state), and the transition state, and so does the temperature dependence. Each translational degree of freedom and each rotational one that the transition state has and the initial state has not, attributes a factor $T^{\frac{1}{2}}$ to the temperature dependence of A. If the initial state is immobile atomic, giving a mobile diatomic transition state with one rotational degree of freedom, the contribution to the temperature dependence of A is $T^{3/2}$. Together with kT/h, we arrive at $T^{5/2}$ as a kind of upper limit for the temperature dependence.

The transmission coefficient κ is usually put equal to 1. There is some evidence, though, that in the case of desorption from paramagnetic metals and alloys, κ might be significantly less than unity (26), and also be temperature dependent (27). According to Solbakken (28) all desorption reactions involving a change in spin multiplicity may exhibit low and temperature dependent values of the transmission coefficient.

The pre-exponential factor A* in eq. (I.17) stands for

$$A^* = \exp(\Delta S/R) \qquad (I.42)$$

where ΔS is the differential entropy of adsorption.

The adsorbed state is always less mobile than the gaseous state, so that $\Delta S \neq 0$, and always dependent on temperature. The temperature dependence is related to the

number and nature of the degrees of freedom that are lost on adsorption.

In the following sections, the influence the temperature dependence of A (or A*) has on the derived equations is discussed.

I.7.2 Effect of the temperature dependence of the pre-exponential factor on the derived equations.

The temperature dependence of A (or A*) may formally be written as

$$A\ (A^*) = B.T^b \qquad (I.43)$$

The extra temperature dependent factor in eq. (I.7) introduces an extra term $b.T^{(b-1)}$ into the derivative (eq.(I.9)) and influences all following equations.

In section I.7.3, we present the revised equations of section I.5. They bear the same numbers, because the equations of section I.5 can be regarded as a special case (b = 0).

I.7.3 The revised equations

I.7.3.1 $T_M = T_M(\beta, E_d)$ or $T_M = T_M(\beta, \Delta H)$

$$(b+2)\ln(T_M) - \ln(\beta) = \frac{E_d}{RT_M} + \ln\left[\frac{(E_d/R + bT_M)}{B}\right] \qquad A.1.1$$

$$(b+2)\ln(T_M) - \ln(\beta) = \frac{\Delta H}{RT_M} + \ln\left[\frac{(1-\theta_M)^2 V_s v_m (\Delta H/R + bT_M)}{FB}\right] \qquad B.1.1$$

$$(b+2)\ln(T_M) - \ln(\beta) = \frac{E_d}{RT_M} + \ln\left[\frac{(E_d/R + bT_M)}{2\theta_M B}\right] \qquad A.2.1$$

$$(b+2)\ \ln(T_M) - \ln(\beta) = \frac{\Delta H}{RT_M} + \ln\left[\frac{(1-\theta_M)^3\ V_s v_m(^{\Delta H}/_R + bT_M)}{2\ \theta_M F B}\right]$$

(B.2.1)

I.7.3.2 $\theta_M = \theta_M\ (E_M, \theta_i)$ or $\theta_M = \theta_M\ (E_M^*,\ \theta_i)$

$$\frac{\ln(\frac{\theta_i}{\theta_M}) - (\theta_i - \theta_M)}{(1-\theta_M)^2} = (E_M^*+b)\ \exp(E_M^*)\, I_{(1)} \qquad (B.1.2)$$

$$2\ \theta_M\left(\frac{1}{\theta_M} - \frac{1}{\theta_i}\right) = (E_M + b)\ \exp(E_M)\, I_{(1)} \qquad (A.2.2)$$

$$\frac{2\ \theta_M}{(1-\theta_M)^3}\left(\frac{1}{\theta_M} - \frac{1}{\theta_i}\right) + \ln\left(\frac{\theta_M}{\theta_i}\right)^2 - (\theta_M - \theta_i) = (E_M^*+b)\exp(E_M^*)\, I_{(1)}$$

(B.2.2)

where $I_{(1)} = \int_0^1 \exp(-E_M/T_n)\, T_n^{\,b}\ dT_n$

E_M is to be replaced by E_M^*, when applicable.

I.7.3.3 $\theta = \theta(\theta_i, E_M, T_n)$ or $\theta = \theta(\theta_i, E_M^*, T_n)$

$$\ln(\theta) - \theta = \ln(\theta_M) - \theta_M - (1-\theta_M)^2\ \frac{(E_M^* + b)}{E_M^*}\ I_{(2)} \qquad (B.1.3)$$

$$\frac{1}{\theta} = \frac{1}{\theta_M} - \frac{1}{2\theta_M}\ \frac{(E_M+b)}{E_M}\ I_{(2)} \qquad (A.2.3)$$

$$\theta - \frac{1}{\theta} - 2\ln(\theta) = \theta_M - \frac{1}{\theta_M} - 2\ln(\theta_M) - \frac{(1-\theta_M)^3}{2\theta_M}\,\frac{(E_M^*+b)}{E_M^*}\,I_{(2)} \qquad \text{(B.2.3)}$$

where $I_{(2)} = \int_0^x \frac{\exp(x)}{(1-x/E_M)}(b+2)\,dx$

E_M is to be replaced by E_M^* when appropriate.

I.7.3.4 $C_n = C_n(\theta_i, E_M, T_n)$ or $C_n = C_n(\theta_i, E_M^*, T_n)$

$$\ln(C_n) = \frac{(E_M+b)}{E_M}\,(x-I_{(2)}) + b\ln\frac{(E_M-x)}{E_M} \qquad \text{(A.1.4)}$$

$$C_n = \frac{\theta}{(1-\theta)} = \frac{(1-\theta_M)}{\theta_M} \cdot T_n^{\,b}\,\exp(x) \qquad \text{(B.1.4)}$$

$$C_n = \frac{\theta^2}{\theta_M^2}\,T_n^{\,b}\,\exp(x) \qquad \text{(A.2.4)}$$

$$C_n = \frac{\theta^2}{(1-\theta)^2}\,\frac{(1-\theta_M)^2}{\theta_M^2}\,T_n^{\,b}\,\exp(x) \qquad \text{(B.2.4)}$$

I.8 Coverage dependent heat of adsorption

Up to now, it has been assumed that the value of E_d (or ΔH) remains constant during the desorption experiment. This will only be true for well defined crystal faces, where all sites are identical, provided that there is no lateral repulsion of the adsorbed molecules.
In the latter case, the system may be regarded as a set of

two types of sites, each type having its own characteristic heat of adsorption (and, consequently, its own characteristic activation energy of desorption)(1).

Polycrystalline filaments, ribbons, or evaporated films, and also supported metal catalysts, usually exhibit a heat of adsorption that is coverage dependent. For the adsorption of hydrogen on an evaporated Ni-film, Sweet and Rideal(29) found the isosteric heat of adsorption to vary from 130 $kJ.mole^{-1}$ (θ=0) to 25 $kJ.mole^{-1}$ (θ=0.8)

The equation:

$$C = \frac{V_s v_m \theta}{F} \cdot A.\exp\,(-E_d(\theta)/RT) \qquad (I.44)$$

can be solved if one assumes E_d to be a simple function of θ(14-16), but even a linear relationship between E_d and θ requires a very tiresome numerical solution.

If readsorption is assumed to occur freely, the equation to be solved reads:

$$C = A^* \exp\,(-\Delta H(\theta)/RT) \cdot \frac{\theta}{(1-\theta)} \qquad (I.45)$$

Now, the mathematical analysis is even more complex than in the former case.

A more convenient approach is the simulation of desorption spectra by means of an analog computer. In this way, Khobert and Knappe (5) arrive at results that are very similar to those obtained by Cvetanovic and Amenomiya (16) as a result of a numerical solution of eq. (I.44).

Solution of the above equations can also be avoided if one assumes the spectrum to be built up by summation of different elementary desorption peaks. It has been shown that ten of these peaks, the energies of which are separated by 2 $kcal.mole^{-1}$ (8.4 kJ $mole^{-1}$) already lead to

the same desorption spectrum as the continuous function would do (4).

The inverse of the latter approach can be used for the analysis of an observed desorption spectrum.
The limits of the energy range are derived from the temperature limits of the desorption trace, assuming $A = 10^{+13}\ s^{-1}$. At each temperature within the range, the desorption rate is to be the sum of n elementary desorption peaks, each peak having its desorption activation energy within the required range. By taking n different temperatures, one obtains n linear equations with n unknowns, the solution of which gives the site distribution.

In general, it can be said that a heterogeneous surface causes a broadening and flattening of peaks, making an unambiguous mathematical analysis impossible. Nevertheless, also in these cases, thermodesorption may provide useful information about the adsorption behaviour, especially when used in combination with other techniques.
In certain cases, determination of the behaviour of the peak maximum, T_M, and the amount adsorbed, V, as functions of the adsorption temperature, T_{ads}, can be used to estimate the energy distribution function (17).

I.9 References.

(1) Goymour, C.G., King, D.A.,
J.Chem.Soc., Faraday Trans. 1, 69, (1973) 749

(2) Contour, J-P., Prud'homme, R.,
Bull.Soc.Chim.Fr., (1969) 2693

(3) Stephan, J.J.
Thesis, Leiden 1975

(4) Czanderna, A.W., Biegen, J.R., Kollen, W.,
J. Colloid Interface Sci., 34 (1970) 406

(5) Khobert K., Knappe B.,
Kinet. Catal., 13 (1972) 948

(6) McCarroll B.,
J. Appl. Phys., 40 (1969) 1

(7) Smith A.W., Aranoff, S.,
J.Phys.Chem., 62 (1958) 684

(8) Redhead, P.A.,
Vacuum, 12 (1962) 203

(9) Carter, G.,
Vacuum, 12 (1962) 245

(10) Erents, K., Grant, W.A., Carter, G.,
Vacuum, 15 (1965) 529

(11) Ehrlich, G.,
Advan. Catal., 14 (1963) 255

(12) Winterbottom, W.L.,
J.Vac.Sci.Technol., 9 (1972) 936

(13) Danson, P.T., Peng, Y.K.,
Surf.Sci., 33 (1962) 565

(14) Grant, W.A., Carter, G.,
Vacuum, 15 (1965) 13

(15) Hansen, R.S., Masushita, K.,
J.Chem.Phys., 52 (1970) 5965

(16) Cvetanovic, R.J., Amenomiya, Y.,
Catal.Rev., 6 (1972) 21

(17) Yakerson, V.I., Rozanov, V.V., Rubinsthein,A.M.,
Surf. Sci., 12 (1968) 221

(18) Lord, F.M., Kittelberger, J.S.,
Surf.Sci., 43 (1974) 173

(19) Cvetanovic, R.J., Amenomiya, Y.,
Advan.Catal., 17 (1967) 103

(20) Edwards Jr., D.
Surf.Sci., 49 (1975) 393

(21) Smutek, M., Cerný,S., Buzek, F.,
Advan.Catal., 24 (1975) 343

(22) Konvalinka, J.A., Scholten, J.J.F., Rasser, J.C.,
J.Catal., in press

(23) Lu, K.E., Rye, R.R.,
Surf. Sci., 45 (1974) 677

(24) Konvalinka, J.A., Scholten, J.J.F.,
J. Catal., in press

(25) Glasstone, S., Laidler, K.J., Eyring, H.,
in "The Theory of Rate Process",
McGraw-Hill Book Company, Inc., New York and
London, 1941

(26) Suhl, H., Smith, J.H., Kumar, P.,
Phys. Rev. Lett., 25 (1970) 1442

(27) Pétermann, L.A., in
"Adsorption - Desorption Phenomena", F. Ricca,ed.
Academic Press, London and New York, 1972,
p. 227 - 243

(28) Solbakken, A.,
Actes 2 ième. Congr. Catal. I. paper 9
Technip., Paris, 1961, p. 341

(29) Sweet, F., Rideal, E.,
Actes 2ième Congr. Catal., I., paper 1
Technip., Paris, 1961, p. 175.

Chapter II

Application of the theoretical Analysis

II.1 Introduction

In this chapter it will be outlined how the equations, derived in chapter I, are to be used in the analysis of experimental desorption spectra.

We wish to emphasize here, that the analysis given in chapter I describes the shape of one simple peak, related to one singular mono-energetic adsorption state. The initial coverage, θ_i, is the initial coverage of the adsorption state in question, and might differ from the overall initial coverage. Generally, a desorption spectrum contains two or more peaks, each of which has to be analyzed separately.

The equations collected in section (I.7.3.1) can be used for a rough estimate of the value of E_d (or ΔH, resp.). For this rough estimate, b may be chosen to be zero, so that $B = A$ (or $B = A^*$).

The equations in sections (I.7.3.2) to (I.7.3.4) are used to compute the theoretical peak shapes for the idealized adsorption states. These theoretical peaks are to be used for comparison with experimental desorption peaks. They can also be used for the determination of the theoretical peak width at half peak maximum (in the following called "half value peak width" or, shortly, "peak width", ΔW) in the cases where an analytical solution of the

appropriate equations is not possible. This peak width plays a key-role in our method of analysis. It is used to discriminate between first and second order desorption peaks, and it gives an indication of the presence or absence of re-adsorption (1).

On this basis it is decided which of the equations of section (I.7.3.1) is to be used for an estimate of E_d or ΔH. It will be outlined that an estimate of A or A* will be necessary.

Hence, from a knowledge of T_M and ΔW, one may derive the initial coverage (θ_i), the enthalpy of adsorption (ΔH), and even the order of the desorption reaction.

II.2 Determination of E_d or ΔH

Many authors suggest the use of the equations presented in section (I.5.1) as a basis for the determination of E_d or ΔH(2-5). These equations predict a shift of T_M to lower values for lower heating rates β. In the ideal case, a plot of $\{2 \ln(T_M) - \ln(\beta)\}$ vs. $^1/T_M$ should be a straight line, the slope of which yields the value of E_d/R or $\Delta H/R$.

For efficient determination of E_d by this method, an experimental variation of β by some orders of magnitude is required. In thermodesorption, where temperature rise is effected by external heating, such a drastic change in heating rate is not very well feasible.
Yakerson et al. (6) propose the use of β-values between 2 and 20 $K.min^{-1}$, where the dependence of T_M on β is much more pronounced. In the region of very low heating rates, however, the desorption peaks become very broad and low, so that accurate experimental determination of T_M becomes difficult.

More serious criticism may arise from the possible

temperature dependence of the preexponential factors A and A*. As shown in section (I.7.3.1), the coefficient of the term $\ln(T_M)$ changes from 2 into (b+2), where $0 \leq b \leq 2.5$.

To investigate the effect this temperature dependence may have on the accuracy of the determination of E_d by the method described above, we computed theoretical values of T_M and β for three different cases:

1) $\frac{E_d}{R} = 10^4$ K, $B = 10^{13}$ s^{-1}, $b = 0$

2) $\frac{E_d}{R} = 10^4$ K, $B = 3.3 \times 10^{10}$ s^{-1} K^{-1}, $b = 1$

3) $\frac{E_d}{R} = 10^4$ K, $B = 1.1 \times 10^{8}$ s^{-1} K^{-2}, $b = 2$

It has to be recalled that the temperature dependence of the preexponential A is given by

$$A = B.T^b \qquad \text{(II.1)}$$

For the present purpose, eq. (A.1.1) was written in the form:

$$\ln(\beta) = (b+2) \ln T_M - \frac{E_d}{RT_M} - \ln\left[\frac{E_d/R + bT_M}{\beta}\right] \qquad \text{(II.2)}$$

and β was calculated for a prefixed value of T_M. Sets of values for T_M and β were used for the plot $\{2 \ln (T_M) - \ln(\beta)\}$ vs. $1/T_M$.

For b = 0 we find, of course, a value of 10^4K for E_d/R; b = 1 gives $E_d/R = 10.2 \times 10^3$K, and b = 2 yields $E_d/R = 10.5 \times 10^3$K.
It is seen that the high value of B as compared with T_M causes the deviation in E_d/R to be small.

The same calculation is performed for the readsorption case (eq. (B.1.1)).
We assumed ΔS to be 125 J mole^{-1} K^{-1} at 550 K. The term $(1-\theta_M)^2 V_s v_m/F$ was set equal to unity. In all cases, $\Delta H/R = 10^4$ K.

1) $B = 10^6$ $b = 0$

2) $B = 1.82 \times 10^3$ K^{-1}, $b = 1$

3) $B = 3.31$ K^{-2}, $b = 2$

For $b = 0$, an "experimental" value for $\frac{\Delta H}{R} = 10000$ K is found. For $b = 1$, this value is 10.39×10^3 K, and for $b = 2$ 10.98×10^3 K. So, an error up to 10% in the determination of ΔH is to be expected, when the use of the $2 \ln(T_M) - \ln(\beta)$ vs. $^1/T_M$ plot is not justified because of temperature dependence of ΔS.

II.3 Determination of the coverage at peak maximum

II.3.1 Introduction

It has been shown in chapter I that for the calculation of theroretical line shapes the value of θ_M, the coverage at peak maximum, has to be known. Therefore, the equations of section (I.7.3.2) have to be solved for various values of E_M (or E_M^*), θ_i, and b.

An iterative approach was not considered useful, because the equations mostly contain both $\ln(\theta_M)$ and $^1/\theta_M$. In the region $0<\theta_M<1$, each of these terms might be predominant, so that an iterative procudure, for which one of the terms should have minor significance, is not well possible.

The equations have been solved by a "trial and error" method, the scheme of which is given in fig. (II.1). For chosen values of E_M and b, the value of the right hand side of the equation can be computed. Then, with a knowledge of θ_i, the value of θ_M is increased stepwise, until the value is found that makes the left hand side just not surpass the right hand side of the equation. The value of θ_M thus found is used as a new starting value, and the procedure is repeated with steps which are one tenth of those in the former sequence. This procedure is repeated until the desired accuracy is achieved.

II.3.2 Results and discussion

First of all, it is necessary to compute the value of the integral $I_{(1)}$, given by:

$$I_{(1)} = \int_0^1 \exp\ (-\ E_M/T_n)\ T_n^{\ b}\ \ dT_n \qquad \text{(II.3)}$$

This integral has been evaluated numerically for a number of E_M and b values. The results are tabulated in table (II.1). The effect the temperature dependence of the pre-exponential factor (b = 2.5) has on $I_{(1)}$ varies from 17% for E_M = 10 to 2% for E_M = 100.

With a knowledge of $I_{(1)}$, the right hand side of the equations of section (I.7.3.2) can be evaluated. Then the equations can be solved for θ_M in the way described in section II.3.1. The results are collected in tables (II.2) to (II.5).

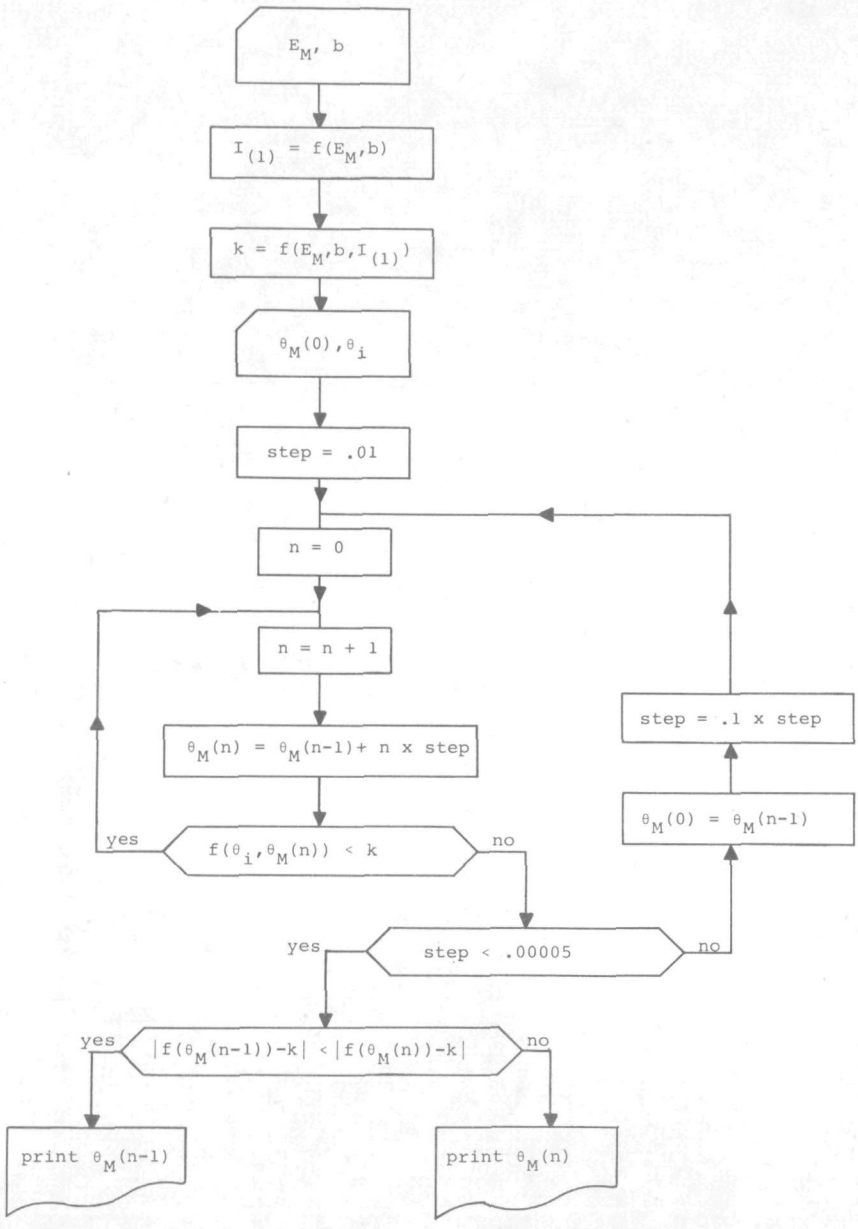

II.1 Scheme of the program for the computation of the coverage at peak maximum, θ_M

Table (II.1) Numerically computed values of the integral $I_{(1)}$ for various values of E_M and b.

E_M	$I_{(1)}$ b = 0	$I_{(1)}$ b = 2.5
10	38.30×10^{-7}	31.93×10^{-7}
15	18.11×10^{-9}	15.86×10^{-9}
20	94.05×10^{-12}	84.72×10^{-12}
25	51.57×10^{-14}	47.31×10^{-14}
30	29.30×10^{-16}	27.22×10^{-16}
40	10.13×10^{-20}	9.57×10^{-20}
50	37.11×10^{-25}	35.44×10^{-25}
100	36.46×10^{-47}	35.60×10^{-47}

Table (II.1)

In general, the desorption peak for second order desorption without readsorption is said to be "symmetric" (2,3) in the sense that at peak maximum about half the initial amount of adsorbed gas has desorbed: $\theta_M/\theta_i \sim 0.5$. In order to check the validity of this statement, θ_M/θ_i - values have been computed. They are presented in tables (II.6) to (II.9). For $\theta_i = 1.00$, the results are presented in fig. (II.2).

For the cases A.1 and A.2, the θ_M/θ_i - values appear to be independent of θ_i. It is seen in fig.(II.2) that the θ_M/θ_i - values for case A.2 are rather close to 0.5, though for low values of E_M the deviation from this value is more than 10%.

In all cases, a temperature dependent preexponential factor tends to decrease the value of θ_M/θ_i, that is, a larger amount of gas is desorbed before the peak maximum is reached. This is clearly demonstrated by fig. (II.3). It is also clear from this figure, that the second order peak in the readsorption case (B-2) is not symmetric.

In general, second order peaks tend to broaden at the high temperature side; first order peaks, on the contrary, exhibit the major part of the desorption at temperatures below T_M. So, a very superficial examination of the shape of an experimental desorption peak can give already strong evidence for first or second order desorption kinetics.

II.4 The theoretical line shape

The theoretical line shapes of reduced desorption peaks can be obtained by the following procedure.
First of all, the integral $I_{(2)}$ has to be computed for a

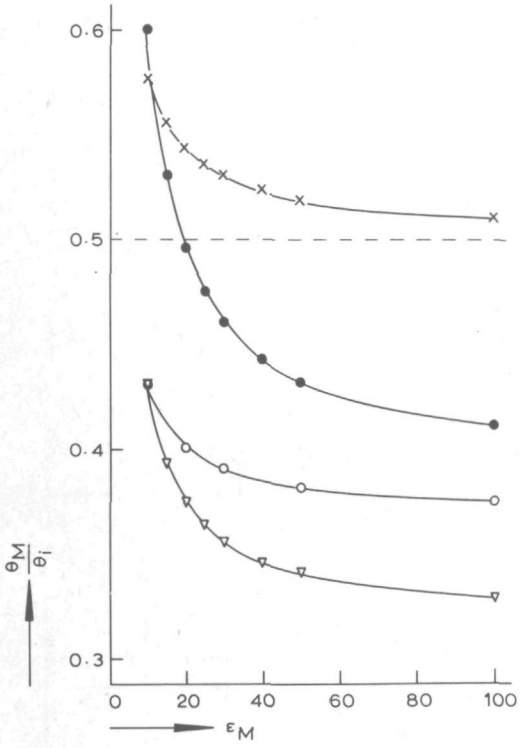

II.2

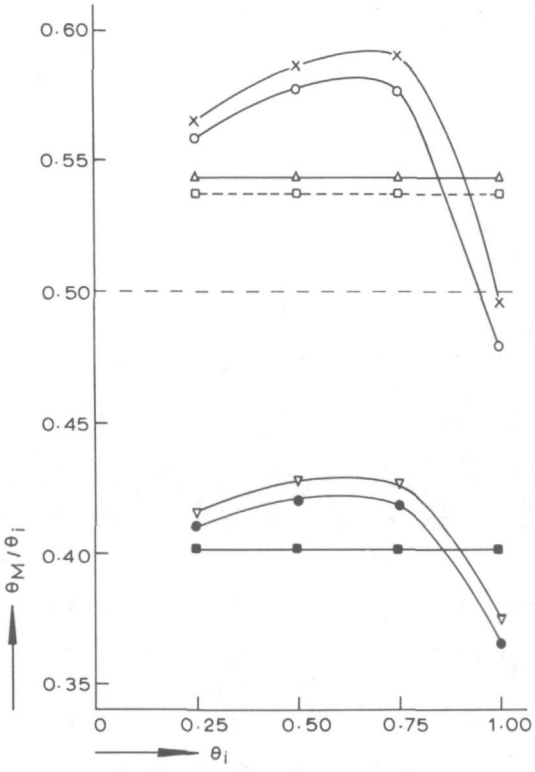

II.3

II.2 Values of θ_M / θ_i (coverage at peak maximum / initial coverage) as a function of the normalized adsorption enthalpy, E_M
X second order without readsorption; ● second order with readsorption; O first order without readsorption; ∇ first order with readsorption
Dashed line: θ_M / θ_i = 0.5. All curves: b = 0

II.3 Values of θ_M / θ_i as a function of initial coverage, for E_M = 20
Δ A-2, b = 0; □ A-2, b = 2.5; X B-2, b = 0; O B-2, b = = 2.5; ■ A-1, b = 0; ∇ B-1, b = 0; ● B-1, b = 2.5
For explanation of symbols, see list of symbols

Table (II.2) Values of the coverage at peak maximum, θ_M, for case A.1

	θ_M							
	$\theta_i = 1.00$		$\theta_i = 0.75$		$\theta_i = 0.50$		$\theta_i = 0.25$	
E_M	b=0	b=2.5	b=0	b=2.5	b=0	b=2.5	b=0	b=2.5
10	.4302	.4151	.3226	.3114	.2151	.2076	.1076	.1038
20	.4015		.3012		.2008		.1004	
30	.3910		.2933		.1955		.0978	
50	.3821		.2866		.1911		.0956	
100	.3753	.3751	.2815	.2813	.1877	.1876	.0939	.0938

Table (II.2)

Table (II.3) Values of the coverage at peak maximum, θ_M, for case A.2

	θ_M							
	$\theta_i = 1.00$		$\theta_i = 0.75$		$\theta_i = 0.50$		$\theta_i = 0.25$	
E_M	b=0	b=2.5	b=0	b=2.5	b=0	b=2.5	b=0	b=2.5
10	.5782	.5604	.4337	.4203	.2891	.2802	.1446	.1402
15	.5561	.5464	.4171	.4098	.2781	.2732	.1391	.1366
20	.5438	.5376	.4078	.4032	.2719	.2688	.1360	.1344
25	.5359	.5317	.4019	.3988	.2680	.2659	.1340	.1330
30	.5305	.5273	.3979	.3955	.2653	.2637	.1327	.1319
40	.5234	.5215	.3925	.3911	.2617	.2608	.1309	.1304
50	.5190	.5177	.3893	.3883	.2595	.2589	.1298	.1295
100	.5100	.5096	.3825	.3822	.2550	.2548	.1275	.1274

Table (II.3)

Table (II.4) Values for the coverage at peak maximum for case B.1

	θ_M							
	$\theta_i = 1.00$		$\theta_i = 0.75$		$\theta_i = 0.50$		$\theta_i = 0.25$	
E_M^*	b=0	b=2.5	b=0	b=2.5	b=0	b=2.5	b=0	b=2.5
10	.4296	.3995	.3577	.3377	.2331	.2229	.1120	.1077
15	.3926	.3777	.3329	.3225	.2204	.2150	.1067	.1044
20	.3738	.3649	.3197	.3134	.2134	.2102	.1038	.1024
25	.3625	.3566	.3117	.3074	.2092	.2070	.1020	.1011
30	.3548	.3507	.3061	.3031	.2063	.2047	.1008	.1001
40	.3453	.3429	.2991	.2974	.2024	.2016	.0992	.0988
50	.3395	.3380	.2949	.2938	.2002	.1996	.0982	.0980
100	.3279	.3278	.2862	.2861	.1954	.1954	.0962	.0962

Table (II.4)

Table (II.5) Values for the coverage at peak maximum for case B.2

	θ_M							
	$\theta_i = 1.00$		$\theta_i = 0.75$		$\theta_i = 0.50$		$\theta_i = 0.25$	
E_M^*	b=0	b=2.5	b=0	b=2.5	b=0	b=2.5	b=0	b=2.5
10	.6007	.5440	.5018	.4772	.3185	.3059	.1512	.1462
15	.5311	.5032	.4647	.4477	.3027	.2955	.1449	.1421
20	.4960	.4795	.4430	.4322	.2935	.2889	.1412	.1396
25	.4749	.4640	.4291	.4216	.2876	.2843	.1390	.1378
30	.4608	.4530	.4194	.4139	.2834	.2810	.1374	.1365
40	.4432	.4386	.4068	.4035	.2779	.2765	.1353	.1348
50	.4326	.4296	.3990	.3968	.2745	.2736	.1340	.1337
100	.4116	.4108	.3831	.3825	.2674	.2672	.1314	.1313

Table (II.5)

Table (II.6) Values of the fraction of the initial coverage that is still adsorbed when the peak maximum is reached, for case A.1

	θ_M/θ_i							
	$\theta_i = 1.00$		$\theta_i = 0.75$		$\theta_i = 0.50$		$\theta_i = 0.25$	
E_M	b=0	b=2.5	b=0	b=2.5	b=0	b=2.5	b=0	b=2.5
10	.4302	.4151	.4301	.4152	.4302	.4152	.4304	.4152
20	.4015		.4016		.4016		.4016	
30	.3910		.3911		.3910		.3912	
50	.3821		.3821		.3822		.3824	
100	.3753	.3751	.3753	.3751	.3754	.3752	.3756	.3752

Table (II.7) Values of the fraction of the initial coverage that is still adsorbed when the peak maximum is reached for case A.2

	θ_M / θ_i							
	$\theta_i = 1.00$		$\theta_i = 0.75$		$\theta_i = 0.50$		$\theta_i = 0.25$	
E_M	b=0	b=2.5	b=0	b=2.5	b=0	b=2.5	b=0	b=2.5
10	.5782	.5604	.5783	.5604	.5782	.5604	.5784	.5608
15	.5561	.5464	.5561	.5464	.5562	.5464	.5564	.5464
20	.5438	.5376	.5437	.5376	.5438	.5376	.5440	.5376
25	.5359	.5317	.5359	.5317	.5360	.5318	.5360	.5320
30	.5305	.5273	.5305	.5273	.5306	.5274	.5308	.5276
40	.5234	.5215	.5233	.5215	.5234	.5216	.5236	.5216
50	.5190	.5177	.5191	.5177	.5190	.5178	.5192	.5180
100	.5100	.5096	.5100	.5096	.5100	.5096	.5100	.5096

Table (II.7)

Table (II.8) Values of the fraction of the initial coverage that is still adsorbed when the peak maximum is reached, for case B.1

	θ_M/θ_i							
	$\theta_i = 1.00$		$\theta_i = 0.75$		$\theta_i = 0.50$		$\theta_i = 0.25$	
E_M^*	b=0	b=2.5	b=0	b=2.5	b=0	b=2.5	b=0	b=2.5
10	.4296	.3995	.4769	.4503	.4662	.4458	.4480	.4380
15	.3926	.3777	.4439	.4300	.4408	.4300	.4268	.4176
20	.3738	.3649	.4263	.4179	.4268	.4202	.4152	.4096
25	.3625	.3566	.4156	.4099	.4184	.4140	.4080	.4044
30	.3548	.3507	.4081	.4041	.4126	.4094	.4032	.4004
40	.3453	.3429	.3988	.3965	.4048	.4032	.3968	.3952
50	.3395	.3380	.3932	.3917	.4004	.3992	.3928	.3920
100	.3279	.3278	.3816	.3815	.3908	.3908	.3848	.3848

Table (II.9) Values of the fraction of the initial coverage that is still adsorbed when the peak maximum is reached, for case B.2

	θ_M/θ_i							
	$\theta_i = 1.00$		$\theta_i = 0.75$		$\theta_i = 0.50$		$\theta_i = 0.25$	
E_M^*	b=0	b=2.5	b=0	b=2.5	b=0	b=2.5	b=0	b=2.5
10	.6007	.5440	.6691	.6363	.6370	.6118	.6048	.5848
15	.5311	.5032	.6196	.5969	.6054	.5910	.5796	.5684
20	.4960	.4795	.5907	.5763	.5870	.5778	.5648	.5584
25	.4749	.4640	.5721	.5621	.5752	.5686	.5560	.5512
30	.4608	.4530	.5592	.5519	.5668	.5620	.5496	.5460
40	.4432	.4386	.5424	.5380	.5558	.5530	.5412	.5392
50	.4326	.4296	.5320	.5291	.5490	.5472	.5360	.5348
100	.4116	.4108	.5108	.5100	.5348	.5344	.5256	.5252

Table (II.9)

preselected value of T_n.

$$I_{(2)} = \frac{\exp(x)}{(1-x/E_M)^{b\mp2}} \quad dx \qquad \text{(II.4)}$$

The solution is carried out numerically. Knowledge of $I_{(2)}$ and θ_M makes evaluation of the right hand side of the equations in section (I.7.3.3) possible. Then, θ can be computed in the same way as has been described in section (II.3.1) for the evaluation of θ_M. The value of θ thus found can be used in the appropriate equation from section (I.7.3.4) to find C_n. By doing so for various values of T_n, a plot of C_n vs. T_n can be obtained. Some of the results are presented in figs. (II.4) to (II.7).

II.5 Determination of peak widths

II.5.1 Introduction

An important parameter for characterizing a desorption peak appears to be the peak width. Traditionally, this peak width is measured at half the peak maximum, where peak broadening effects are most pronounced. We shall call the so measured peak width the "half value peak width", or, shortly, "peak width", for current reference.

II.5.2 Peak widths for desorption without readsorption.

For first and second order desorption without readsorption (case A.1 and A.2, respectively), Edwards (7) derived the following equations relating the peak widths ΔW (in T_n-units) with E_M.

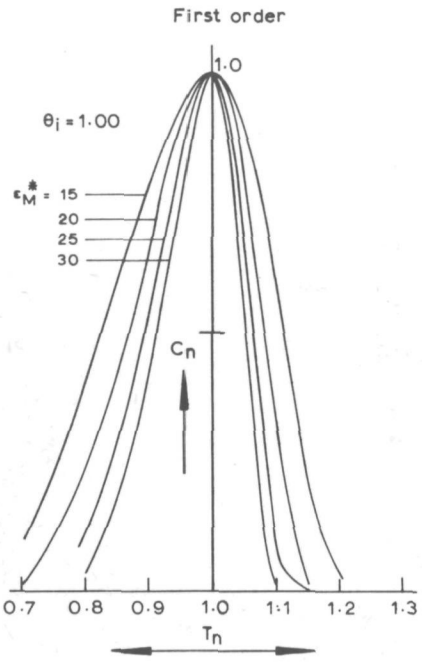

II.4

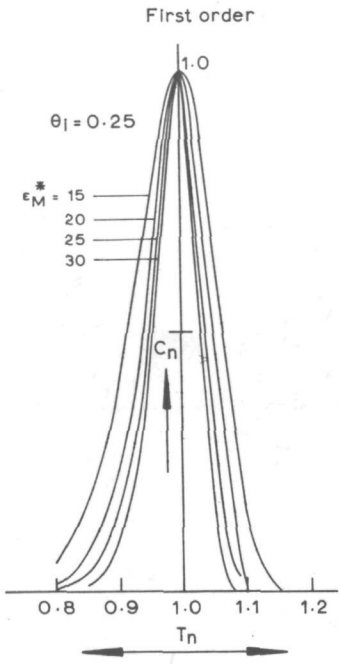

II.5

II.4 Theoretical peak shape for case B-1 (first order desorption with freely occurring readsorption); initial coverage is 1.00, various values of E_M^*

II.5 As figure II.4, but $\theta_i = 0.25$

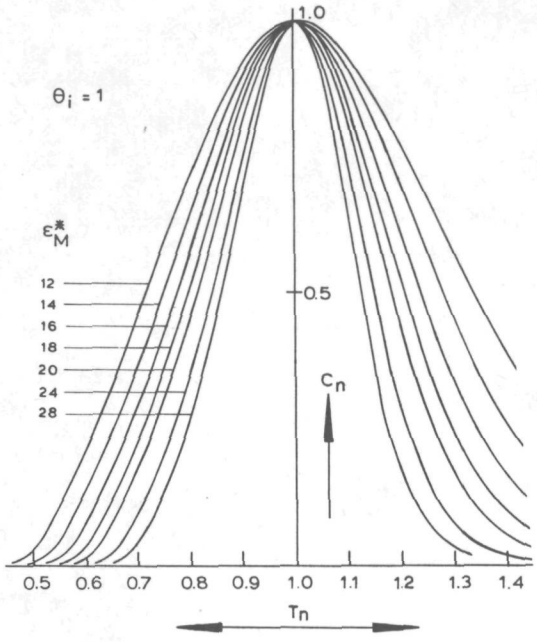

II.6

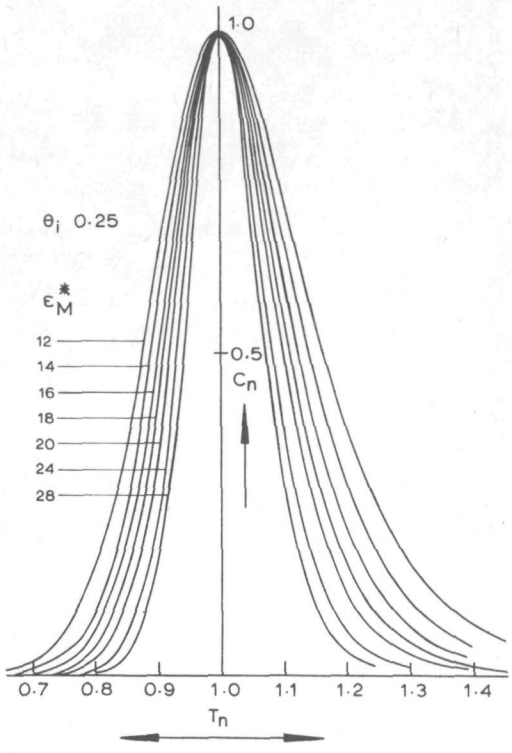

II.7

II.6 Theoretical peak shape for case B-2 (second order desorption with freely occurring readsorption, various values of E_M^*, $\theta_i = 1.00$

II.7 As figure II.6, but $\theta_i = 0.25$

First order:

$$\Delta W = \frac{2.4464}{E_M} \{ 1 - \frac{1.4005}{E_M} + \frac{3.5325}{E_M^2} + \ldots \} \qquad (II.5)$$

Second order:

$$\Delta W = \frac{3.5255}{E_M} \{ 1 - \frac{2.000}{E_M} + \frac{6.941}{E_M^2} + \ldots \} \qquad (II.6)$$

The peak width appears to be independent of coverage. So, the value of ΔW is characteristic for E_M, and can in principle be used for direct determination of E_d, the desorption activation energy. This has been recognized by Edwards (7), and he also derived the inverse equations.

First order:

$$E_M = \frac{2.4464}{\Delta W} (1 - 0.5725 \ \Delta W + 0.2625 \ (\Delta W)^2 + ..) \qquad (II.7)$$

Second order:

$$E_M = \frac{3.5255}{\Delta W} (1 - 0.5673 \ \Delta W + 0.2366 \ (\Delta W)^2 + ..) \qquad (II.8)$$

The coverage independence of ΔW in the case of first order desorption follows directly from the equation describing the peak shape, i.e. eq. (A.1.4).

$$\ln (C_n) = \frac{(E_M+b)}{E_M} (x - I_{(2)}) + b \ln (\frac{E_M-x}{E_M}) \qquad (A.1.4)$$

It is seen that, for given values of E_M and b, C_n depends only on T_n. So, the values of T_n for which $C_n = 0.5$ are independent of θ, and so is ΔW.

The peak shape of second order peaks is given by eq. (A.2.4):

$$C_n = \frac{\theta^2}{\theta_M^2} \; T_n^{\,b} \exp(x) \qquad (A.2.4)$$

From eq. (A.2.3) we get:

$$\frac{1}{\theta} = \frac{2 - \{(E_M+b)/E_M\} \; I_{(2)}}{2\theta_M} \qquad (II.9)$$

On substitution of θ from eq. (II.9) into eq. (A.2.4) we obtain:

$$C_n = \frac{4}{\{2 - (\frac{E_M+b}{E_M}) \; I_{(2)}\}^2} \; T_n^{\,b} \exp(x) \qquad (II.10)$$

which is consistent with a coverage independent peak width. It also provides us with a more direct method for determination of the theoretical peak shape, as determination of θ_M and of θ can be left out.

Making use of eqs. (II.5) and (II.6), values of ΔW for E_M in the range 10 to 100 have been determined. They are presented in fig. (II.8).
Except for very high values of E_M, second order peaks are appreciably broader than first order peaks. This feature may be used for discrimination between the two cases.

II.5.3 Peak widths for desorption with readsorption

It can be seen in figs. (II.9) and (II.10) that in the cases B.1 and B.2 (freely occurring readsorption, first and second order desorption kinetics, respectively) the peak width is strongly dependent on the initial coverage, θ_i.

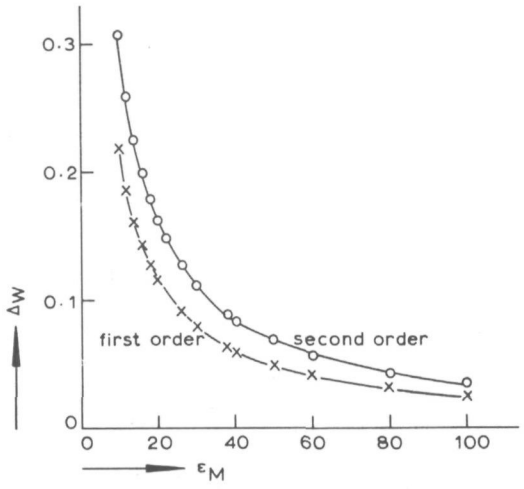

II.8 Half value peak widths for first and second order desorption without readsorption, as a function of the normalized desorption activation energy, E_M

As a consequence, no analytical expression for the peak width can be derived. The ΔW-values can only be determined by construction of a theoretical peak in the way described in section (II.4). This has been done for various values of E_M^*, θ_i and b.

Again, second order peaks are appreciably broader than first order peaks. The readsorption also causes an appreciable peak broadening. The half value width for a second order peak with a relatively low E_M^* -value may be as high as 0.5. This means that for T_M = 400K, the half value peak width is 200K. Since the peak area is limited by the total amount that can be absorbed, the peak will be

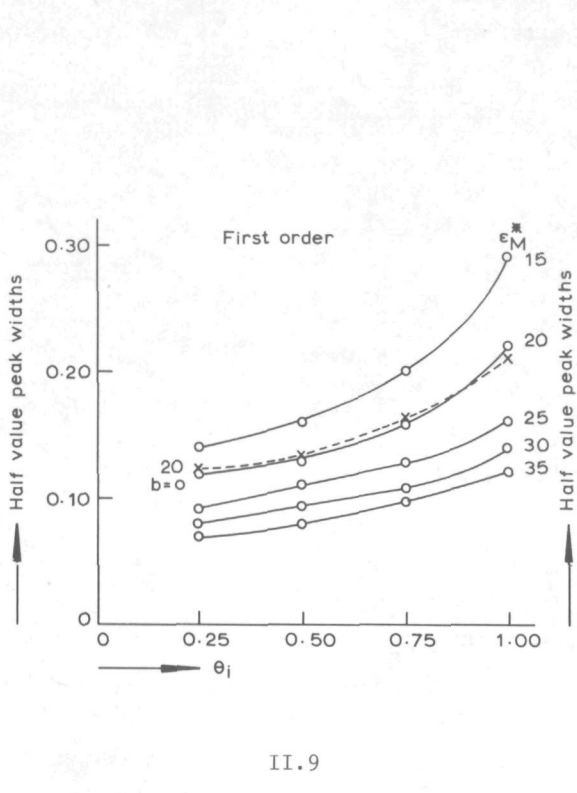

II.9

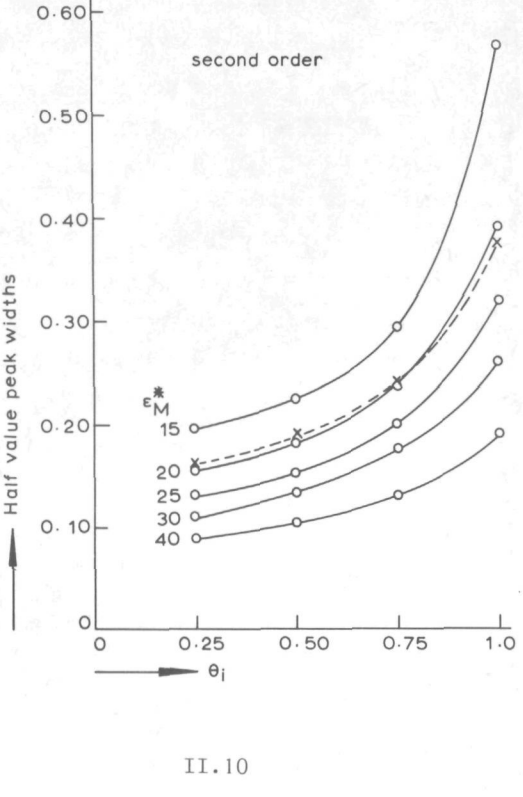

II.10

II.9 Half value peak widths for first order desorption with freely occurring readsorption as a function of initial coverage, for various values of the normalized adsorption enthalpy E_M^*
Solid lines: b = 2.5 (temperature dependent pre-exponential)
Dashed line: E_M^* = 20, b = 0 (temperature independent pre-exponential)

II.10 As figure II.9, for second order desorption

very low, and may in some cases even be overlooked.

II.6 Analysis of a desorption spectrum

This section deals with the application of the derived method in the analysis of the different peaks in an experimental desorption spectrum.

In general, one single desorption spectrum does not yield all the information needed for a thorough analysis. So, several adsorption/desorption runs have to be carried out, preferably with various initial coverages. It has been shown in section (II.5.2) that in case the readsorption is inhibited, the peak width is independent of the initial coverage. If readsorption can occur, the peak width does depend on the initial coverage, the dependence being more pronounced in the second order case. Moreover, second order peaks are broader than those arising from first order desorption. So, two or three desorption runs, starting at different initial coverages, enable us to determine unambiguously the type of desorption kinetics the peak is caused by (first or second order, readsorption or not). Now that the desorption order is known, fig.(II.8), (II.9) or (II.10) can be used for a determination of E_d or ΔH.

The value of E_d or ΔH can also be found with the aid of the appropriate $\ln(T_M)$-formula in section (I.7.3.1). Therefore, an estimate of the values of B and b will be necessary. It has been shown in section (II.2) that the influence of a temperature dependent preexponential on the estimate of E_d or ΔH is only marginal (< 10%), so that for the present purpose, b may be assumed to be zero. As for an estimate of B(= $\exp(\Delta S/R)$, if b=0) it should be kept in mind that the loss of entropy on adsorption (= the gain of entropy on desorption) is larger for higher heats of adsorption.

In case of second order desorption with and without readsorption (and of first order desorption with readsorption) the value of T_M indirectly depends on θ_i, via the θ_i-dependence of θ_M (eqs. (A.2.1), (B.1.1) and (B.2.1)). Cvetonovic and Amenomiya (8) showed the effect to be small for case (B.1). The effect will be somewhat more pronounced for the second order cases. The equations cited show, however, that the effect is not unique for second order desorption kinetics, so that it cannot be used as a criterion for second order desorption, as has been proposed (2,3).

Since the derived peak widths and the $\ln(T_M)$ formulae stem from the same model, their application on a desorption peak should yield the same value for E_d, or ΔH. A small difference can be accounted for by the choice of B. A large difference in the E_d- or ΔH-values found via both methods points to the inapplicability of our model. This may be caused by:

- diffusion limitation
- coverage dependent heat of adsorption or desorption activation energy
- the presence of a shoulder on the desorption peak studied.

Diffusion limitation has been dealt with theoretically by Cvetanovic and Amenomiya (8) for case (A.1). The value of T_M appears to be somewhat higher than when diffision is absent. The effect on the peak width is a small increase. The latter result can be understood as follows. According to their assumption, the transport of the desorbing gas is fully governed by the diffusion phenomenon:

$$V_D = \pi r^2 D \frac{dC}{dz} \quad , \qquad \text{(II.11)}$$

where r is the pore radius, and z is the position parameter along the axis of the pore. D is the effective diffusion coefficient. The concentration inside the pore, C, is governed by the desorption process. If we deal with first order desorption without readsorption, C is given by:

$$C = K.\theta \quad , \tag{II.12}$$

where K is a combination of several constants. This leads to the equation (ref.(8)):

$$\ln C_n = x - I_{(2)} \tag{II.13}$$

$$I_{(2)} = \int_o^x \frac{e^x}{(1-x/E_M)^{(2+\alpha)}}\, dx$$

with $0<\alpha\leq 0.5$

So, the effect on the peak shape is comparable with the effect of a temperature dependent preexponential, but less pronounced (see for comparison eq. (A.1.4)). As α will not exceed 0.5, the effect of diffusion control will be negligible.

The problem caused by a coverage dependent heat of adsorption has been dealt with in section (I.8), together with the approach required in such case.

If a second peak exhibits itself as a shoulder on the main peak, there are several effects to be noticed:
- the peak width suggests a lower value for ΔH or E_d than is found with the $\ln(T_M)$ formula.
- the value of θ_M/θ_i is much higher (or lower) than is to be expected theoretically.

The position of the peak maximum can be used for the determination of the theoretical shape of the main peak, as will

be described below. Afterwards, the shoulder can be isolated.

So far, only the position of the peak maximum and the half value peak width have been used. The values of θ_i and E_M thus found can be used to compute the theoretical line shape in the way described in section (II.4). Comparison of this theoretical line shape with the one obtained experimentally yields information about the applicability of the model, the correctness of the estimated E_M-value, etc.

A more satisfactory approach may be the following. In principle, the detected concentration of desorbing gas results from the net desorption, governed by kinetic and thermodynamic properties of the system. This is reflected by the equations, reconsidered below.

A.1 $$C = \frac{V_s v_m}{F} \cdot A \exp\left(\frac{-E_d}{RT}\right) \theta \qquad (I.7)$$

B.1 $$C = A^* \exp\left(\frac{-\Delta H}{RT}\right) \frac{\theta}{(1-\theta)} \qquad (I.16)$$

A.2 $$C = \frac{V_s v_m}{F} A \exp\left(\frac{-E_d}{RT}\right) \theta^2 \qquad (I.29)$$

B.2 $$C = A^* \exp\left(\frac{-\Delta H}{RT}\right) \frac{\theta^2}{(1-\theta)^2} \qquad (I.35)$$

Using $A = B.T^b$ and writing the equation in the logarithmic form we obtain:

A.1 $$\ln(C_n) - \ln(\theta) - b \ln(T) = \ln\left(\frac{V_s v_m}{F C_M}\right) + \ln(B) - \frac{E_d}{R} \cdot \frac{1}{T} \qquad (II.14)$$

B.1 $$\ln(C_n) - \ln\left\{\frac{\theta}{(1-\theta)}\right\} - b \ln(T) = \ln\left(\frac{B}{C_M}\right) - \frac{\Delta H}{R} \cdot \frac{1}{T} \qquad (II.15)$$

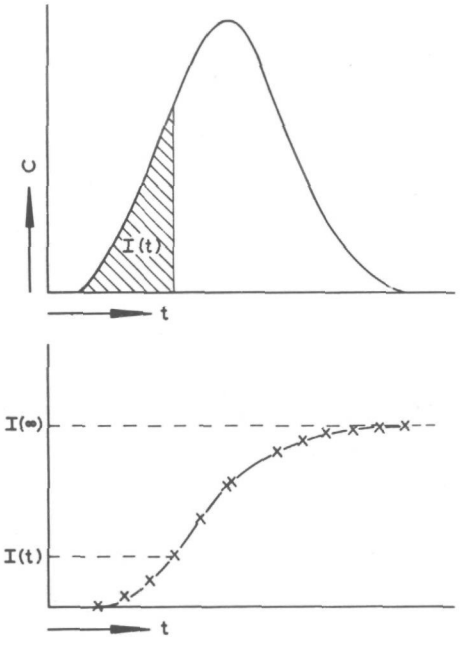

II.11 Concentration of the desorbing gas, and the integrated peak area, both as a function of time

The integrated peak area is used in computing the fractional coverage as a function of time, using the equation:

$$\theta(t) = \frac{I(\infty) - I(t)}{I(\infty)} \cdot \theta_i$$

$$\text{A.2}\quad \ln(C_n)-\ln(\theta^2)-b\ln(T) = \ln\left(\frac{V_s V_m}{FC_M}\right)+\ln(B)-\frac{E_d}{R}\cdot\frac{1}{T} \qquad \text{(II.16)}$$

$$\text{B.2}\quad \ln(C_n)-\ln\frac{\theta^2}{(1-\theta)^2}-b\ln(T)= \ln\left(\frac{B}{C_M}\right) - \frac{\Delta H}{R}\cdot\frac{1}{T} \qquad \text{(II.17)}$$

A plot of the left hand side of the equation vs. $^1/T$ should yield a straight line, from the slope of which E_d or ΔH can be determined. The intercept yields the value of B. The factor b is an adjustable parameter, the value of which is to be chosen as to give the best straight line.

Knowledge of θ as a function of temperature, or as a function of time, is necessary for application of the method described above. This function can be obtained by continuous analogue integration of the signal which is proportional with the concentration C (i.e. the katharometer signal, compare section (IV.2)); see fig.(II.11).

$$I(\infty) = \int_0^\infty C\,dt \equiv \theta_i \qquad \text{(II.18)}$$

$$I(t) = \int_0^t C\,dt \equiv \theta_i - \theta(t) \qquad \text{(II.19)}$$

$$\theta(t) = \frac{I(\infty) - I(t)}{I(\infty)} \qquad \text{(II.20)}$$

So, a desorption peak can be described as a family of sets of values for C_n, θ, and T. When plotted according to the appropriate equation, the straight line obtained yields E_d, or ΔH, and B by its slope and intercept, respectively. The correlation can be improved by an appropriate choice of the factor b.

In principle, peaks of nearly any form can be forced into a straight line by the method described above. One should be very careful, therefore, when applying this

method. The parameters derived should have physical significance. The heat of adsorption has to agree with the value obtained by the $\ln(T_M)$ formula. Moreover, the values of B and b are related to the value of ΔH. A high heat of adsorption predicts a high adsorption entropy, and a high value of b.
However, if all necessary care is taken, TPD can be used fruitfully in the exploration of the nature of chemisorption, as will be described in chapter IV.

Summarizing, the procedure is as follows:

- The peak width, and its dependence on θ_i, are used for determining the order of the description reaction, and for an estimate of E_M.
- The position of the peak maximum independently yields an estimate of E_M, which is to be compared with the value, determined by the peak width.
- Estimated values of E_M and θ_i are used for a calculation of the theoretical peak shape, or the experimental peak shape is compared with a family of theoretical peaks from the file.
- A logarithmic plot provides us with E_M and A ($= BT^b$).

We wish to stress the fact, that the final analysis uses the whole peak shape, which is a combination of a nearly infinite number of measurements of desorption rates. The normalized peak shape is independent of the position of the peak maximum, so they independently yield information about the desired kinetic parameters. We did already outline the limits of the validity of our model. The use of the peak shape, rather than merely the position of the maximum, provides us with a reliable criterion if application of the model is justified.

References

1. Konvalinka, J.A., Scholten, J.J.F.,
J. Catal., in press

2. Redhead, P.A., Vacuum, 12 (1962) 203

3. Carter, G., Vacuum, 12 (1962) 245

4. Ehrlich, G., Advan. Catal., 14 (1963) 255

5. Smutek, M., Cerny, S., Buzek, F.,
Advan. Catal., 24 (1975) 343

6. Yakerson, V.I., Rozanov, V.V., Rubinsthein, A.M.,
Surf. Sci., 12 (1968) 221

7. Edwards Jr., D., Surf. Sci., 54 (1976) 1

8. Cvetanovic, R.J., Amenomiya, Y.,
Advan. Catal., 17 (1967) 103

Chapter III

The platinum - iridium system

III.1 The phase-diagram

Platinum and iridium, both members of the eighth group of the third transition series, are neighbours in the periodic table of the elements (fig. III.1).

Both metals crystallize in a face centered cubic (fcc) lattice, the lattice constant for platinum being 391.6 pm, and for iridium 383.1 pm (3). On this basis, one would expect both metals to be miscible in any ratio. Indeed, unbroken series of solid solutions have been reported by several investigators (1). The observed age hardening effects, firstly attributed to ordering at temperatures below 1200K, appeared to result from the existence of a miscibility gap below 1250K (2) (fig. III.2).

The very sluggish rates of precipitation make an unambiguous determination of the exact position of the miscibility gap very difficult. In X-ray diffraction the demixing at 10% - 20% iridium is not observable at all. This is ascribed to the small difference in lattice constant between both phases, and the small amount of iridium-rich phase that is to be expected.

Now that the existence of a miscibility gap has been established convincingly, the question arises why the two metals, being so closely related, show such a large miscibility gap. Raub (3) suggested a relationship between the difference in the melting points of two fcc platinum metals

	IIIB	IVB	VB	VIB	VIIB	VIII	VIII	VIII	IB
4th period	Sc	Ti	V	Cr	Mn	Fe	Co	Ni	Cu
5th period	Y	Zr	Nb	Mo	Tc	Ru	Rh	Pd	Ag
6th period	La	Hf	Ta	W	Re	Os	Ir	Pt	Au

III.1 Part of the periodic table of the elements, showing the three transition series and the neighbouring I b - metals

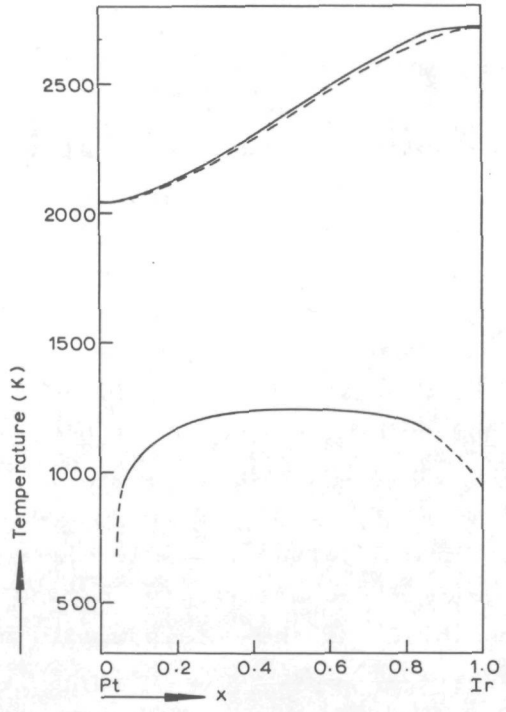

III.2 Phase diagram for the platinum-iridium system, showing a miscibility gap below T = 1248 K; after Raub and Plate (2)

on the one hand, and the critical temperature of the miscibility gap of the corresponding binary system on the other. In this way, the question is transposed to the nature of the chemical bond in transition metals. Fig.III.3 shows the melting point of a transition metal to be closely related to the number of d-electrons. Pauling (14) introduced the concept of the "percentage d-character" of the metallic bond. This quantity refers to the degree of participation of d-orbitals in the metallic bond, and is a measure of its strength, i.e. the higher the percentage d-character, the greater the bond strength.

III.2 Intermetallic interaction

III.2.1 Pauling's approach

According to Pauling's concept, transition metals will form stable alloys if the bond between dissimilar atoms has a higher percentage d-character than A-A and B-B bonds. This will in general be the case if a metal from the left hand side of a transition series is mixed with a metal from the right hand side. If both metals stem from the same region of the transition series, it is not likely that d-character is gained by breaking bonds between similar atoms and forming bonds between dissimilar atoms. If the bonds in both metals differ appreciably in d-character, i.e. if both metals have an appreciable difference in melting point, gain in d-character by forming dissimilar bonds is not possible, and the metals will show limited mutual solubility.

Raub's rule for the critical temperatures of the miscibility gaps for binary platinum-metal systems can be regarded as an example of the d-character concept of

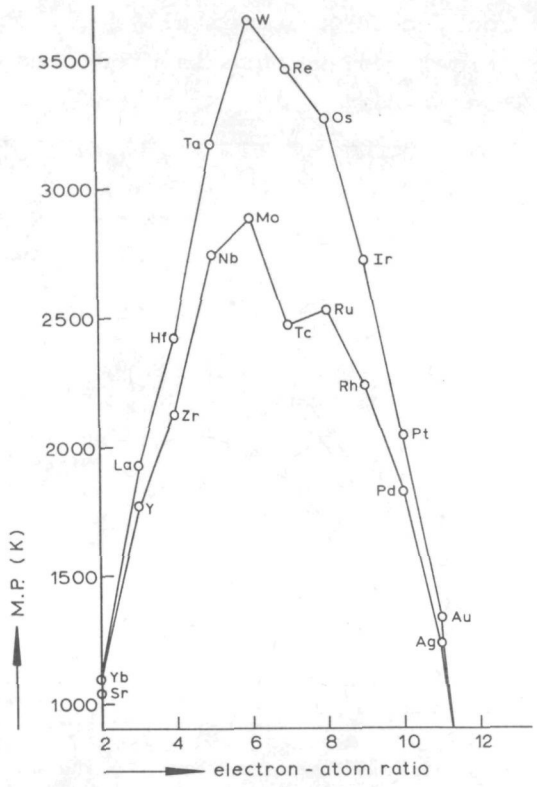

II.3 Melting points of transition metals as a function of the number of atoms in excess of the inert gas configuration.
Lower line : second transition series
Upper line : third transition series

Pauling. It should be emphasized here that this rule only applies for binary combinations of Pt, Pd, Rh, and Ir, and that even within this limited number of systems the predicted miscibility gaps for Rh-Pt and Rh-Ir have never been confirmed experimentally, although in the latter case the critical temperature is predicted to be as high as 1100K (3).

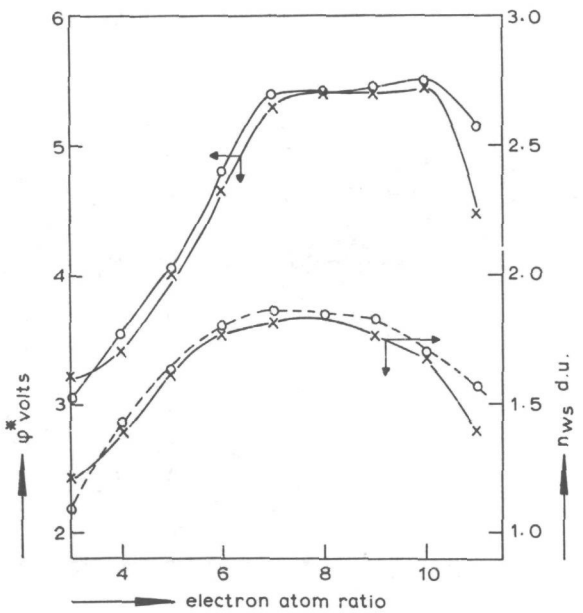

III.4 The electronegativity parameter, φ^*, and the electron density parameter, n_{WS}, for various transition metals, as a function of the number of electrons in excess of the inert gas configuration; after Miedema et al.(6)
X second transition series
O third transition series

III.2 The Engel-Brewer approach

According to the model developed by Engel and Brewer, considerable increase in bond strength is achieved when the early transition metals (Ti, Ir, Hf, etc.) are alloyed with the latter transition metals (Pd,Rh,Ir,Pt,etc.) as a result of the d-orbitals (4,5). This is consistent with fig.III.3,

in which the number of unpaired d-electrons appears to be decisive in the bond strength of transition metals.

However, the Engel-Brewer approach assumes electron transfer from the d-electron rich to the d-electron poor metal, which is in contradiction with the values of the electronegativity parameters (6) (fig. III.4). Another draw-back of the above described approach is that it is unable to explain the magnetic properties of Pd-Y, Rh-Y and Pd-Zr alloys.

III.2.3 Electronegativity and electron density

To eliminate the draw-backs of the Engel-Brewer approach, Miedema et al. propose another model (6,7), according to which Wigner-Seitz atomic cells are taken from the pure metals to form an alloy. It is assumed that the volumes of the atomic cells do not change, so that the energy effect only arises from the boundary conditions between dissimilar cells.

In the pure constituent metals, the electron density, n_{ws}, and the chemical potential for electrons, ϕ^*, will be different for each metal. The electron density discontinuity, Δn_{ws}, has to be smoothed, which leads to a positive contribution to the enthalpy of alloying. In a first approximation, this positive contribution is proportional to $(\Delta n_{ws})^2$. The difference in the chemical potential for electrons causes a charge transfer, so that the chemical potential becomes uniform throughout the alloy. This results in a negative energy-effect, proportional to $-(\Delta\phi^*)^2$.

The enthalpy of formation of a binary alloy, consisting of two transition metals, is given by

$$\Delta H = 96.48 \quad f^1(C_A,C_B)\ P\{-e(\Delta\phi^*)^2 + \frac{Q_o}{P}\ (n_{ws}^{1/3})^2\} \quad \text{(III.1)}$$

where $f^1(C_A,C_B)$ is a function of C_A and C_B that accounts for the composition dependence of ΔH,

e is the elementary charge,

$P = 0.147\ V^{-1}\ cm^{-2}\ (d.u)^{-1/3}$

$Q_o/P = 9.4\ \ eV(d.u.)^{2/3}$

$1\ d.u. = 10^2\ kg^{1/2}\ cm^{-5/2}$

The electronegativity parameter, ϕ^*, is expressed in Volts, the charge density, n_{ws}, in d.u., so that the enthalpy is obtained in eV per molecule. The factor 96.48 converts it to kJ $mole^{-1}$.

It is assumed that the chemical potential for electrons, ϕ^*, is closely related to the electronic work function, ϕ_{exp}, of the metal. At first, ϕ^* was assumed to be equal to ϕ_{exp}. Later on in the analysis, the authors use ϕ^* as a "best fit" parameter, though only slightly different from ϕ_{exp}. This procedure illustrates the semi-empirical character of the method.

For an estimate of n_{ws}, the relation between the charge density and the bulk modulus B, i.e. $(n_{ws})^2 = B/V_m$ (V_m = molar volume), has been used. Though this equation may hold for alkaline metals, it certainly will not for transition metals.

The model predicts electronic charge transfer from metals like Y and Zr (ϕ^* = 3.20 and 3.40 V, respectively) to the Rh or Pd atoms (ϕ^*= 5.40 and 5.60 V, resp.), thus reducing the number of Y and Zr d-electrons and filling the Rh and Pd d-levels. Strong experimental support for

this model is the correct prediction of the magnetic properties of Pd-Y, Rh-Y and Pd-Zr alloys. Mössbauer isomeric shifts and Knight shifts, on the contrary, show a behaviour that is appreciably different from predictions on the basis of the Miedema model. These experiments, as cited by Clarke (15), on the systems Pd-Ag, Pt-Sn, Ag-Au, Au-Sn, Pt-Co, Pt-Fe, and Pt-Ni, strongly suggest the following picture: there is a charge transfer by conduction-electron shift (s-electron shift) towards the more electronegative element, which is compensated by a d-electron transfer in opposite direction, so that the Pauling electronegativity principle is maintained.

In our opinion, however, the Miedema model correctly considers the competition between difference in electronegativity ($\Delta\phi^*$) and difference in charge density (Δn_{ws}) as the principle criterion for alloy formation. Group VIII metals have virtually the same electronegativity value, whereas the charge density differs significantly (fig. III.4). Thus, binary group VIII systems are expected to show limited mutual solubility.

The derivation of the composition dependent function $f^1(C_A,C_B)$ is based upon a regular solution model (8), with a correction for ordered structures (6). In case that the model predicts a positive enthalpy of formation, demixing and clustering is likely to occur in the binary system, and the regular solution model does not apply any more. If the Miedema model is to be used for an estimate of the critical temperature of miscibility, only qualitative agreement is to be expected. In table III.1 we compare our estimated critical temperatures for the system Pt-Ir and related systems with those obtained by Raub on the basis of the difference in melting point (3), and with the experimental values, where available.

Table III.1

	ϕ^*(Volts)	n_{ws}(d.u.)
Rh	5.40	1.76
Pd	5.45	1.67
Ir	5.55	1.83
Pt	5.65	1.78

Table III.1.a Values for the chemical potential for electrons (ϕ^*) and for the charge density (n_{ws}) of some group VIII metals, as reported by Miedema et al. (6,7)

System	T_c a)	T_c b)	T_c c)
Pd-Ir	6619	-	1749
Pt-Ir	89	-	1248
Pd-Rh	487	-	1103
Ir-Rh	156	1150	-
Pd-Pt	488	1050	-
Pt-Rh	<0	1040	-

Table III.1.b Critical temperatures of miscibility, in Kelvin

a) Computed with eq.(III.1), values of ϕ^* and n_{ws} after Miedema et al. (6,7), see above

b) Estimated by Raub (3), on basis of difference in melting point

c) Experimental values, reported by Raub

Table III.1 Theoretical and experimental values of critical temperatures of miscibility for some group VIII binary systems.

Summarizing, we obtain, apart from the correct prediction of heats of formation for exothermic ($\Delta H<0$) alloys and compounds, the following credit points for the Miedema cellular approach:

- a theoretical basis for the miscibility gaps in binary group VIII alloy systems,
- a correct qualitative prediction of the critical temperatures of these miscibility gaps.

III.3 Thermodynamics

Recently, thermodynamic data on the Pt-Ir system have become available from the work done by Ramakrishnan and Chandrasekharaiah (9). They measured the activity of iridium in Pt-Ir alloys, using the volatility of IrO_3, at 1568K and at 1518K. The authors were aware of the effect surface depletion may have on their results. They neglected, however, the possibility of enrichment of the surface in one of the two constituents under an oxygen atmosphere. This effect may have caused the measured IrO_3-pressures to be somewhat too high, since the Ir-O bond is stronger than the Pt-O bond (10) (c.f. section III.4). We expect this error to be small, the contact time of oxygen being in the order of 20 s.

From the thus measured activities, the authors derive the free enthalpy of mixing for different alloy compositions. Its temperature dependence can be used in calculating the enthalpy and the entropy of mixing, according to the equation:

$$\Delta G(x) = \Delta H(x) - T\,\Delta S(x) \qquad \text{(III.2)}$$

where x is the atomic fraction of iridium.
The results are collected in table III.2.

The values of $\Delta H(x)$ and $\Delta S(x)$ thus obtained can be used in the same equation to derive $\Delta G(x)$ for different temperatures. In doing so, it has been assumed implicitly, that $\Delta S(x)$ and $\Delta H(x)$ are independent of temperature, i.e., it was assumed that:

$$C_{p,alloy} = x\, C_{p,Ir} + (1-x)\, C_{p,Pt} \qquad \text{(III.3)}$$

$$\Delta C_p = 0$$

(C_p is the specific heat capacity at constant pressure)

Iridium and platinum are both non-ferromagnetic, and their respective $C_p(T)$-curves show a "normal" behaviour (11). Moreover, the C_p-values for Ir and for Pt are virtually the same. So, extension of the observed thermodynamic properties to lower temperatures seems justified. The results are presented in table III.3.

If the alloy is an ideal solid solution, the enthalpy and the entropy of formation are given by:

$$\Delta H_{ideal} = 0 \qquad \text{(III.5)}$$

$$\Delta S_{ideal}(x) = -R\,[\, x \ln(x) + (1-x) \ln(1-x)] \qquad \text{(III.6)}$$

In non-ideal cases, the equation for $G(x)$ reads (8):

$$\Delta G(x) = x(1-x)\Omega + RT[x\ln(x) + (1-x)\ln(1-x)] \qquad \text{(III.7)}$$

At constant temperature, the interaction parameter Ω is either a constant or a smooth function of x.

As very dilute alloys behave ideally, it follows from eqs. (III.2) and (III.6) that for both ideal and non-ideal solid solutions the following equations can be derived:

x	ΔG(x) J.mol^{-1}		ΔH(x)	ΔS(x)
	T= 1468K	T= 1518K	J.mol^{-1}	J.mol^{-1}K^{-1}
0.101	- 3778	- 4000	2732	4.435
0.124	- 4360	- 4515	799	3.515
0.162	- 5071	- 5293	1439	4.435
0.243	- 6004	- 6029	-5268	0.502
0.333	- 5766	- 6071	3201	6.109
0.458	- 5297	- 5849	10920	11.046
0.585	- 4494	- 5301	19213	16.150

Table (III.2)

Free enthalpies of mixing at different temperatures, and the derived enthalpies and entropies of mixing, after (9)

	ΔG(x) J.mol^{-1}						
x	T=300	T=500	T=600	T= 700	T=1000	T=1200	T=1300
0.101	1402	515	71	-372	-1703	-2590	-3033
0.124	-255	-958	-1310	-1661	-2715	-3418	-3770
0.162	109	-778	-1222	-1665	-2996	-3883	-4323
0.243	-5418	-5519	-5569	-5619	-5770	-5870	-5920
0.333	1368	146	-464	-1075	-2908	-2874	-4740
0.458	7607	16443	4293	3188	-126	-2335	-3439
0.585	14368	11138	9523	7908	3063	-167	-1782

Table (III.3)

Free enthalpies of mixing, calculated for different temperatures (in Kelvin)

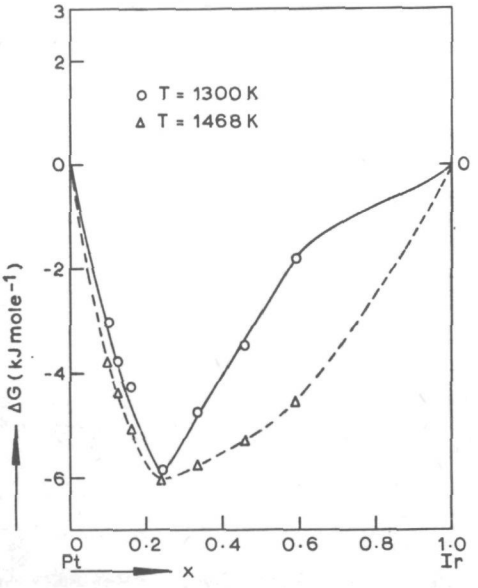

III.5 The free enthalpy of mixing for the Pt-Ir system, at 1468 K (after lit. (9), and at 1300 K (extrapolated from data, reported in lit. (9)).

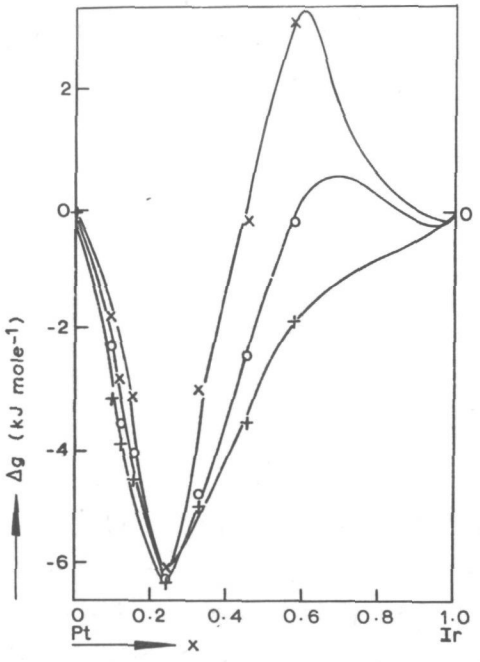

III.6 As fig. III.5, for lower temperatures, indicating a miscibility gap below 1300 K
× T = 1000 K; O T = 1200 K;
+ T = 1300 K

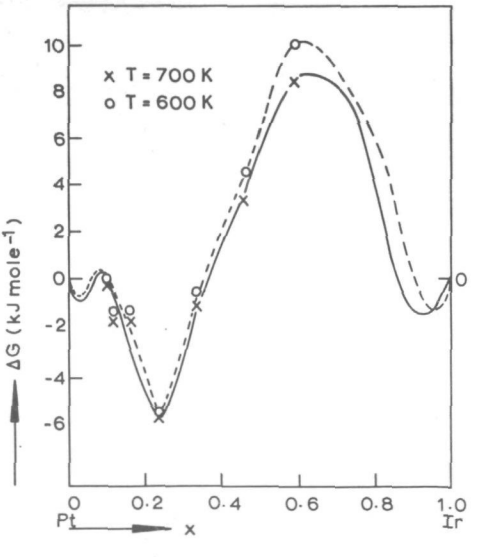

III.7 As figure III.5 and III.6, for still lower temperatures, suggesting a saturation boundary near x = = 0.05, and compound formation near x = 0.25

$$\lim_{x \to 0} \frac{d(\Delta G(x))}{dx} = - \infty \qquad \text{(III.8)}$$

$$\lim_{x \to 1} \frac{d(\Delta G(x))}{dx} = + \infty \qquad \text{(III.9)}$$

These features should be kept in mind when constructing $\Delta G(x)$ plots from the available data. Some of these plots are presented in figs. III.5 to III.7.

It is seen from fig. III.5 that at $T \geq 1300K$, platinum and iridium are miscible in any ratio, and a complete series of solid solutions is obtained. However, the asymmetrical shape of the curves suggests the inapplicability of simple solution models, such as the regular solution model, or the quasi-chemical one. In fact, the minimum value for $\Delta G(x)$ being at $x \approx 0.25$ might suggest a compound Pt_3Ir to be favoured thermodynamically. The large negative value of $\Delta H(0.25)$ may also point into this direction. Moreover, $\Delta S(0.25)$ appears to be very low, as compared with the value of 4.7 J $mole^{-1}$ K^{-1}, that should be found for ideal solid solutions (c.f. table III.2). So, the possibility of short range ordering near $x = 0.25$ may not be excluded.

In fig. III.6, it is seen that the minimum at $x = 0.25$ is also found for lower temperatures. Below 1200K, $\Delta G(x)$ is positive for $x > 0.6$, and, because of eq. (III.9), a second minimum is found for $x = x_2$, with x_2 near 1.0. For compositions $0.25 < x < x_2$, there will be segregation into two phases, the compositions of which being $x = 0.25$ and $x = x_2$, respectively. It is seen that the critical temperature of the miscibility gap lies between 1200K and 1300K, in remarkable agreement with the value of 1250K,

reported by Raub and Plate (2).

At still lower temperatures ($T \lesssim 700K$), positive values of $\Delta G(x)$ are found for $x \gtrsim 0.1$. Now, because of eq.(III.8), a third minimum at $x = x_3 \approx 0.05$ is to be expected. It is true, however, that extrapolation of thermodynamic data, measured near 1500K, to temperatures as low as 600K, may not be justified. It is also true, that this third minimum results, in fact, from only one activity measurement at $x = 0.1$, which might be in error. However, the data reported by Raub and Plate do not seem unambiguous either, especially with respect to extrapolation to lower temperatures. On the basis of the available thermodynamic data, three different phase diagrams for the Pt-Ir system can be postulated:

1. The phase diagram proposed by Raub and Plate (fig.III.2) is correct. So, the minimum in $\Delta H(x)$, observed by Ramakrishnan and Chandrasekharaiah at $x = 0.25$, should shift to a value of x as low as 0.07 for T falling from 1468K to 975K. So, extrapolation of the thermodynamic properties appears to be not justified, and one should only be content that the thermodynamic data of the latter authors correctly predict the critical temperature of miscibility to be between 1200K and 1300K. The question remains, however, why phase separation has not been observed by X-ray diffraction for $x = 0.10$ and for $x = 0.20$ (2).
2. There is a miscibility gap which has its critical temperature at 1250K, and its composition boundaries at $x = 0.25$ and $x \gtrsim 0.99$. This phase diagram will not be able to explain the observed age hardening, nor the change in specific resistivity, for $x = 0.10$ and for $x = 0.20$. Support for this model is yielded by the X-ray

diffraction experiments by Raub and Plate, which suggest a lattice constant for the platinum-rich phase that is compatible with a composition $Pt_{0.75}\ Ir_{0.25}$ (or with a composition $Pt_{0,81}\ Ir_{0.19}$, if only the sharp diffraction lines are taken into account). This model disregards the minimum near $x = 0.05$ in the $\Delta G(x)$-curves for $T \lesssim 700K$.

3. The phase diagram exhibits a miscibility boundary at $x \approx 0.05$, an ordered compound Pt_3Ir, and a second miscibility boundary at $x \approx 0.99$. So, for $0.05 < x < 0.25$, segragation is expected to take place into a phase with composition $Pt_{0.95}\ Ir_{0.05}$, and into an ordered compound Pt_3Ir. For $0.25 < x < 0.99$, the phase diagram predicts segregation into Pt_3Ir and into $Pt_{0.01}\ Ir_{0.99}$. This model nicely explains the observed phenomena with respect to age hardening and specific electric resistivity. It also gives merit to the minimum at $x = 0.05$ in fig. III.7. The fact that phase segregation cannot be observed by X-ray diffraction techniques can be understood as well. The lattice constant of the ordered compound Pt_3Ir will be somewhat higher than the one observed at higher temperatures for the disordered solid solution $Pt_{0.75}Ir_{0.25}$. The former lattice constant is equal to the one for the solid solution $Pt_{0,80}Ir_{0.20}$, which differs very little from the value for $Pt_{0.95}Ir_{0.05}$ (only 1 pm), so that phase separation cannot be observed in X-ray. It has already been mentioned that the observed lattice constants suggest a platinum rich phase with composition $Pt_{0.80}Ir_{0.20}$, rather than $Pt_{0.95}Ir_{0.05}$.

It should be noted that the latter postulated phase diagram is not in contradiction with postulate number 1, but is merely a refinement of it. It is true, that the current theories on transition metal alloys do not predict

compound formation in the Pt-Ir system (4-7, 12), but they do not predict a critical temperature as high as 1250K either (7,13). Moreover, there is some evidence for compound formation in related binary systems, like Ni_3Co, Pt_3Co, Pt_3Rh, and Ni_3Pt (1).

Summarizing, we conclude that the available theories are not able to give a correct description of the platinum-iridium binary system. Though the mutual miscibility of the two metals is limited, there is some evidence for the existence of an ordered compound Pt_3Ir.

III.4 Surface composition

For catalytic activity, it is not just the (bulk) alloy composition that counts, but merely the composition of the outer atomic layer of the alloy particles, usually referred to as the surface composition.

In general, the surface composition differs from the overall alloy composition. Qualitatively, this can be understood as follows. The creation of a surface introduces a positive contribution to the free energy of the system, because of the incomplete coordination of the atoms at the surface. This effect can be minimized by filling the surface planes preferentially with atoms of the constituent which has the lowest surface free energy (i.e. the lowest heat of atomization). If the constituent atoms have a large difference in atomic radius, there is a tendency for the surface to be enriched in the element having the larger atomic radius. It should be noted that these effects may cause surface enrichments of opposite sign. In the case of Au-Cu, they are believed to cancel each other (16). In the case of Pt-Ir, where the atomic radii of the con-

stituents hardly differ, the effect caused by strain will not play a role, so that only the effect due to difference in heat of atomization should be taken into account.

III.4.1 Difference in heat of atomization

The effect different heats of atomization have on the composition of the surface has been dealt with by several authors (17-19). Their theories are based upon the regular solution model for alloys (8), and apply for disordered solid solutions.
The theoretical predictions are plausible:

- sites with a low coordination number are enriched in the constituent having the lowest heat of atomization
- the degree of enrichment increases with decreasing coordination number of the site
  (enrichment: corners > edges > planes)
- the degree of enrichment decreases with increasing temperature (the enriched surface has a lower entropy than a surface with a statistically more probable composition).

The same principles also apply for binary systems exhibiting a miscibility gap, and also for systems forming ordered compounds.

If the binary system shows a miscibility gap, phase separation is expected to occur in such a way that the sum of the free energy of the created interface and that of the surface is minimal. In general, this requirement leads to the so-called "cherry-model", as introduced by Sachtler and co-workers (20-23). The phase which is richest in the more volatile constituent envelops a kernel, consisting of the phase which is richer in the element having the higher heat of atomization. For the surface of the

outer phase, the above mentioned rules for disordered solutions apply, so that the surface of the particle is enriched in the more volatile component, relative to the volatile-rich phase. A consequence of this model is, that the surface composition of the particle remains constant over an appreciable range of alloy compositions (fig.III.8).

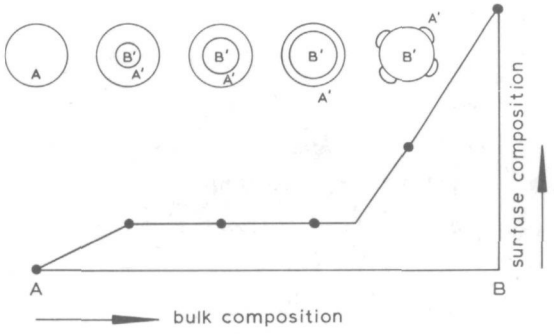

III.8 Cherry model for the surface composition of an alloy, composed of two metals with limited miscibility. The A-rich phase A' envelopes the B-rich phase B'. As a consequence, the surface composition is constant over a long range of bulk compositions

A theoretical model for the surface composition of the ordered compound Pt_3Sn has been developed by van Santen and Sachtler (24). The enrichment is assumed to take place by interchange of atoms in the surface layer with atoms in the layer just below the surface. Thus, the surface layer becomes enriched in the element with the lower heat of sublimation, while the opposite is true for the subsurface layer. As the existence of an ordered structure implies

stronger interaction between dissimilar atoms than in the case of disordered solid solutions, ordered compounds are expected to show less surface enrichment than disordered alloys do. Also, since surface enrichment means the introduction of a certain degree of disorder (i.e., a raise in entropy), the surface enrichment will decrease with decreasing temperature. For instance, the surface enrichment of the (111)-plane of Pt_3Sn is zero at very low temperatures, and 12.5% at 872K, while for a disordered solution the enrichment would be 25% at that temperature (24).

III.4.2 The influence of chemisorption

The theories discussed so far are based upon the assumption that the increase in free energy results from the creation of a solid-vacuum interface. This surface free energy can be minimized by placing the constituent having the lowest surface energy in the outer layer. A different situation, however, will be met if the alloy particle is surrounded by gases. In this case, there are two effects:

- tendency of the element with the lowest heat of atomization to migrate to the surface
- tendency of the element on which the gases in question have the highest heat of chemisorption, to migrate to the surface, in order to form as many chemisorption bonds as possible.

These effects may enhance each other, or, on the contrary, tend to cancel each other out. The system Pt-Sn, for instance, shows an appreciable surface enrichment in tin after annealing at 500°C in vacuum. This enrichment is enhanced by chemisorption of oxygen but reduced by exposition to hydrogen at 500°C (25).

III.4.3 Coke-formation

Chemisorption of hydrocarbons on the platinum metals is often accompanied by dehydrogenation of the species, resulting in the deposition of a carbonaceous residue on the surface (26). Diffusion of carbon to a considerable depth into the bulk of the metal has been observed by Schmidt and Luss in the case of Pt-Rh (27). Consequently, near the surface we deal with the ternary system Pt-Rh-C, for which the above described rules governing surface enrichment may not hold. An analogous situation is to be expected for the Pt-Ir system under reaction conditions.

III.4.4 Particle-size effect

For very small particles, the surface enrichment might be limited by the limited availibility of the atoms in which the surface is expected to be enriched (19). Moreover, small alloy particles on a carrier may exhibit a broad composition distribution, as a result of the catalyst preparation (28). In reference (28) the expected "cherry"-model is not found applicable for small silica-supported Cu-Ni particles.

Ollis (29) gives a theoretical basis for the thermodynamic stability of small particles, having a composition lying within a miscibility gap. Hoffman (30) arrives at the same result on basis of a kinetic reasoning. Ruckenstein (31) emphasizes the effect of straining of the small particle by the support, and of the configurational changes occurring in small assemblies of atoms because of their smallness. It has been argued that microcrystals of platinum metals have icosahedron symmetry, rather than the fcc structure, shown by larger crystals (32).

The arguments mentioned above show the surface

enrichment in the case of small (supported) particles to be more or less unpredictable, and to be probably less pronounced than what is expected on basis of current theories.

III.4.5 Application to the platinum-iridium system

Our present concern is, how the theories outlined above can be applied to increase our understanding of the platinum-iridium system.

The derived equations describing surface enrichment are based upon the regular solution model. It is shown in section III.3 that this model does not hold for the Pt-Ir system, so that no better than qualitative agreement with theory is to be expected. On basis of the surface energy of platinum (1.865 J m^{-2}) and that of iridium (2.250 J m^{-2}), and their respective melting points (2042K and 2716K) (10), the surface should be enriched in platinum. The miscibility gap, that is predicted by any of the three postulated phase diagrams (section III.3) suggests applicability of the cherry-model, the cherry consisting of an iridium-rich kernel, enveloped by a platinum-rich skin.

However, small alloy particles may exhibit much larger mutual miscibility than one would expect on the basis of the phase diagram, as outlined in section III.4.4. Moreover, the very sluggish rates of precipitation make undercooled solid solutions possible (2). Indeed, Raney platinum-iridium alloys, having particle sizes up to 6.5 nm, appear to consist of solid solutions in any Pt-Ir ratio (33). In such case of undercooled solid solutions, the thermodynamically favourable phase segregation will be restricted to the outermost atomic layers, where the mobility of the atoms is higher, due to the incomplete coordination.

As to the influence of chemisorption, it can be said

that the initial heat of chemisorption of hydrogen is slightly higher on platinum (34), but we do not consider a difference of 2 kcal $mole^{-1}$ to be significant (c.f. chapter IV). The chemisorption of hydrocarbons, however, is appreciably stronger on iridium (35), which might invert the surface enrichment into the direction of iridium.

Summarizing, we can say about surface enrichment in the platinum-iridium system, that:

- the theoretical equations, based on the regular solution model, do not apply
- undercooled solid solutions being likely for practical platinum-iridium catalysts, the cherry model does not apply either
- ordering, to be expected near 25% iridium, will suppress the surface enrichment as compared with the value predicted for disordered solid solutions
- under reaction conditions, the hydrocarbons present may provoke a relative enrichment in iridium, (partly) cancelling the theoretically predicted enrichment in platinum under vacuum conditions.

III.5 Catalytic activity of transition metal alloys

III.5.1 Rigid band theory

The remarkable catalytic activity of transition metals, as compared with, for instance, metals from the IB group of the periodic table (see fig. III.1), suggests an important role to be played by d-electrons in catalysis. Dowden (36) explained differences in catalytic activity from the differences in electronic structure, shown by members of a transition metal series. According to his model, catalytic reactions can be classified with respect to the kind of

chemisorbed complex that is involved (ionic or covalent). If the rate is limited by the formation of a positive ion at a metal surface, the process is most favoured and fastest when the ionisation potential of the metal and the metal work function are both large, and when the gradient of the density of states function at the Fermi-surface is large and positive. Formation of negative ions is optimum with small ionisation potentials and work functions but with an electron level density of states gradient which is large and negative. Covalent bonding requires a large density of electron levels close to the Fermi surface.

Properties like the density of states at the Fermi surface, and the density of states gradient, can be obtained experimentally or by application of the band theory of metals (37). The rigid band theory assumes that there is a common energy band for all metals of the same transition series, the filling of which is determined by the electron-atom ratio (i.e. in these considerations the number of electrons in excess of the inert-gas configuration) the metal in question possesses. (c.f. fig. III.9, and ref. (38)). This theory gives a simple explanation for the effect of alloying on catalytic activity. Addition of gold to platinum, for example, increases the electron-atom ratio, thus shifting the Fermi surface to a higher energy. It is seen from fig. III.9 that the density of states is lowered markedly. If about 60% of gold is added, the d-band is assumed to be full, and the catalytic activity should drop down considerably.

On alloying platinum with rhodium, an increase in d-band vacancies, or unpaired d-electrons, should be achieved. Mc Kee and Norton (39) found the fastest methane deuterium exchange on Pt-Rh alloys containing 60-70% Rh, corresponding with one unpaired d-electron per metal atom.

Similar arguments were used by Gray et al (40), and by Bond and Webster (41,42) in explaining optimum catalytic activity by transition metal alloys. The latter authors stress the inability of the model in explaining the activities of Pt-Pd alloys, and the impossibility to reproduce the properties of rhodium by blending equiatomic parts of ruthenium and palladium (42).

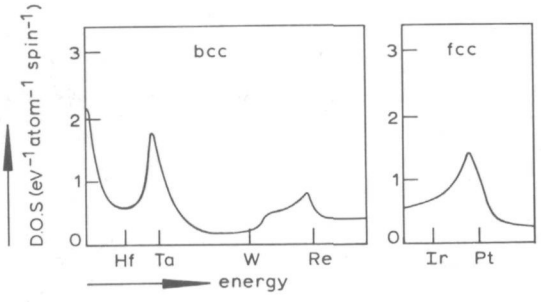

III.9 Rigid band density of states for 5 d transition metals; after lit. (38)

III.5.2 Individual surface atom concept

Describing behaviour of alloys in terms of rigid band theory implies the assumption that the individual constituent atoms become indistinguishable. Further, according to Dowden's theory, the catalytic activity is fully determined by the collective electronic properties of the crystal as a

whole. Rienäcker (43) adopts this picture in explaining the activity of alloys of Ni, Pd and Pt with Cu, Ag and Au in para-hydrogen conversion, decomposition of formic acid and hydrogenation of ethene. In the case of manganese alloys, however, the author reports the existence of localized electrons in Mn, which do not join the d-bands of the IB-metal. Other interesting features, mentioned in this paper, are a sharp drop in the activation energy of formic acid decomposition on ordered alloys, and the same effect on solid solutions having a composition near the boundary of a miscibility gap. The first effect might, according to Rienäcker, be explained by an increase in localization of the bonding electrons, resulting in a lowering of the Fermi level. The latter result might be related with the observed straining and hardening effects near a saturation boundary.

Friedel (44) showed, that the nuclear charge of an "impurity" atom in a metal lattice is screened by conduction electrons, so that the effect of the impurity is restricted to a spherical region, determined by the screening radius, R_o. For very dilute solutions, R_o only depends on $n(E_F)$, the density of states at the Fermi level. For Cu, Fe and Ni, R_o values are reported of 0.47, 0.17 and 0.11 nm, respectively. A more recent extension of the model describes screening as being concentrated close to the impurity, but with a smaller, long-range component of electron density (45). An important difference with rigid band theory is the localized nature of the influence of the solute, so that the constituent atoms retain their individuality in this model.

Chemisorption can be treated in the same way, as has been shown by Grimley (46). The existence of two groups of d-orbitals, having different symmetries (i.e. eg- and t_{2g}-

symmetry) requires the distinction of several types of chemisorption (fig. III.10). For interstitial adsorption, the analogy with solution is appropriate. It appears that pronounced changes in chemisorption take place when $n(E_F)$ and $\partial n(E)/\partial E_F$ become small and the gradient changes sign (47). A hydrogen atom, atop a metal atom, (type C) overlaps negligibly with other centres, and the interaction with d-orbitals (d_z^2) is essentially localized.

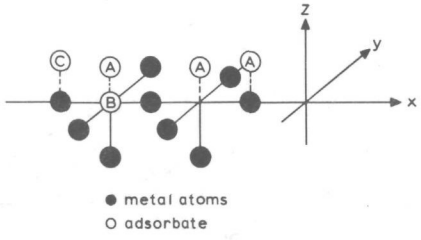

III.10 Different adsorption sites on a metal surface, having different orbital symmetry; after Dowden (47)

Combination of d_z^2 (Ni) and 1s (H) gives bonding and antibonding orbitals, respectively, below the 1s level and above E_F. If d_z^2 is initially full, then one electron must go to the lowest unfilled level, E_F, and the Ni-H surface complex will be screened like a quasi Cu-atom.

Soven (56,57) introduced the coherent potential model

of disordered substitutional alloys. The scheme is based on the idea that in metallic alloys the mean free path of an electron is relatively long, so that at every lattice site the electron experiences a coherent potential, V_o. This potential has been defined in such a way, that it only depends on the average distribution of constituent atoms. Thus, the problems arizing from the disordered nature of the alloy have been circumvented. On the basis of the coherent potential, the averaged alloy Green's function is derived. Again, the assumption is made that the alloy wave functions are sufficiently spread out, so that only the coherent part of the Green's function is to be taken into account.

An important feature of the model is, that it can be used in computing separately the contribution to the total density of states from each of the constituents. The constituent atoms appear to retain their individual character when forming alloys. In the case of Cu-Ni, for instance, the d-holes are localized on the Ni-atoms (58).

An important consequence of the atoms retaining their individuality when forming an alloy, is the possibility of "titration" of the surface atoms of one constituent by means of selective chemisorption (23,48). In alloys of a group VIII metal with a group IB metal, only the transition metal atoms are catalytically active. So, when the electronic structure of individual atoms does not vary with alloying, the effects of alloying on the catalytic activity can be explained by the dilution of active sites in an inert matrix and the relative preponderance of sites consisting of few active atoms over the larger sites (49,50). Apart from this effect, the alloy partner may also influence the electronic structure of the catalytically active metal. In the case of Pt-Sn, such effect has been reported by several authors (48,51).

If two catalytically active metals are blended, a new kind of sites may be created, consisting of both types of atoms. The catalytic activity of this type of sites is expected to be intermediate between the activities of both constituents. If the atoms of one of the constituents are selectively poisoned, the atoms of the other metal form active sites, diluted in a more or less inactive matrix. However, a poison may influence the electronic structure on the active site, via the poisoned metal atom.

Summarizing, the effects can be classified as follows:

1) creation of new sites (geometric effect)
   a) by dilution of (groups of) active atoms in a more or less inactive matrix
   b) by formation of sites consisting of atoms of both constituents.
2) change in electronic structure
   a) by metal atoms surrounding the site
   b) by species adsorbed on the metal atoms surrounding the site.

Since both the geometric effect and the electronic effect may play a role simultaneously, the above scheme is only a formal one. The geometric effect is often called "ensemble effect", a term that we judge to be misleading. For the same reason we avoided use of the term "ligand-effect" for the effects mentioned under 2), because it is also erroneously used for the phenomenon depicted under 1 b).

III.5.3 Application to the platinum-iridium system

Platinum and iridium are both catalytically active in hydrocarbon conversion reactions. The available theories predict little mutual interaction, so that, on this basis, little mutual influence on the electronic structure of the metals is to be expected. Experimental thermodynamic data, however, reveal the formation of an alloy $Pt_{0.75}Ir_{0.25}$ to be appreciably exothermic (section III.3), so that in the composition range around 25% iridium a strong, electronic interaction between both metals should take place. Mössbauer isomer shifts and Knight shifts, determined for related systems, suggest s-charge transfer towards the more electronegative element (i.e. Pt), compensated by d-electron shift in opposite direction (15). The result would be an increase in the density of states at the Fermi level, if the rigid band theory holds for the Pt-Ir system (c.f. fig. III.9). According to Gautier (52), the rigid band theory can still be used if the difference in electronic band energy of the two constituents is considerably less than the width of the band in question, which is certainly the case for the d-bands of platinum and iridium (55). Velicky et al. (53), however, show that the coherent potential approximation (CPA) also in such case yields a better description of reality. Qualitatively, the latter approximation leads to the same result, i.e. an increase of the density of states at the Fermi level if platinum is alloyed with iridium (see fig. 3 of ref. (53)).

Raub and Plate (2) report an increase of the electrical resistance when iridium is added to platinum, although the specific resistance of iridium is lower than that of platinum (38). This also points to an enhancement of the density of states at the Fermi level (37,38,54).

The possible existence of an ordered structure, and the mutual influence on the electronic structure of both constituents, may have considerable effect on the catalytic activity (43). Since saturation boundaries may also exhibit enhanced catalytic activity (section III.5.2), interesting alloy compositions can be derived from the phase diagram to be $Pt_{0.95}Ir_{0.05}$, $Pt_{0.75}Ir_{0.25}$, and $Pt_{0.01}Ir_{0.99}$.

Besides the electronic effect, the geometric effect may play an important role, in producing sites having hybride Pt-Ir character. The influence of more or less selective poisoning by carbon and sulfur will be discussed in some detail in chapter V.

III.6 Summary

The three theoretical approaches of transition metal alloy formation we discussed in this chapter (i.e. the Pauling, the Engel-Brewer and the Miedema approach, respectively) have in common that they predict heats of formation for platinum-iridium alloys which are close to zero or slightly positive. The phase diagram reported by Raub and Plate (2) shows the critical temperature of miscibility to be as high as 1248K, which suggests a larger positive enthalpy of alloy-formation than is predicted by any of the three theoretical approaches.

The thermodynamically determined free energies of mixing (9), which we extrapolated to lower temperatures, show large positive values near 50% iridium. However, near 25% iridium, the $\Delta G(x)$ value is negative at all temperatures. These thermodynamic data clearly show the limited validity of the theoretical models mentioned earlier. On the basis of the $\Delta G(x)$-curves constructed by us, we postulate three possible phase-diagrams, taking the experimental results

from ref. (2) into account.

In section III.4 we discussed the current theories describing surface enrichment, and the parameters this effect is influenced by, i.e. chemisorption, coke-formation, particle-size, ordering, and the existence of undercooled solid solutions. We concluded that, though enrichment of the surface is to be expected under vacuum conditions, the surface composition under reaction conditions is subject to many unknown influences, and cannot be predicted.

In the last section, III.5, we outlined some properties of transition metal alloys which are believed to be important in catalysis. The distinction between geometric effect and electronic effect, though a rather artificial one, provides us with a basis, with aid of which we can try to understand the catalytic behaviour of alloys. On a theoretical basis, the electronic effect is expected to be small in the case of platinum-iridium. However, the thermodynamic properties cited suggest an important mutual interaction to exist in the composition range around 25% iridium.

As main results of the theoretical discussion, presented in this chapter, we mention

- the thermodynamic properties of the Pt-Ir system suggest a more complex behaviour than can be described by available theories
- phase segregation, if any, will be restricted to the outermost layers of the alloy particles
- interesting catalytic properties of Pt-Ir alloys may be expected near 5%, 25% and 99% iridium.

References

1. Hansen, M.,
"Constitution of binary alloys"
Mc-Graw-Hill, New York 1949

2. Raub, E., Plate, W.,
Z. Metallkd., 47 (1956) 688

3. Raub, E.,
J. Less-Common Met., 1 (1959) 3

4. Engel, N.,
Powder Met. Bull., 7 (1954) 8

5. Brewer, L.,
Acta Metall., 15 (1967) 553

6. Miedema, A.R., Boom, R., de Boer, F.R.,
J. Less-Common Met., 41 (1975) 283

7. Miedema, A.R.,
J. Less-Common Met., 46 (1976) 67

8. Swalin, R.A.,
"Thermodynamics of solids", 2nd edition
John Wiley & Sons, New York, 1972. p.p. 141-148

9. Ramakrishnan, E.S., Chandrasekharaiah, M.S.,
J. Less-Common Met., 37 (1974) 269

10. "Handbook of Chemistry and Physics", R.C. Weast, ed.
52nd edition. The Chemical Rubber Co., Cleveland (Ohio)
(1971)

11. Hultgren, R., Orr, R.L., Anderson, P.D., Kelley, K.K., "Selected values for the thermodynamic properties of metals and alloys" John Wiley & Sons, Inc., New York (1963)

12. Choudary, U.V., Gingerich, K.A., Cornwell, L.R., J. Less-Common Met., 50 (1976) 201

13. Kaufmann, L., Bernstein, H., "Computer calculation of phase diagrams" pp. 129,133 Academic Press, New York (1970)

14. Pauling, L., Proc. Roy. Soc. (London), A 196 (1949) 343

15. Clarke, J.K.A., Chem. Revs., 75 (1975) 291

16. van Santen, R.A., Toneman, L.H., Bouwman, R., Surf. Sci, 47 (1975) 64

17. van Santen, R.A., Boersma, M.A.M., J. Catal., 34 (1974) 13

18. Williams, F.L., Nason, D., Surf.Sci., 45 (1974) 377

19. Burton, J.J., Hyman, E., Fedak, D.G., J. Catal., 37 (1975) 106

20. Bouwman, R., Sachtler, W.M.H., J. Catal., 19 (1970) 127

21. van der Planck, P., Sachtler, W.M.H., J. Catal., 7 (1967) 300

22. Bouwman, R., Sachtler, W.M.H.,
J. Catal., 26 (1972) 63

23. Sachtler, W.M.H., Vide, 164 (1973) 67

24. van Santen, R.A., Sachtler, W.M.H.,
J. Catal., 33 (1974) 202

25. Bouwman, R., Toneman, L.H., Holscher, A.A.,
Surf. Sci., 35 (1973) 8

26. Ramaswamy, A.V., Ratnasamy, P., Sivisanker, S.,
Leonard, A.J.,
Proc. 6th. Int.Congr.Catal.,London (1976), paper B 25

27. Schmidt, L.D., Luss, D., J. Catal., 22 (1971) 269

28. Robertson, S.D., Kloet, S.C., Sachtler, W.M.H.,
J. Catal., 39 (1975) 234

29. Ollis, D.F., J. Catal., 23 (1971) 131

30. Hoffman, D.W., J. Catal., 27 (1972) 374

31. Ruckenstein, E., J. Catal., 35 (1974) 441

32. Burton, J.J., Catal.Rev.Sci.Eng., 9 (1974) 209

33. Kropotova, N.V., Semenova , A.D., Fadeeva, V.I.,
Vovchenko, G.D., Russ.J.Phys.Chem., 50 (1976) 226

34. Clark, A., "The chemisorptive bond",
Academic Press, New York - London (1974), p. 12

35. Nieuwenhuys, B.E., Hagen, D.I., Rovida, G.,
Somorjai, G.A., Surf.Sci., 59 (1976) 155

36. Dowden, D.A., J.Chem.Soc., (1950) 242

37. Mott, N.F., Jones, H., "The theory of the properties of metals and alloys", Oxford Univ.Press, London (1936)

38. Shimizu, M., in "Electronic density of states", L.H. Bennett, ed., N.B.S. Special Publication 323, Washington, D.C. (1971) p. 685

39. McKee, D.W., Norton, F.J., J.Catal., 4 (1965) 510

40. Gray, T.J., Masse, N.G., Oswin, H.G., Actes 2ième Congr.Int.Catal., Technip Paris (1961) 2, 1697

41. Bond, G.C., Webster, D.E., Plat.Met.Rev., 10 (1966) 10

42. Bond, G.C., Webster, D.E., Ann. N.Y. Acad. Sci., 158 (1969) 540

43. Rienäcker, G., Proc. 4th. Int. Congr. Catal., Moscow (1968), p. 537

44. Friedel, J., Adv. Phys., 3 (1954) 446

45. Friedel, J., Trans.Metall.Soc. A.I.M.E.,230 (1964) 616

46. Grimley, T.B., Proc.Phys.Soc., 92 (1967) 776

47. Dowden, D.A., in: "Chemisorption and catalysis", E.P. Hepple, ed., Inst. of Petroleum, London (1970),p.1

48. Verbeek, H., Sachtler, W.M.H., J.Catal.,42 (1976) 257

49. Ponec, V., Sachtler, W.M.H., J.Catal., 24 (1972) 250

50. Dessing, R.P., Thesis, Leiden (1974)

51. Karpinski, Z., Clarke, J.K.A.,
J. Chem. Soc., Faraday Trans. I., 71(1975) 893

52. Gautier, F., in: "Propriétés electroniques des métaux et alliages", Janot,ed., Masson (1973), p. 157 - 377

53. Velicky, B., Kirkpatrick, S., Ehrenreich, H., Phys. Rev., 175 (1968) 747

54. Hume-Rothery, W., "Electrons, atoms, metals and alloys", 3rd. ed., Dover Publications, Inc., New York (1963), p. 257

55. Smith, N.V., Wertheim, G.K., Hüfner, S., Traum, M.M., Phys. Rev. B., 10 (1974) 3197.

56. Soven, P., Phys.Rev., 156 (1967) 809

57. Soven, P., in "Energy bands in metals and alloys", L.H. Bennet and J.T. Waber, ed. Gordon and Breach, New York, 1967, p. 139.

58. Stocks, G.M., Williams, R.W., Faulkner, J.S., Phys. Rev., B 4 (1971) 4390.

Chapter IV

Application of the thermodesorption technique

IV.1 Introduction

In this chapter, our temperature programmed desorption (TPD) experiments are presented, and the analysis of the results is discussed.

As we wished to investigate supported metal catalysts (Pt, Pt-Ir and Ir), our apparatus is based upon the gas-chromatographic technique, described by Cvetanovic et al. (1). TPD-spectra reported by these authors (1-3) and by others (4-6) usually show a rather poor resolution of desorption peaks partially caused by non-optimum experimental conditions. For a successful application of the analysis described in chapter II, a better resolution of desorption spectra was required. So, much work has been done in order to improve peak separation. The resulting apparatus and standard experimental conditions are described in section IV.2.

In order to eliminate effects due to spill over of hydrogen from the metal to the support, and other carrier effects, a series of hydrogen desorption experiments was carried out on metal powders, prepared by the so-called Kulifay method (7). The alloys thus obtained were subjected to X-ray diffraction techniques. They appeared to be solid solutions in all compositions, so that the lattice constant can be used in determining the platinum/iridium ratio. The surface compositions of these powders were determined by Auger electron spectroscopy (AES).

The theoretically predicted surface enrichment in platinum was confirmed by this technique. Moreover, AES showed platinum to be easily contaminated with carbon, in contrast to iridium metal, which appeared to be relatively resistant to carbon poisoning.

Supported catalysts have been prepared by ion exchange, and by impregnation. Because of its importance in reforming catalysis, γ-alumina was used most frequently, but also α-alumina, activated carbon, and silica have been employed. The samples were examined by means of X-ray analysis, in order to check for alloy formation, and to determine the mean particle size of the metal crystallites. The metal content of those samples containing only Pt or Ir could be determined spectrophotometrically. The composition of some of the supported bimetallic catalysts was determined by activation analysis.

The hydrogen TPD-spectra for platinum and iridium powders are nearly identical. The main difference is the existence of two peaks in the H_2/Pt spectrum which are not found for hydrogen desorption from iridium. It will be shown in section IV.5.5 that at least one of these peaks is due to carbon-covered platinum. One of the peaks, exhibited by both metals, can be ascribed to hydrogen dissolved in the bulk of the metal.

Supported catalysts show the same peaks as the corresponding Kulifay-powders do. The relative preponderance of the peaks may however be different. This can be explained by particle-size effects. Silica and alumina supported catalysts show an additional peak, pointing to intimate interaction between metal and support (section IV.5.7).

The γ-alumina and the silica supports have been investigated by temperature programmed desorption of ethene (ethylene), and of butene (butylene). Silica appears to possess one type of acidic sites, alumina, however, two.

Even these rather large and heavy gas molecules do not show effects that could be due to diffusional limitation of the desorption process.

IV.2.1 Apparatus and procedure

The apparatus used for thermodesorption experiments is depicted in fig. IV.1.

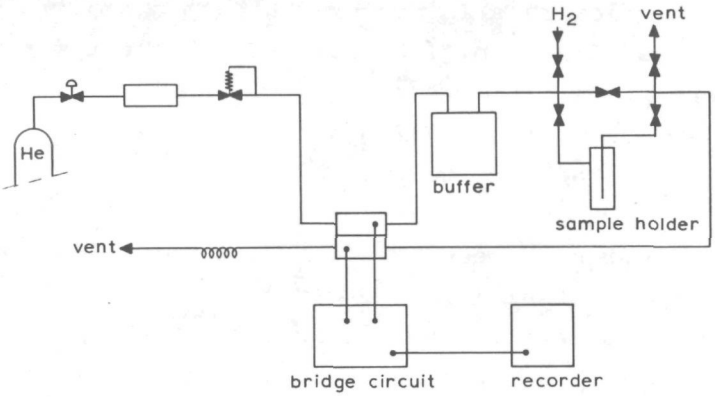

IV.1 Flow apparatus for TPD - experiments (see text)

The carrier gas, mostly helium, sometimes nitrogen, is dried over molecular sieves (Linde 3A), freed from traces of oxygen by copper on alumina (R 3-11 from B.A.S.F.), and again led over mol. sieve 3A. The initial pressure of 8 bar is reduced to 4 bar by a Dräger pressure reducer. The precision flow controller (Brooks model 8744 A) maintains a constant carrier gas flow rate (to within 1%), provided that some necessary precautions were taken to be discussed below. The carrier gas then passes through the reference part of the detection system. This consists of four Gow-Mac

thermistor cells, combined in a bridge-circuit, which is connected with a chart recorder via an amplifier. This way of detection against an on-stream reference requires equal pressure in both parts of the detection system. Therefore, a buffer volume is incorporated, to prevent pressure build-up in the sample holder as a result of the temperature rise during the desorption run. Fluctuations in the back pressure are smoothed by means of an adjustable restriction in the vent. The flow rate is measured at atmospheric pressure by means of a soap flow-meter. The whole apparatus is in stainless steel.

The sample-holder (fig. IV.2) is designed as to bring the carrier gas on the same temperature as the catalyst by external heating (or cooling), before it reaches the sample. Besides, the linear gas speed is low in the outer part of the sample holder, but high in the catalyst bed. The volume between the catalyst and the measuring cell of the detection unit is kept as small as possible, so that desorbing gas reaches the measuring cell within one second. The platinum resistance thermometer is placed in the axis of the catalyst bed. External heating causes a temperature gradient between the outer wall of the sample holder and the center of the catalyst bed, which is, however, smoothed by the carrier gas flow. For linear heating schedules, this temperature gradient appeared to be constant, so that it can be corrected for. The platinum resistance thermometer was chosen for its reliability and linearity over the whole temperature range (80 - 720 K). Thermocouples need calibration after any twenty adsorption/desorption runs.

Heating and cooling is effected externally by means of the cryostate-oven, depicted in fig. IV.3. The oven contains a thermo-coax heating coil, and a cooling coil for liquid nitrogen.

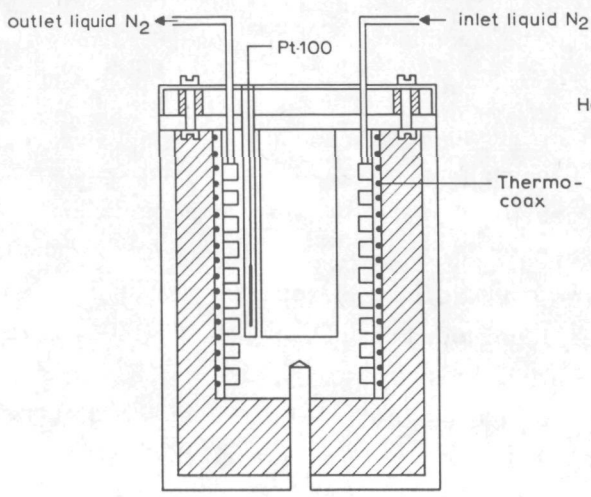

IV.2

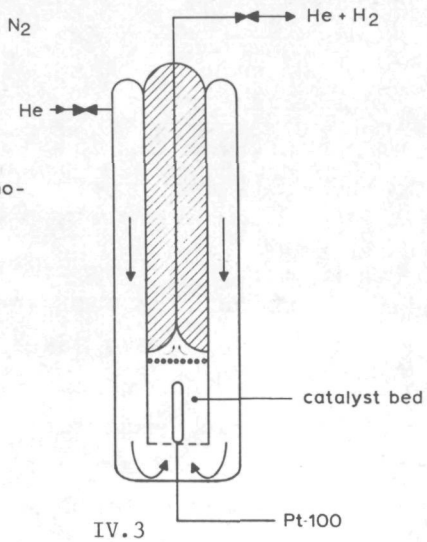

IV.3

IV.2 Cryostate / furnace combination used for heating and cooling of the sample holder in TPD - experiments

IV.3 Sample holder for TPD - experiments
The diameter of the catalyst bed is 12 mm. The height of the catalyst bed varies from about 3 mm to about 30 mm, dependent on the amount of catalyst. The latter is chosen as to make $V_s v_m \approx$ $\approx$ 2 (see list of symbols for V_s and v_m)

Heating is controlled by a Becker proportional linear temperature programmer model 753. Constant temperatures in the region 80 K to 250 K can be obtained by a liquid nitrogen cryostate of the on/off type (Cryoson, type TRL 1B).

The sample can be pretreated in situ, in hydrogen or in a helium/oxygen mixture. Adsorption of hydrogen takes place in pure hydrogen at atmospheric pressure, or by pulsing hydrogen into the carrier gas (pulse volume $\simeq$ 78.5 mm^3 NTP). Ethene and butene adsorption is done exclusively pulswise.

For most experiments the carrier gas flow F was maintained at 1.02 $\pm$ 1 cm^3 (NTP) s^{-1}, the heating rate β was 0.25 K min^{-1}, and the amount of catalyst was taken as to make $V_s v_m \approx 2$ cm^3 (NTP). For definitions see section I.3.1 and I.3.2.

IV.2.2 Materials

All gases were of high purity quality. Hydrogen was further purified by means of a palladium diffusion unit (Johnson - Matthey, type H28/1). Helium and, incidentally, nitrogen were purified in the way described above. Ethene and butene were Baker high purity gases ("Lecture-bottles").

Platinum sponge and iridium sponge were obtained from Drijfhout, Amsterdam, and manufactured by Johnson-Matthey. The main contaminant of Pt (catalogue no. J.M.C. 1010) was reported to be Pd (3 ppm), and that of Ir (catalogue no. J.M.C. 991) was Ba (5 ppm). It is interesting to note that in iridium no other platinum metals were present. In the preparation of Kulifay-powders and supported catalysts we used chloroplatinic acid (H_2PtCl_6) or "spec pure" platinum powder, and iridium dioxide ($IrO_2.xH_2O$) or sodiumchloroiridate ($Na_2IrCl_6.6H_2O$), all obtained from Johnson - Matthey. All other chemicals used in catalyst preparation were reagent grade.

IV.3.1 Catalyst preparation

IV.3.1.1 Kulifay - powders

High surface area (about 10 $m^2\ g^{-1}$) metal and alloy powders have been prepared by reduction of solutions of H_2PtCl_6 and/or H_2IrCl_6 with hydrazine ($N_2H_4.2\ HCl$), following the method proposed by Kulifay (7).

IV.3.1.2 Supported catalysts

About 5 grams of the support is stirred in 30 cm^3 of water. Chlorine is added in the form of five drops of con-

centrated HCl. A solution containing the required amounts of H_2PtCl_6 and/or H_2IrCl_6 is added dropwise. After one hour of stirring, the thick paste is dried in a porcelaine crucible at 360 K for 16 hours. The impregnated support is calcined in air at 820 - 870 K for 16 - 20 hrs.

IV.3.2 Analysis

IV.3.2.1 Composition

The concentration of both the H_2PtCl_6 and the H_2IrCl_6 solution can be determined spectrophotometrically (8,9). In both analyses, the absence of other platinum group metals is essential, so that mixtures of both metals cannot be analyzed in this way. However, the coloured complexes used in these analyses can be employed for a check on the completeness of the reduction (in the case of preparation of Kulifay-powders), or of the impregnation (when preparing supported catalysts). When the reaction is complete the overall composition is known, as one started with known amounts of dissolved platinum and iridium salts.

For some catalysts, the composition thus derived has been verified by means of activation analysis. Since these results confirmed the calculated compositions to within 2%, it is assumed that for each catalyst the metal content and the platinum/iridium ratio correspond with the amounts of dissolved transition metal salt used in the preparation.

IV.3.2.2 Particle size and alloy formation

The Kulifay-powders and a number of the supported catalysts have been subjected to X-ray diffraction. All Kulifay-powders appeared to be monophasic solid solutions,

the lattice parameters of which corresponded with the expected composition, when using the lattice constants reported by Raub and Plate (10). Moreover, the average particle diameter as obtained from X-ray line broadening (30 nm) agreed with the values derived from the BET surface area, determined for some of the samples by means of physical adsorption of methane (10 $m^2\ g^{-1}$). (Pt-powder: S_{BET} = 11.1 $m^2\ g^{-1}$, $\bar{d}_w$ (X-ray) = 26 nm; Ir-powder: S_{BET} = 9.8 $m^2\ g^{-1}$, $\bar{d}_w$ = 30 nm; Pt/Ir 50/50: S_{BET} = 9.6 $m^2\ g^{-1}$, $\bar{d}_w$ = 29 nm).

In an early stage of our research work, supported catalysts were prepared by ion exchange, rather than with the impregnation technique described in section IV.3.1.2. The ion exchange technique is based on exchange of surface protons against cations containing Pt or Ir. After exchange, the metal is obtained by careful, mild reduction, for example with methanol. The metal particles were very small (< 3 nm) but of varying composition: pure platinum, pure iridium and one or even two solid solutions in one bi-metallic catalyst.

The impregnated catalysts have rather large metal particles (ca. 30 nm), but only one solid solution is present, and unalloyed platinum or iridium cannot be detected. When investigating synergistic effects of the platinum-iridium system in catalysis, the impregnated mono-phasic catalysts are to be preferred, in spite of the larger crystallite size.

IV.3.2.3 Auger electron spectroscopy

Auger electron spectroscopy (AES)[1], carried out on some of the Kulifay-powders, confirms the high purity of the metals used, carbon and oxygen, and sometimes sulfur, being the most important contaminants.

Though this technique is known to be a tool for surface analysis, it should be noted that electrons of rather high energy (in the order of 2000 eV, 1 eV $\approx$ 1.6×10^{-19} J) have an escape depth of 2 nm, or ten atomic layers. Even electrons having an energy of 50 or 60 eV still have an escape depth of about 0.5 nm, that is two atomic layers.

The intensities of the platinum and iridium peaks in the 50 - 60 eV range have been used in determining the surface composition of the powders. It was assumed that the Auger electron yields and the back scattering factors are the same for both metals, as they are neighbours in the periodic table. The peaks near 2000 eV appear to reflect the bulk composition.

The results obtained are collected in table IV.1 and in fig. IV.4. It is seen that for iridium contents up to 50%, the surface is appreciably enriched in platinum. Surfaces of iridium-rich samples seem to be slightly enriched in iridium. This may be an artefact, caused by the method of preparation: it is known that platinum (IV) is reduced more rapidly by hydrazine than iridium (IV). So, it is possible that when all the available platinum has reacted, there is still iridium in the solution, so that

1) AES measurements have been carried out in the apparatus of the department of heterogeneous catalysis of the Gorlaeus Laboratoria in Leiden, by Dr. F.J. Kuyers. For experimental details, see: Kuyers, F.J., Thesis, Leiden (1977)

Table IV.1

Bulk composition % Ir [a]	Bulk composition (Auger) % Ir [b]	Surface Composition (Auger) % Ir [c]
12 [e]	11	5
16	15-19	6-9
20 [e]	54	66
50	50-51	70
50 [d]	63-64	90-93
85	77-79	90-93

a) Based upon the assumption of complete reduction of the transition metal salt solutions

b) Based upon the intensity ratio $I_{Ir} / (I_{Pt} + I_{Ir})$ of the Auger peaks near 2000 eV

c) Based upon the intensity ratio of the Auger peaks in the energy range 50 - 60 eV

d) Reduction of the metal salt solution with hydrazine was incomplete

e) Samples contaminated with aluminium

Table IV.1 The surface composition of Pt - Ir Kulifay-powders as a function of bulk-composition

the platinum-rich kernel is covered with a skin of pure iridium. Repeated oxygen/hydrogen treatment at 600 K will not be able to produce thermodynamic equilibrium if the iridium skin is thick, i.e. if the overall iridium content is high. It is interesting to note that, in spite of the relative enrichment in platinum, even for bulk compositions 98% Pt / 2% Ir, still some iridium ($\approx$ 1%) can be detected in the surface.

The influence of hydrocarbon chemisorption on surface composition has been investigated with the sample containing 50% iridium. Some high purity propane was admitted to the AES vacuum chamber, which was still connected with the vac - ion pumps, so that a steady state partial pressure of 8×10^{-6} Pa propane was built up. The 280 eV carbon peak showed a considerable growth, indicating that some kind of carbon-containing deposit was formed at the surface. Simultaneously, the intensities of the low-energy platinum and iridium peaks dropped markedly, but the effect is far more pronounced for platinum than for iridium (fig.IV.5). This is consistent with the Auger spectra taken from pure platinum and iridium powders, which show that platinum covers more rapidly and more extensively with carbon, and that a carbon deposit on iridium is removed far more easily by a hydrogen treatment. Heats of formation of the respective carbides (620 ± 14 kJ mole^{-1} for iridium, 610 ± 5 kJ mole^{-1} for platinum) show that chemisorption-induced surface enrichment of iridium in the alloy is a much less probable explanation for the effects caused by propane adsorption. Possibly, dehydrogenation accompanying hydrocarbon chemisorption is less on iridium as compared with platinum, or the reverse process (hydrogenation of the absorbed species) has a lower activation energy on the former metal. This will be discussed in more detail in

section V.4.3.2.

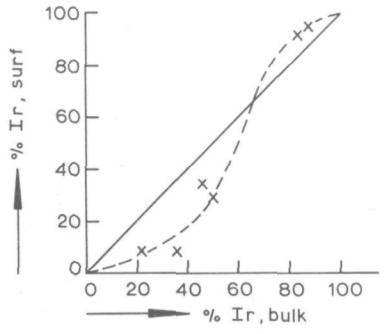

IV.4

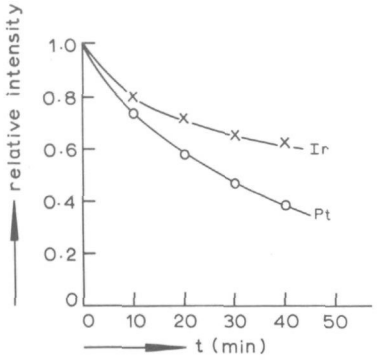

IV.5

IV.4 Surface composition versus bulk composition of Kulifay Pt-Ir powders, as determined by AES
Solid line: *theoretical curve for surface composition* = bulk composition
Dashed line : experimental curve

IV.5 Decline of the relative Ir and Pt Auger peak intensities upon exposure to propane

IV.4 Description of TPD experiments

IV.4.1 Desorption of hydrogen

IV.4.1.1 Kulifay-powders

Standard adsorption/desorption experiments with Kulifay-powders were carried out as follows. The metal powder was saturated with hydrogen at room temperature (297 K) in a hydrogen flow during five minutes. Then, the sample holder was closed, and cooled in three minutes to 80 K. At that temperature the sample was purged with helium for five minutes, during which the Gow-Mac cell signal

returned to the base-line, indicating that no more hydrogen was evolved. At this moment, the linear heating program was started (heating rate $\beta = 0.25\ K\ s^{-1}$), and the sample was heated up to 500 K. Before the first adsorption/desorption run, the sample was cleaned by repeated treatment in hydrogen and a helium/oxygen mixture (20% oxygen) at 550 K. The last treatment before a series of adsorption/desorption runs was always in hydrogen, followed by purging with helium at 620 K for at least 16 hrs. Except for the first desorption run, this procedure yielded reproducible results. Between two adsorption/desorption runs, the sample was kept in a helium stream at room temperature. In fig. IV.6, typical desorption spectra for platinum and iridium powders are presented. We wish to stress the relatively good resolution, as compared with literature (1-6), revealing an appreciable number of desorption peaks and - shoulders, especially in the case of platinum.

Platinum shows peaks with their maxima at 123 K, 167 K, 224 K, 324 K and 500 K, and shoulders at 186 K and 376 K. In the following, desorption peaks will be referred to by the temperature at which they have their maximum. The H_2/Ir spectrum contains peaks at 123 K, 186 K, 332 K and 500 K, and shoulders at 230 K and at 389 K. (In order to establish the existence of a peak at 500 K, for some experiments the heating has been extended up to 550 K).

It is interesting to investigate in how far these spectra depend on sample history. A more severe oxygen pretreatment (50% oxygen in helium, 670 K) of the platinum powder makes the 167 K peak and the 224 K peak to disappear, while the shoulder at 196 K is now fully resolved. The same pretreatment of the iridium sample causes the disappearance of the shoulder at 230 K, so that now both metals exhibit qualitatively the same desorption spectrum (fig. IV.7).

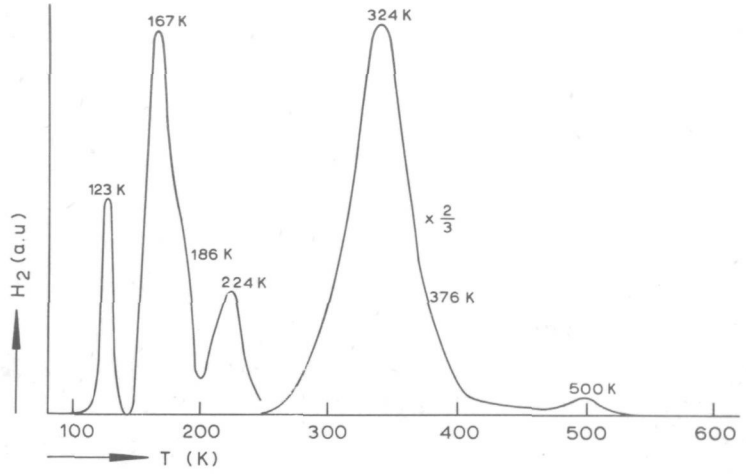

IV.6[a] H_2/Pt desorption spectrum after mild pretreatment of the platinum powder

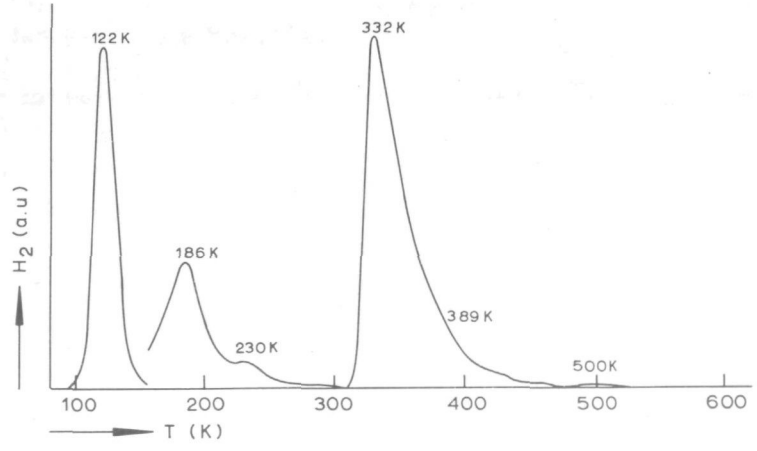

IV.6[b] Idem for H_2/Ir

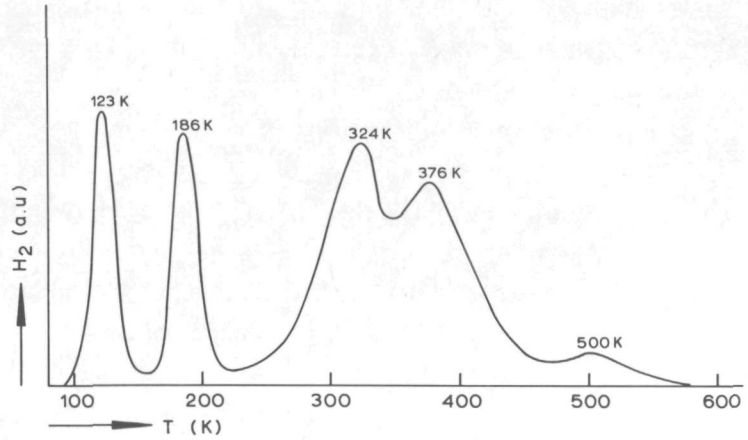

IV.7[a] H_2/Pt desorption spectrum after severe oxygen pretreatment and prolonged exposure to hydrogen

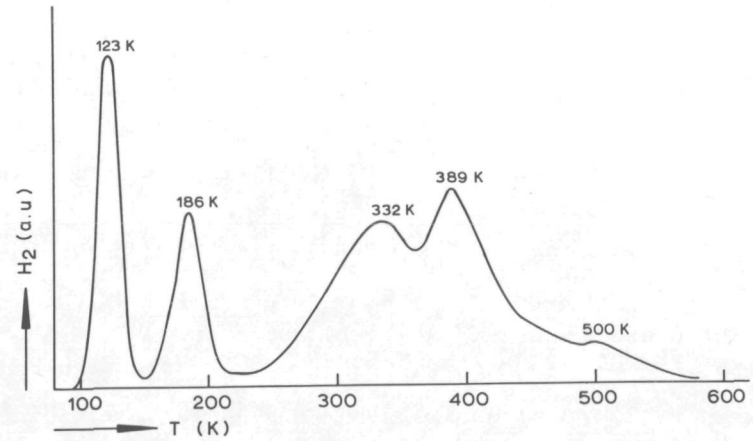

IV.7[b] Idem for H_2/Ir

However, after a number of adsorption/desorption runs, shoulders can be observed in the platinum spectrum at 167 K and at 224 K, whereas the iridium spectrum remains virtually unchanged.

The first desorption run after a hydrogen treatment at 550 K, followed by degassing at 620 K, yields a much higher peak at 186 K than the following, reproducible, runs do. Moreover, if the desorption run is not preceded by hydrogen adsorption (in a "blank" experiment), all peaks are lacking, except for the peak at 186 K, and, incidentally, the peak at 324 K (332 K in the case of iridium). The behaviour of the 186 K peak was further investigated by doing desorption experiments, preceded by

- hydrogen treatment at 550 K (5 minutes)
- purging with helium at 620 K (16 hrs)
- purging with helium at 80 K (t minutes) with varying purging times t at 80 K. The resulting desorption spectra exhibit one peak at 186 K, the height of which appears to be roughly linearly proportional to the purging time t (IV.8). The peak width at half peak maximum, ΔW, was observed to be independent of peak height, so that the peak height directly reflects the peak surface, or the initial coverage θ_i.

When hydrogen adsorption at room temperature is proceeded for 30 minutes or more, the top of the peak at 324 K for platinum (332 K for iridium) shifts to a higher temperature, and the peak becomes broader. Adsorption during 16 hrs results in a peak at 376 K (Ir: 389 K) and a shoulder at 324 K (Ir: 332 K), so that the hydrogen desorbing at 324/332 K appears to be a precursor of the hydrogen which desorbs at 376/389 K.

Four different Kulifay alloy powders have been investigated, containing 10, 24, 50 and 75% iridium (sample A, B, C and D, respectively). The latter sample shows an

iridium-like behaviour with respect to the position of the peaks in the 300 - 400 K region. Shoulders in the low temperature branch of these peaks suggest the presence of platinum in the surface. Sample C (50% Ir) exhibits a broad peak between 300 and 400 K, in which three or four maxima may be observed.

Sample A yields a desorption spectrum which is about the same as the one found for pure platinum. If iridium is present in the surface, it does not give rise to visible shoulders at 332 K or at 389 K. It is important to note, that this sample did not need the "severe" oxygen pre-treatment for elimination of peaks at 224 K and 167 K. The peak at 224 K was found only incidentally, and could not be reproduced. A shoulder at 167 K could not be detected, though in certain cases the peak at 186 K was broadened

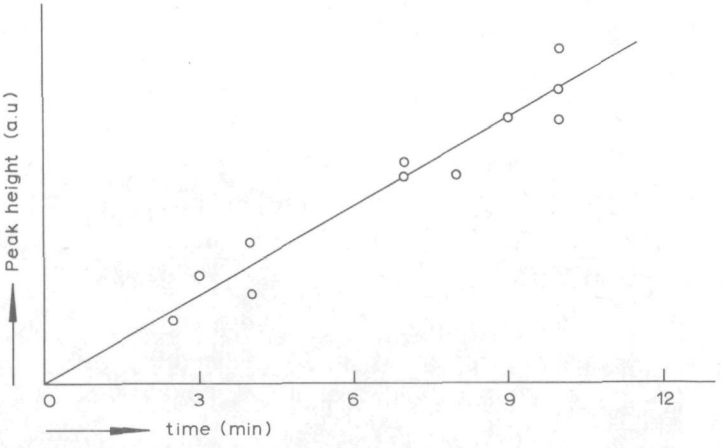

IV.8 Height of the 186 K peak as a function of time of purging in helium at 80 K

at the low temperature side.

The behaviour shown by sample B is quite different from that of the other samples. The peaks expected to be found at 186, 324/332 and 376/389 K seem to have shifted to 173, 298 and 350 K, respectively. A more rigorous pretreatment of the sample did not bring about any change in the desorption spectra. An additional sample B^1, containing 28% iridium, during the preparation of which special precautions were taken to avoid contamination, yielded the same desorption spectra as sample B, though the peaks might be somewhat broadened at the high temperature side.

The peaks in the desorption spectra of alloy powders showed the same dependence on catalyst pretreatment as has been reported for the corresponding peaks in the spectra of pure platinum and pure iridium.

IV.4.1.2 Silica supported catalysts

Five silica supported samples have been prepared, following the method described in section IV.3.1.2, containing 100, 80, 73, 50 and 0 atom % platinum, the rest, up to 100%, being iridium. The silica used was Ketjen F 2, S_{BET} = 340 m^2 g^{-1}. The total metal load was about 6 weight% and the mean metal particle diameter was in the order of 50 nm for all catalysts. The bimetallic catalysts were monophase. The samples were pretreated in hydrogen and in a 50% oxygen 50% helium mixture at 700 K, and degassed at 750 K. It is important that these samples can be treated at higher temperatures without sintering of the metal, in contrast with the Kulifay-powders.

Representative hydrogen desorption spectra are collected in fig. IV.10. The spectra of the samples 100/0, 80/20 and 0/100 all show a peak at 183 K, having the same

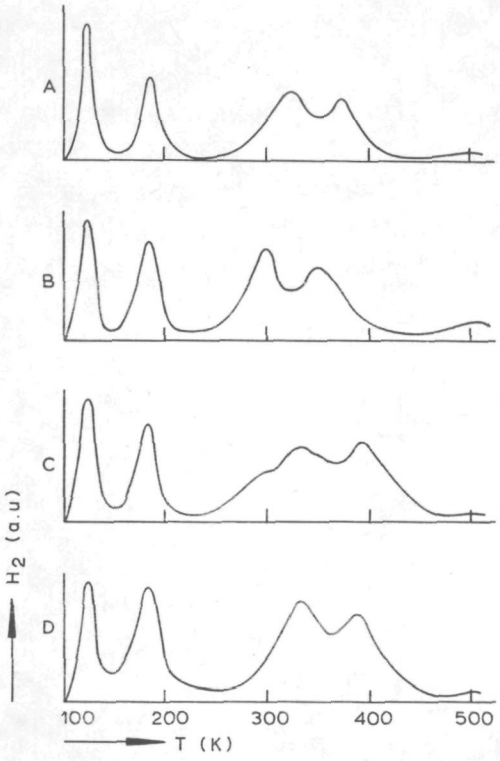

IV.9

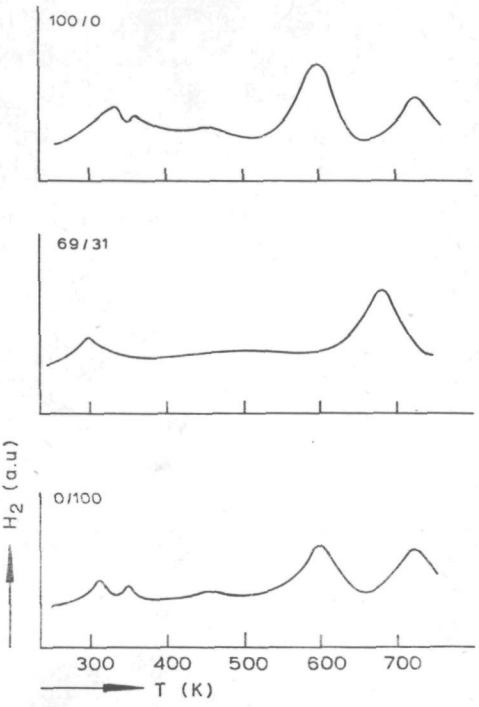

IV.11

IV.9 H_2 desorption spectra for various Kulifay alloy powders
A : 90% Pt, 10% Ir;
B : 76% Pt, 24% Ir;
C : 50% Pt, 50% Ir;
D : 25% Pt, 75% Ir.

IV.11 Hydrogen TPD -spectra for various alumina supported catalysts

characteristics (ΔW, θ_M/θ_i, overall line shape) as the one found at 186 K for Kulifay powders. Sample 73/27 has this peak at 174 K, to be compared with the value of 173 K for the Kulifay-powder containing 24% iridium. Sample 50/50 shows a twin peak with maximum at 177/183 K.

The 100/0 sample shows peaks at 166 K and at 225 K, but these can be eliminated by a more severe pretreatment, using pure oxygen at 750 K.

All catalysts show desorption of water, detected by separate gaschromatographic analysis, at temperatures above 670 K. This phenomenon can be suppressed by a heat

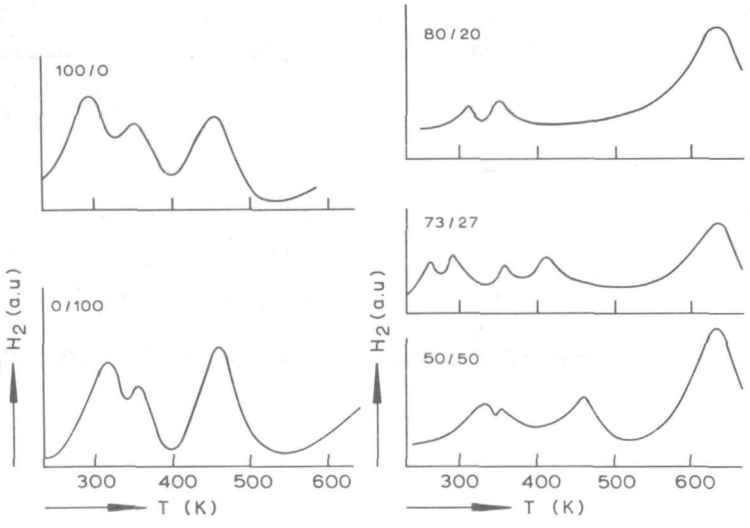

IV.10 Hydrogen TPD - spectra for various silica supported Pt-Ir catalysts
100/0 : 100% Pt; 80/20 : 80% Pt, 20% Ir, etc.

treatment in helium at 770 K for at least 16 hrs, but it cannot be fully eliminated in this way. The spectra presented in fig. IV.10 are from water-poor samples.

Ir/SiO_2 exhibits a desorption peak at 316 K. Corresponding peaks are found at 312 K for 80/20, at 280 K for 73/27, and at 298 K for 100/0. All iridium-rich samples show a peak at 355 K. For 80/20, this peak is shifted to 350 K, and for 100/0 to 346 K. A peak near 450 K is found for all samples, except for 73/27, where it has shifted to 410 K.

Bimetallic catalysts show a peak near 630 K, which is not observed in the spectra of the pure constituents. In the region between 350 K and 550 K, desorption from bimetallic catalysts is almost continuous.

In general, the spectra do not differ much from those obtained from Kulifay-powders. Peaks near 450 K have not been detected by us on Kulifay-powders, and peaks above 600 K, if any, were beyond the heating range of those powders.

IV.4.1.3 Alumina supported catalysts

From the point of view of reforming catalysis, samples on γ-alumina as a carrier (AKZO 000-3P, $S_{BET} = 248\ m^2\ g^{-1}$) are the most important ones. To check in how far diffusional retardation may influence the observed TPD-spectra, samples on α-alumina (Rhône-Progil SCS 9) have also been investigated. Since the latter samples yielded the same desorption spectra as those from γ-alumina supported catalysts, it was concluded that diffusional retardation does not play a role, and the α-alumina results will not be discussed further.

Some of the obtained desorption spectra are collected in fig. IV.11. It is seen that they are all characterized

by a narrow and high peak near 190 K, a very broad and low peak between 300 K and 500 K, and two somewhat more pronounced peaks at 600 K and at 720 K. These spectra are obtained after pulse loading. The hydrogen adsorption step consists of dosing four pulses of 78,5 mm^3 (NTP) hydrogen at 298 K, so that only hydrogen that is irreversibly adsorbed at this temperature will remain on the surface of the catalyst. It is, therefore, surprising that in the subsequent desorption step an important desorption peak near 190 K is detected. The height of this peak is dependent on the time during which the sample is purged at 80 K.

Desorption runs after saturation of the sample with hydrogen at room temperature reveal nearly the same desorption picture, be it that the broad peak between 300 K and 500 K is somewhat higher, and very small peaks at the familiar positions (330, 350, 445 K) can be observed.

Alumina-supported samples exhibit the same peaks as those on silica, but are poorly resolved in the region 300 K - 550 K. The pure metals on γ-alumina show peaks at 600 K and 720 K, that could not be observed when investigating silica supported platinum or iridium.

IV.4.1.4 Carbon supported platinum

Several activated carbon supported platinum catalysts were obtained by ion exchange on a hydrophylic (oxygen-rich) carbon support. Hydrophobic carbon (oxygen-poor) was loaded with platinum via adsorption of H_2PtCl_6, and subsequent reduction with methanol. It will be clear that these samples cannot be treated in oxygen at elevated temperatures. Desorption peaks have been recorded at 227 K, 323 K, 376 K and 453 K, and are independent of the oxygen content of the support (fig. IV.12).

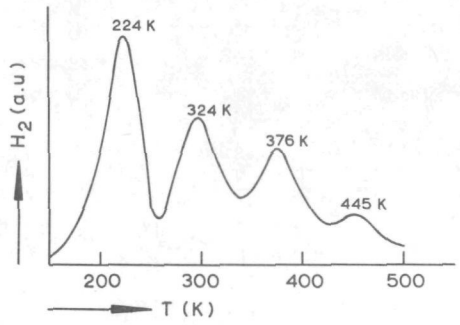

IV.12 Part of a desorption spectrum for carbon supported platinum. The peak at 445 K is associated with hydrogen desorption from the support

IV.4.2 Desorption of ethene and butene

Hydrogen desorption experiments with non-impregnated silica and γ-alumina, the same used as supports, reveal these species to be inactive towards hydrogen. Desorption of water, which is found at temperatures above 600 K, can be reduced by a prolonged heat treatment in nitrogen or helium at 750 K. We did not succeed in completely suppressing this water desorption.

Both supports have been investigated by adsorption and desorption of ethene (ethylene), and the γ-alumina support also with butene (butylene) (fig.IV.13). Ethene desorption spectra from silica show one peak near 380 K, whereas on γ-alumina as much as three peaks are detected (340 - 360 K,

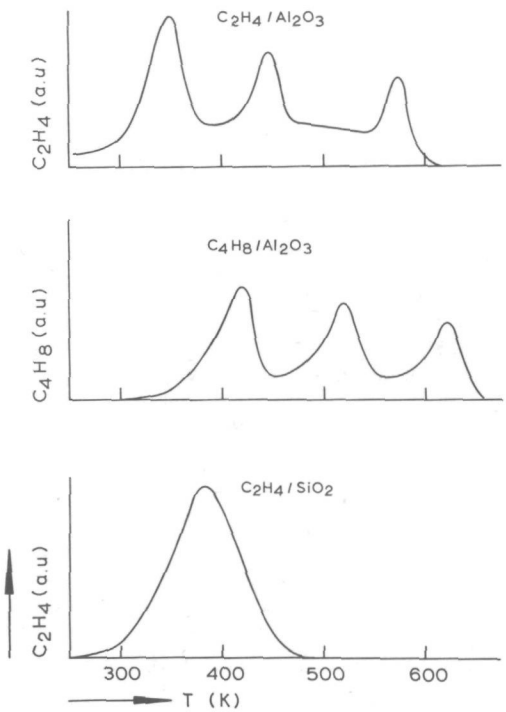

IV.13 Desorption of ethene and butene from alumina. Desorption of ethene from silica

430 - 460 K, and 540 - 620 K resp.). All these peaks have their maxima at varying temperatures, suggesting energetically heterogeneous surfaces. The same holds for the three peaks in the butene/alumina spectra, 405 - 445 K, 503 - 545 K and 578 - 635 K being the regions in which peak maxima can be found.

IV.5 Discussion

IV.5.1 Introduction

The information presented in IV.4 reveals, that platinum and iridium and their alloys differ only slightly in their behaviour towards hydrogen. On this basis one might conclude that hydrogen thermodesorption experiments with platinum - iridium catalysts will contribute little to our understanding of the platinum - iridium bimetallic system. However, a more thorough analysis is necessary to appreciate fully the value of the obtained thermodesorption results. This can best be done by analyzing each peak separately.

IV.5.2 The 123 K peak

The peak at 123 K is found for all samples, supported or not, monometallic or bimetallic. The peak is recorded only if the sample has been in contact with hydrogen at temperatures below 123 K. Some of this type of adsorbed hydrogen can be desorbed by purging with helium at 80 K. By varying the purging time, the peak surface area can be varied. The peak width, ΔW, appeared to be dependent on the peak surface area, that is, on the initial coverage (fig. IV.14). This feature is, as argued in section II.5.2, an indication of the occurrence of readsorption. The value

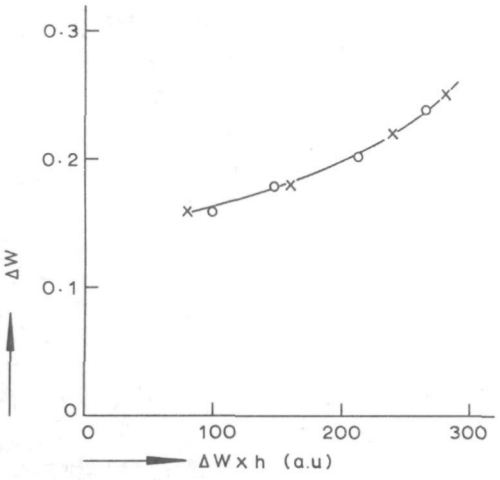

IV.14 Peak width of the 123 K - peak as a function of initial coverage
× platinum powders;
O iridium powders

	SiO_2	γ-Al_2O_3
Na_2O (weight %)	0.014	0.086
SO_4	0.05	1.1
Fe	0.022	0.03
SiO_2		1.22
Al_2O_3	0.18	
Surface area ($m^2\ g^{-1}$)	403	247
Pore volume (N_2) ($cm^3\ g^{-1}$)	1.06	0.85
Pore volume (Hg) ($cm^3\ g^{-1}$)		
Average particle diameter	150 μm	3.0 mm

Table IV.7

Chemical composition and some physical properties of silica F_2 and γ-alumina 000-3P, as stated by the supplier.

of θ_M/θ_i, approximated by the value of ΔW ($T_n > 1$)/ ΔW (total) (see fig. IV.14), is 0.38 or less, indicating first order desorption kinetics (c.f. table II.4). Comparison of fig. IV.14 with fig. II.9 reveals the value of E_M^* to be less than 15. A plot of $\ln(C_n) - \ln\{\theta/(1-\theta)\} - b \ln(T)$ versus $1/T$ (c.f. eq.(II.15)), constructed for some experiments in which the 123 K peak was well resolved, yielded a best fit for $b = 1$, and a slope ($= \Delta H/R$) of $(1.35 \pm 0.2) \times 10^3$ K, so that $\Delta H = 11 \pm 2$ kJ mole^{-1}. The value $b = 1$ suggests limited mobility of the adsorbed molecules at this temperature. Substitution of the appropriate parameters into equation B.1.1 (see section I.5.1) gives $\ln A^* (= \Delta S/R) = 7.99$, or $\Delta S = 60$ J mole^{-1} K^{-1}.

We conclude that the hydrogen desorbing at 123 K is adsorbed molecularly and rather weakly, the adsorbed molecules having limited mobility.

It is hard to say if the hydrogen, associated with this peak, is physically or chemically adsorbed. Physisorbed hydrogen has a low heat of adsorption (ca. 6 kJ mole^{-1}), and has unrestricted mobility in two dimensions. This is certainly not the case with the hydrogen desorbing around 123 K. One may think of it as being adsorbed at so-called B5 - sites, but it is doubtful if the rather large crystallites ($\sim$ 30 nm) provide enough of these sites to account for the rather large amount of molecularly adsorbed hydrogen. Without further experimental information, no definite conclusion concerning the nature of this type of hydrogen adsorption can be drawn.

IV.5.3 The peak at 186 K

This peak shows a very interesting dependence on sample history. It is strongly enhanced if adsorption takes place at a temperature below 186 K, but it is also found after

pulsewise adsorption at room temperature (298 K) or at even higher temperatures. Moreover, the peak is also found in blank experiments, when the sample is kept in helium at 80 K for some time, without preceding adsorption of hydrogen. The experimental results give the impression that the peak surface area is governed by the time during which the sample was kept at 80 K (c.f. fig. IV.8), provided that the catalyst was not treated in hydrogen at elevated temperatures just before the desorption run. In the latter case, the surface area is much higher than indicated by the straight line in fig. IV.8. These features, which we reported already for Kulifay-powders in section IV.4.1.1 have been found to apply also for supported catalysts, regardless of the metal involved (platinum, iridium, or their alloys). As the peak width ΔW (= 0.10) is independent of coverage, we deal with desorption without readsorption. The values of θ_M/θ_i point to "second order" desorption kinetics. Now, E_M formally can be determined with the aid of eq. (II.6) (section II.5.2) to be 27, so that E_d = 42 kJ mole^{-1}, a value that is more or less confirmed by plots, constructed according to equation (II.14) : 49 $\pm$ 3 kJ mole^{-1}. The former value for E_d, together with T_M = 186 K, suggest $A(= \kappa.kT/h \exp(\Delta S_d^{\dagger}/R)) \approx 2 \times 10^{10}$. The transmission coefficient κ may be as small as 10^{-3} (c.f. section I.7.1 and reference (27) of chapter I), but if we assume that $\kappa \approx 1$, then $\Delta S_d^{\dagger}$ should be as small as - 41 J mole^{-1} K^{-1}, i.e., the transition state should be much less mobile than the initial state.

In our opinion all these phenomena can be accounted for by assuming that hydrogen can be dissolved in platinum and iridium. Dissolution takes place during hydrogen treatment at elevated temperatures (600 - 800 K), but the dissolved hydrogen cannot be removed completely by vacuum treatment or purging with helium at the same or a slightly higher

temperature. At very low temperatures, however, sites at the surface and the subsurface are more attractive, from a thermodynamic point of view, than the bulk, because of the higher adsorption enthalpy at the (sub)surface. The lower entropy is of less importance at low temperatures. So, at low temperatures, part of the dissolved hydrogen migrates to the surface, or to the subsurface sites, when the surface is already covered with hydrogen.

When the temperature is raised, that part of the hydrogen which is near the surface, can desorb, either as molecules via defects in the lattice near the surface ("porthole - mechanism"), or after recombination with a surface hydrogen atom, via octahedral holes in the subsurface. The latter possibility is analogous to the "breakthrough" model, proposed by Konvalinka and Scholten for the desorption of hydrogen, dissolved in palladium (11). However, whereas the latter authors found "first order" desorption kinetics, our results point to "second order". This might suggest that in the case of platinum and iridium, diffusion of hydrogen from the bulk to the surface becomes rate-determining. The desorbed hydrogen may readsorb, but will not penetrate into the bulk, because the loss of enthalpy, associated with dissolution of chemisorbed hydrogen, is not balanced by the gain of entropy at this temperature.

It will be clear that our theoretical line shape analysis does not apply in this case. The unreasonably high value of E_d, together with the large negative activation entropy, clearly demonstrate the breakdown of the mathematical analysis. On the basis of the assumption that $\Delta S_d^{\dagger} \approx 0$, we compute $E_d \approx 32$ kJ mole^{-1}.

The main points of the model can be summarized as follows:

- hydrogen is absorbed by platinum and iridium at elevated temperatures, but does not desorb at these temperatures, because of the high entropy of hydrogen atoms in the bulk
- at low temperatures (80 K) absorbed hydrogen migrates to the surface, because of the high enthalpy of asorption at the surface, but desorption is not possible, due to the high activation energy
- since in desorption at least one of the atoms involved is a subsurface hydrogen atom, the activation energy of desorption is lower than when desorption involves recombination of two surface hydrogen atoms (section IV.5.4).

Dissolution of hydrogen in platinum has been reported by various authors (12,13). The results mentioned by Aben c.s. (14) when discussing hydrogenation of benzene over supported platinum, are in fact in remarkable agreement with our findings. They report a treatment of the catalyst in hydrogen at 770 K to result in a higher low-temperature desorption peak. It is interesting to note that this behaviour is associated with an increase of the benzene hydrogenation activity.

It will be clear that a high peak at 186 K causes a reduction of the height of peaks desorbing at higher temperatures, since desorption of subsurface hydrogen causes a depletion of chemisorbed hydrogen. This is indeed what has been observed by us, and what has also been reported by Aben et al. (14). However, desorbing hydrogen may readsorb at surface sites, from which it can desorb at higher temperatures. This effect has been observed in blank experiments: incidentally, a peak in the 300-400 K region is observed in desorption experiments that were not preceded by adsorption, but showed a high peak at 186 K. This readsorption may cause

the peak at 186 K to be somewhat narrower than the theoretically computed desorption peak. Indeed, some of the derived θ_M/θ_i-values are somewhat too low for second order desorption kinetics. This may, however, be caused by a shoulder at 167 K, or, in the case of supported catalysts, by spilled over hydrogen (section IV.5.7).

Concluding, we may state that the unexpected features of the peak at 186 K, being:

- relative inertness with respect to the adsorption procedure, as long as adsorption is carried out at temperatures above 230 K and below 600 K
- dependence on duration of purging at low temperatures
- strong influence of the conditions of pretreatment of the catalyst
- apparent absence of readsorption,

can be explained by a model, including:

- penetration of hydrogen into the bulk of platinum and iridium at elevated temperatures (> 600 K)
- migration of dissolved hydrogen to the surface being favoured thermodynamically, but rather slow because of the low temperature
- desorption at a temperature as low as 186 K, in which diffusion of bulk hydrogen atoms is rate-determining.

IV.5.4 Peaks in the temperature region above 300 K

All peaks detected for various samples in the temperature region above 300 K have the following main characteristics in common:

- second order desorption
- freely occurring readsorption
- a value of E_M^* in the order of 20
- almost complete loss of entropy on adsorption.

Table IV.2

$T_{M\ K}$	E_M*	ΔH	ΔS	Pt	Ir	A	B	C	D
				100	0	90	76	50	25
298	18.6	46	120				+	+	
324	19.0	51	122	+		+			
332	19.6	54	127		+			+	+
350	19.4	56	125				+	+	
376	20.2	63	132	+		+			
389	20.1	65	131		+			+	+
500	21.0	87	136	+	+	+	+	+	+

Table IV.2

Kulifay powders. Occurrence of desorption peaks on various samples, and their adsorption enthalpy and entropy. The platinum contents of the samples are given in atomic %.
Values of ΔH in kJ $mole^{-1}$
Values of ΔS in J $mole\ K^{-1}$

Table IV.3

T_M K	E_M*	ΔH	ΔS	100/0	80/20	73/27	50/50	0/100
263	17.9	39	115			+		
292	18.0	44	115	+				
295	18.2	45	116			+		
312	18.2	47	116		+			
316	18.2	48	116					+
330	18.3	50	116				+	
346	19.0	55	122	+				
350	18.9	55	121		+			
355	19.4	57	125			+	+	+
410	19.4	66	124			+		
445	20.1	74	129	+				
460	20.2	77	130				+	+
630	22.1	116	144		+	+	+	

Table IV.3

Silica supported catalysts
Occurrence of desorption peaks on various samples, and their adsorption enthalpy and entropy.
Values of ΔH in kJ $mole^{-1}$
Values of ΔS in J $mole^{-1}$ K^{-1}

Table IV.4

T_M K	E_M*	ΔH	ΔS	100/ 0	90/ 10	69/ 31	50/ 50	30/ 70	0/ 100
298						+			
311								+	+
319							+		
333				+					
350							+	+	+
362				+					
445				+	+			+	+
600	21.9	109	143	+				+	+
680	22.4	126	146		+	+			
720	22.6	135	147	+			+	+	+

Table IV.4

Alumina supported catalysts
Occurrence of desorption maxima on various samples, and the enthalpy and entropy of adsorption of some of them.
Values of ΔH in kJ $mole^{-1}$
Values of ΔS in J $mole^{-1}$ K^{-1}

Table IV.6

C_2H_4/Al_2O_3	T_M K	E_M^*	ΔH	ΔS
first peak	340 - 360	24.4	69 - 73	169 ± 2
second peak	430 - 460	25.6	91 - 98	177 ± 3
third peak	540 - 620	20.4	91 - 105	130 ± 1
C_4H_8/Al_2O_3	T_M K	E_M^*	ΔH	ΔS
first peak	405 - 445	29	97 - 107	207 ± 5
second peak	503 - 545	31	129 - 140	222 ± 6
third peak	578 - 635	26	124 - 137	178 ± 10
C_2H_4/SiO_2	T_M K	E_M^*	ΔH	ΔS
one peak	373 - 392	28	87 - 91	ca. 200

Table IV.6

Olefine desorption from silica and alumina
Values of ΔH in kJ $mole^{-1}$
Values of ΔS in J $mole^{-1}$ K^{-1}

T_{M_K}	E_M^*	ΔH	ΔS
323	19.0	51	122
376	20.2	63	132
453	21.1	79	138

Table IV.5

Carbon supported platinum
Desorption peaks in the region 300 K - 500 K

The results are collected in tables IV.2 to IV.6. In agreement with the dissociative character of the adsorption, almost complete loss of entropy is associated with the adsorption process. This, however, does not necessarily imply total immobility of the adsorbed atoms. If the chance to find an atom moving from one site to another is about, say, 1%, and the chance to find it on an adsorption site, where it can only vibrate a bit, is about 99%, the entropy of the adsorbed state is about zero.

IV.5.5. Peaks at 167 K and at 224 K

The peaks at 167 K and 224 K have been found especially on pure platinum powders and supported platinum catalysts. They can be eliminated by a more severe pretreatment of the sample, of which a heat treatment in oxygen is an essential part. The oxygen treatment is followed by a thorough treatment in hydrogen (700 K, 1 bar), in order to remove chemisorbed oxygen. Repeated adsorption/desorption runs caused the reappearance of the 224 K - peak. This behaviour suggests these peaks to be caused by a kind of bulk contamination. In view of the reported AES-results, the most probable contaminant seems to be carbon. Therefore, experiments have been carried out in which a "clean" $Pt/\gamma\text{-}Al_2O_3$ catalyst was poisoned by pulsewise adsorption of ethane (one pulse of 78.6 mm^3 (NTP)) at room temperature, followed by purging in helium at 700 K. The results are shown in fig. IV.16. It is seen that the 224 K is markedly enhanced by preceding coverage of the surface with carbon. This is consistent with the results of experiments with carbon supported platinum. These samples cannot be treated in oxygen at elevated temperatures, and carbon will most probably be a contaminant of the platinum surface. It is

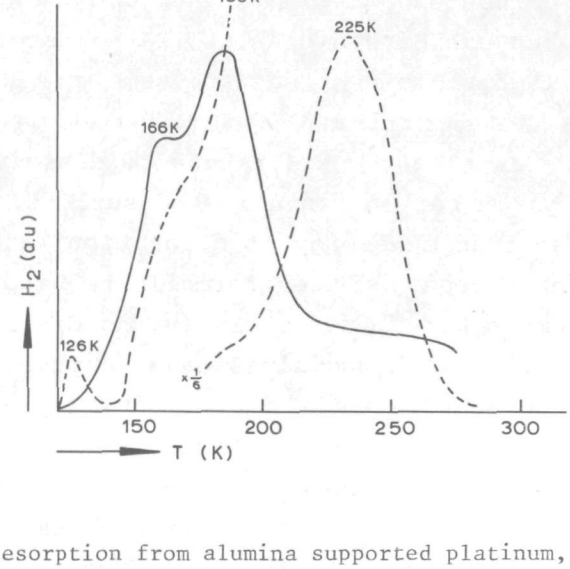

IV.16 Hydrogen desorption from alumina supported platinum, showing the influence of carbon
Solid line : "clean" platinum surface
Dashed line : after ethane pretreatment

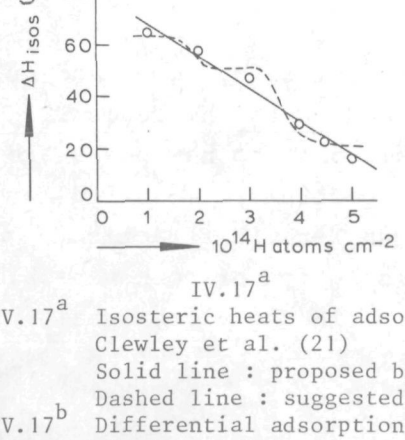

IV.17[a]

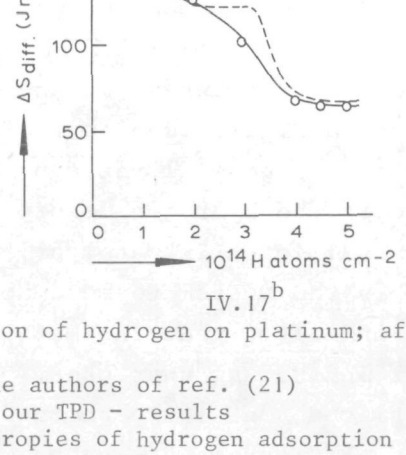

IV.17[b]

IV.17[a] Isosteric heats of adsorption of hydrogen on platinum; after Clewley et al. (21)
Solid line : proposed by the authors of ref. (21)
Dashed line : suggested by our TPD - results

IV.17[b] Differential adsorption entropies of hydrogen adsorption on platinum; after Clewley et al. (21)
Solid line : proposed by the authors of ref. (21)
Dashed line : suggested by our TPD - results

seen that carbon supported platinum does not show a peak at 186 K, but exhibits a peak at 224 K instead (fig. IV.12 and table IV.5). The peak has the same characteristics (ΔW, θ_M/θ_i) as the one at 186 K for non-contaminated samples. We ascribe the 224 K peak to dissolved hydrogen, desorbing via a carbon contaminated surface.

The "activation energy of desorption" and the activation entropy" have been computed formally to be 52 kJ $mole^{-1}$ and -42 J $mole^{-1}$ K^{-1}, respectively. As discussed above (section IV.5.3), these values have no physical meaning, but merely demonstrate the inapplicability of our model.

The peak at 167 K does not seem to be related with carbon, though it can be eliminated by a thorough oxygen/hydrogen pretreatment. It is therefore tempting to ascribe this peak also to a contamination of some kind. It should be a species which is found often on platinum, and can be removed by oxygen and/or hydrogen, e.g. sulfur. No experiments with deliberate sulfur poisoning have been performed, so that the origin of the 167 K peak remains obscure.

IV.5.6 Effect of alloying

Our main interest is the effect of alloying Pt and Ir on the catalytic behaviour of Pt and on the hydrogen TPD spectra. In general, it can be said that no new peaks are found if the hydrogen desorption spectrum is measured for a bimetallic Pt/Ir catalyst, though X-ray diffraction reveals the system to be a solid solution of both metals. This indicates that the metal atoms in the alloy retain their individual character.

Alloys containing up to 20% iridium show a platinum-like behaviour in the sense that the desorption peaks have the same position as found for platinum. This is in agree-

ment with the platinum enrichment of the surface, as observed in AES. The slight difference between Pt and Ir in the interaction energy with hydrogen will not be able to cause induced surface enrichment in iridium due to hydrogen adsorption. In spite of the platinum-like behaviour of these alloys, the peak at 224 K is found only incidentally, and can be removed by moderate hydrogen treatment. We conclude that only a small amount of iridium in the surface is sufficient to remove the carbon deposit from neighbouring platinum sites, if hydrogen is present. Hydrogenation of the carbonaceous species on the platinum sites by atomic hydrogen from iridium sites is a probable mechanism for this phenomenon. We return to this question in chapter VI.

When the iridium content is in between 20 and 30%, the alloy behaves quite differently. The peak at 186 K has shifted to ca. 174 K, and other peaks are observed at 298 K, 350 K and 410 K, whereas platinum shows peaks at 324 K, 376 K and 445 K (fig. V.10), and iridium has its corresponding peaks at still higher temperatures. These values indicate the chemisorption enthalpies to be about 10% lower on these alloys than those of the corresponding chemisorption complexes on platinum (c.f. table IV.2 and IV.3). It is important that this effect is found in the region of alloy composition where thermodynamic data suggest the existence of an ordered compound, as discussed in chapter III. We consider the thermodesorption results as a proof of the predicted intermetallic interaction, the formation of covalent metal-metal bonds in the alloy causing a weakening of the interaction with chemisorbed species, e.g. hydrogen, as will be discussed in more detail in chapter VI.

Samples having an iridium content of more than 30%

exhibit dual character: that of the Pt_3Ir "compound", and that of iridium. For iridium contents higher than 50%, the iridium character prevails (fig. IV.9). However, the accuracy of the determination of maxima of broad and low second order peaks is not sufficiently high to establish if the peak maxima for iridium-rich samples are shifted to a somewhat lower temperature, due to the presence of platinum in the surface.

All silica supported alloys show an extra peak at 630 K (fig. IV .10). The peak is highest on sample 50/50 suggesting that atoms of both metals contribute to the site responsible for this type of chemisorption.

TPD experiments with γ-alumina supported samples reveal desorption peaks near 720 K for both the platinum and the iridium sample (table IV.4). It is possible that these peaks would have been found for silica supported platinum and iridium as well, when the desorption experiments with these samples would have been extended to temperatures above 650 K. Literature reports significant desorption of hydrogen above 700 K for most transition metals. This matter will be returned to in chapter VI.
The peaks near 630 K on the silica supported alloy samples may be associated with a type of hydrogen chemisorption which desorbs from the silica supported pure metals at temperatures above 650 K.
(c.f. the peaks near 689 K on γ-alumina supported alloys and those at 720 K for γ-alumina supported platinum and iridium, table IV.4). This interpretation remains hypothetical, unless more experimental data become available.

The effects of alloying on the TPD-spectra can be summarized as follows:

- up to 20% iridium: a behaviour like pure platinum, except for the influence of carbon contamination

- between 20% and 30% iridium: a new "compound" is formed, which exhibits weaker chemisorption of hydrogen than Pt, resp. Ir.
- between 30% and 50% iridium: two phases are present, one being the compound which exhibits relatively weak chemisorption, the other has iridium-like behaviour
- more than 50% iridium: an iridium-like behaviour is found.

IV.5.7 Effect of the support

The use of a support may influence the TPD-spectrum by desorption of hydrogen, previously spilled over from the metal to the support (23), and by direct interaction of the support with the metal deposited on it. Since our supported catalysts have metal particles of rather large diameter, both effects will be small.

Direct evidence of hydrogen spill-over has not been found. However, γ-alumina and silica supported samples evolve large amounts of water in each desorption run. The amount of water can be reduced considerably by heating the catalyst at 750 K in helium, but complete elimination of water is not possible in this way. In our opinion, spilled over hydrogen chemisorbs on dehydroxylated sites and subsequently reacts with hydroxyl groups at the surface of silica or alumina. Surface hydroxyl groups can be removed by heat treatment, but for complete removal, temperatures of about 1100 K are required (24, 25).

As discussed above in section IV.5.3, the peak at 186 K is virtually insensitive to the preceding exposure to hydrogen. This is not always true for silica and γ-alumina supported catalysts. These samples show an increase of the height of the 186 K peak on prolonged exposure ($> 30 \times 10^6$ N m^{-2} s) to hydrogen. Moreover, the value of

θ_M/θ_i tends to decrease from about 0.54 to 0.48. We suppose that this effect may be due to spilled over hydrogen, desorbing via a first order mechanism at that temperature.

Another explanation may be that the supported samples contain, apart from the rather course metal crystallites ($\bar{d}_w$ (X-ray) $\gtrsim$ 30 nm) an appreciable amount of very small particles (d < 2 nm) which are not detected in X-ray diffraction. Hydrogen is assumed to dissolve readily into these small particles at room temperature. Desorption of this hydrogen will not suffer diffusion limitation, because of the small particle size, and hence the desorption peaks show first order characteristics (θ_M/θ_i < 0.5).
It should be noted that the 186 peak of these samples faithfully follows the behaviour described in section IV.5.3 if no previous hydrogen adsorption has taken place.

Silica and γ-alumina supported samples show peaks near 450 K (figs. IV.10 and IV.11), which are not found for Kulifay-powders. It has been shown by Leclère et al.(16) that part of the iridium, deposited on η-alumina is incorporated in the support as Ir(III) aluminate, which cannot be reduced by hydrogen to metallic iridium. Elsewhere, these authors report a hydrogen desorption peak near 400 K which they ascribe to this iridium being in interaction with the support (17). A similar phenomenon in the case of platinum would explain the (partial) solubility of platinum, deposited on alumina or silica-alumina, in 2,4-pentane dione, which has been reported by several authors (18,19). It might be that the peaks in the region around 450 K, observed for silica and alumina supported samples, are to be ascribed to hydrogen, chemisorbed on platinum or iridium in interaction with the support. The peak near 450 K in the spectra of carbon supported platinum is desorption from the support.

A more general effect of the support γ-alumina is the very flat structure of the hydrogen desorption spectrum between 200 K and 550 K. The total amount of hydrogen desorbing between these two temperatures, when expressed per m^2 of metal, is about the same as for carbon supported metals or for Kulifay-powders. So, the alumina support seems to induce an energetically heterogeneous metal surface. This can occur only when an appreciable amount of very small metal particles (< 2 nm) is present on the support, which would be consistent with the observed behaviour of the 186 K peak, as discussed above. Most of the hydrogen adsorbed on small particles apparently desorbs at temperatures above 550 K, which would explain why the amount of hydrogen evolved between 200 K and 550 K is still consistent with the X-ray value for $\bar{d}_w$ ($\approx$ 30 nm), though the existence of non-detected small particles implies a higher metal surface. Since all hydrogen desorbs in this part of the spectrum via second order desorption kinetics with an E_M^* value of about 20, the shape of this part of the desorption spectrum reflects the shape of the site/energy distribution.

IV.5.8 Ethene desorption from silica and alumina

The experiments with ethene and 1-butene have been undertaken in order to investigate if the TPD-spectra of these relatively heavy molecules are influenced by diffusion retardation. A thorough analysis of the systems ethene/γ-alumina and ethene/silica would justify a whole research program, and falls outside the scope of this thesis. Moreover, a fundamental attack of this problem requires the use of samples of higher purity than our samples had (c.f. table IV.7). Furthermore, we neglected, for example,

the possibility of isomerization of the double bond in 1-butene, and of other oligomerization reactions than the dimerization reported by Cvetanovic and Amenomiya (20). However, in spite of the preliminary character of our experiments, they may contain valuable information for other investigators, and hence we shall subject them to a brief discussion.

The analysis of the ethene desorption spectra is complicated by the energetical heterogenity of the silica and alumina surfaces. However, in the case of alumina, the individual peaks appear to be well described by the theoretical model for first order peaks with freely occurring readsorption. The position of the peak maximum depends on the pretreatment of the sample, rather than on the initial coverage with ethene. When the adsorption/desorption experiment is preceded by a heat treatment of the sample at 770 K for 16 hrs in helium, the peak maxima shift to higher temperatures, suggesting competitive chemisorption of hydroxyl groups on the sites on which ethene is chemisorbed. As the peaks of the spectra fitted well to our model, the heats of adsorption and the adsorption entropies could be calculated. The results are presented in table IV.6.

In the case of silica, the varying position of the peak maximum could not be related with the sample pretreatment at 770 K. The peak is broadened at both sides, and, as a consequence, does not fit theoretically calculated peaks. If the peak is regarded as an analogon of the first peak of the alumina spectrum, the heat of adsorption can be estimated to be 87 kJ $mole^{-1}$.

Determination of the enthalpies and entropies of adsorption of 1-butene on alumina is less accurate than those of ethene adsorption on the same oxide, the resolution of

butene peaks being poorer. By varying the carrier gas flow rate F, it was established that the poorer resolution was not caused by diffusion retardation.

Cvetanovic and Amenomiya (20) also report three desorption peaks in the ethene/γ-alumina spectrum, at about 350 K, 470 K and 570 K, respectively. They computed the activation energy of desorption to be 113 kJ mole^{-1} for the first peak, and 155 kJ mole^{-1} for the second. Consequently, the adsorption of ethene on γ-alumina is activated, the activation energy being 40-44 kJ mole^{-1} for the first peak, and 57-64 kJ mole^{-1} for the second. However, the author's analysis (20) was based on the assumption that they dealt with negigible readsorption, which is very improbable, since their apparatus and their experimental conditions were of the same type as ours. Moreover, for the determination of E_d they used the plot $2\ln(T_M) - \ln(\beta)$ versus $1/T_M$ for various values of β between 0.12 and 0.35 K s^{-1}. Use of this method is not justified because of the dependence of T_M on catalyst pretreatment. We note that their reported values of T_M agree well with these measured by us.

The authors of reference (20) show that the species desorbing at 570 K in the ethene/γ-alumina spectrum is a mixture of n-butenes, formed during the adsorption via a Rideal mechanism. This is in agreement with the first order desorption kinetics that we observed for this third peak. The low values of ΔH and ΔS (table IV.6) suggest that two ethene molecules are adsorbed at the same site, and recombine to desorb as butene. Apparently, the two ethene molecules are rather loosely bound to the site, so that ΔS, being the difference in entropy between one mole gas phase butene and two moles of adsorbed ethene, is relatively small. Application of this reasoning to the third peak of the butene spectrum suggests that this peak is associated

with the formation of an octene species.

The values of ΔS have been computed using equation (B.1.1) of section I.5.1. A plot of $\ln(C_n) - \ln\{\theta/(1-\theta)\} - b \ln(T_n)$ versus $1/T_n$ for the first peak of the ethene/ alumina spectrum gives the best straight line for b = 2, the slope of which ($= - E_M^*$) = - 24.43. The value of b = 2 suggests loss of three translational degrees of freedom, and a rotational one. For this theoretical case we calculate ΔS = 172 J mole^{-1} K^{-1}, in good agreement with the empirical value. The very limited mobility of the adsorbed ethene is consistent with the reported Rideal mechanism for butene formation.

IV.5.9 Evaluation of the TPD-method

Now that the theoretical backgrounds of the method have been discussed in detail (chapters I and II), and the results of the application on experimental desorption spectra have been presented in the preceding sections of this chapter, the relation between theory and experiment should be discussed critically.

In spite of the simplifying assumptions made when deriving the theoretical equations, the most important being the energetical homogeneity of the surface, most experimental peaks could be described astonishingly well by the theoretical model. This is the more surprising as one knows that in general the heat of adsorption strongly depends on coverage. Clewley, Lynch and Flanagan (21), for example, report an almost linear decrease in enthalpy of adsorption with coverage of the hydrogen chemisorbed on platinum in excess of the hydrogen irreversibly adsorbed at room temperature (fig. IV.17a). In view of these enthalpies of adsorption, together with E_M^* about constantly $\approx$ 20, a

more or less constant desorption rate between 100 K and 490 K is to be expected. However, when incorporating the differential entropies of adsorption, reported by the same authors (fig. IV.17b), it can be shown that 50% of this hydrogen desorbs between 320 K and 329 K. This is in remarkable agreement with the value of 324 K, measured by us, for which we computed ΔH = 51 kJ $mole^{-1}$, and ΔS = 122 J $mole^{-1}$ K^{-1}. Thus, the existence of this desorption peak, rather than a constant desorption rate, is caused by a kind of internal "compensation-effect", and the computed values of ΔH and ΔS are sort of weighted averages of the real values.

On the other hand, the enthalpies reported by Flanagan et al (21) are isosteric enthalpies, derived from Temkin isotherms, and the differential entropies are derived from them. One should therefore be careful in drawing conclusions. It can as well be argued that the resolution of thermodesorption peaks which has been obtained by us suggests the existence of a horizontal part in the $\Delta H(\theta)$ - curve (fig. IV.17a, dotted line). In fact, Cristmann and Ertl (22) report isosteric heats of hydrogen adsorption on a Pt(111) surface, derived from work function changes, to be virtually constant (40 kJ $mole^{-1}$) for $0.1 < \theta < 0.5$.

Sweet and Rideal (26) show that the enthalpy of hydrogen chemisorption on polycrystalline nickel varies little over a long range of θ. Theoretical calculations, carried out by van der Avoird et al (27) also show the enthalpy of adsorption of hydrogen on transition metals to be virtually constant over a long range of θ-values, because of the localized character of the chemisorptive bond. Nevertheless, second order peaks may be very broad, so that, in spite of the validity of the assumption of energetical homogeneity for each peak, resolution of peaks may be poor

(c.f. section II.5.3). Since Cvetanovic et al (1-3) were very well aware of external reasons for peak broadening (eddy-diffusion, pore diffusion, etc.), when constructing their apparatus, the resolution of peaks in their TPD-spectra will be governed by the physical properties of the sample, rather than by non-optimum experimental conditions. Our experiments with ethene demonstrate that the same applies for our TPD-spectra.

Recently, Verbeek and Sachtler (13) expressed their doubts about the possibility of a kinetic analysis of TPD-spectra. We agree with them insofar one deals with poorly resolved desorption spectra. Our results show that well resolved spectra lead to a consistent picture of types of adsorption and their respective enthalpies and entropies of adsorption. This picture can be used for theoretical resolution of a shoulder, for example a shoulder at 167 K on the 186 K peak of platinum (fig. IV.18), or to attack a complicated spectrum of a bi- or tri phase platinum/iridium/alumina catalyst, apparently partly covered with carbon (fig. IV.19).

IV.6 Summary

The thermodesorption apparatus designed and built by us yields satisfactory well resolved TPD-spectra of hydrogen, desorbing from platinum, iridium and their alloys. This good resolution enabled us to check the validity of our theoretical models. In spite of the simplifying assumptions underlying the model, experimental peaks could be fitted reasonably well by theoretically calculated peaks (fig. IV.20). Moreover, the enthalpies of adsorption, as obtained from the line shape analysis, are consistent with those derived from the position of the peak maxima, and led to

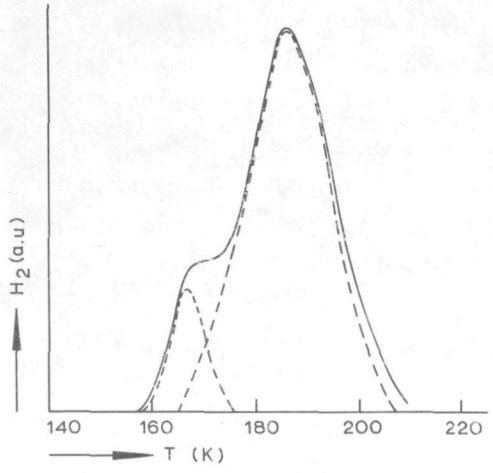

IV.18

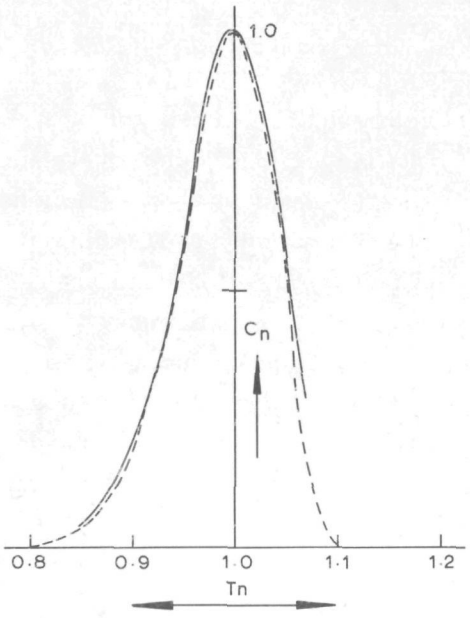

IV.20

IV.18 Deconvolution of a shoulder at 167 K in a peak at 186 K (H_2 / Pt)
Dashed lines : composing peaks
Solid line : experimental desorption curve

IV.20 Fit of a theoretical peak on an experimental desorption peak
Solid line : experimental peak at 352 K in the C_2H_4 / Al_2O_3 desorption spectrum
Dashed line : theoretical peak for first order desorption with freely occurring readsorption, $E_M^* = 24.43$, $b = 2$, $\theta_i = 0.50$, $\theta_M = 0.2077$

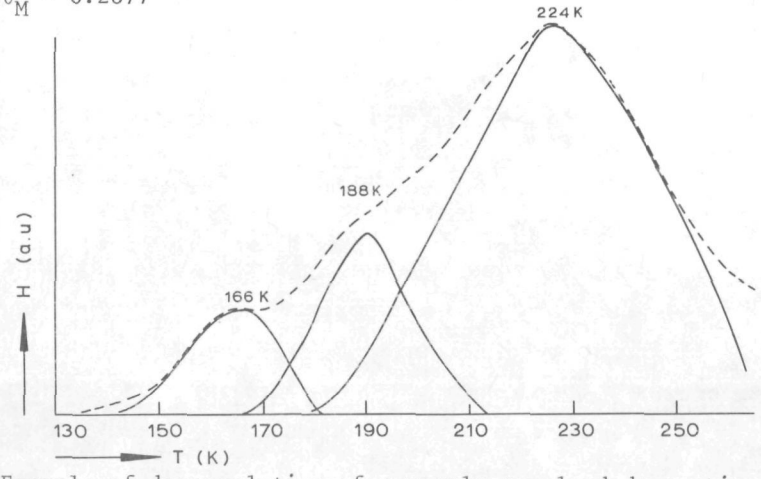

IV.19 Example of deconvolution of a poorly resolved desorption curve
Solid lines : composing peaks
Dashed line : experimental curve

reasonable values of the entropy of adsorption.

One of the desorption peaks has been tentatively ascribed to the phenomenon of dissolution of hydrogen in platinum and iridium. Another peak, found on platinum, appears to be caused by contamination of the surface with carbon. The presence of only a small amount of iridium in the surface reduces this peak to virtually zero, suggesting that a carbonaceous deposit on platinum can be removed by atomic hydrogen from iridium sites.

The TPD results confirm the surface enrichment in platinum, as observed by AES. Though platinum and iridium differ only slightly in their behaviour towards hydrogen, some of their alloys show a shift of peak maxima to lower temperatures. This seems to be consistent with the postulated phase diagram no. 3 (section III.3), according to which ordering should occur near 25% iridium.

Thermodesorption of ethene from silica and alumina reveals the existence of one type of site on the former, and two types on the latter oxide.
Moreover, dimerization to butene on alumina takes place via a Rideal mechanism: a second ethene molecule adsorbs on an occupied site, and both ethene molecules combine to desorb as one butene molecule, the desorption process being rate determining.

Concluding remarks:

- The theoretical model can be applied successfully to experimental desorption spectra, provided that the peaks are sufficiently resolved
- when treated in this way, thermodesorption spectra yield valuable information with respect to surface contamination, dissolution of hydrogen, the effect of alloy formation, and possible carrier effects.

References

1. Komers, R., Amenomiya, Y., Cvetanovic, R.J., J. Catal., 15 (1969) 293

2. Tsuchiya, S., Amenomiya, Y., Cvetanovic, R.J., J. Catal., 19 (1970) 245

3. Cvetanovic, R.J., Amenomiya, Y., Advan. Catal., 17 (1967) 103

4. Stephan, J.J., Thesis, Leiden (1975)

5. Escard, J., Leclère, C., Contour, J.P., J. Catal., 29 (1973) 31

6. Mimeault, V.J., Hansen, R.S., J. Chem. Phys., 45 (1966) 2240

7. Kulifay, S.M., J. Am. Chem. Soc., 83 (1961) 4916

8. Platinum determination
   a) Beamish, F.E., "The Analytical chemistry of noble metals", Pergamon Press (1966) p. 454 - 460
   b) Ayres, G.H., Meyer, A.S., Anal. Chem., 23 (1951) 299

9. Iridium determination
   Mac Nevin, W.M., Kriege, O.H., Anal. Chem., 28 (1956) 16

10. Raub, E., Plate, W., Z. Metall kd., 47 (1956) 688

11. Konvalinka, J.A., Scholten, J.J.F., J. Catal., in press

12. Paal, Z., Thomson, S.J., J. Catal, 30 (1973) 96

13. Verbeek, H., Sachtler, W.M.H., J. Catal., 42 (1976)257

14. Aben, P.C., van der Eyk, H., Oelderik, J.M., Proc. 5th. Int. Congr. Catal., North Holland, Amsterdam / London (1973) Vol. 1, p. 717

15. Kinoshita, K., Lundquist, J., Stonehart, P., J. Catal., 31 (1973) 325

16. Leclère, C., Contour, J.P., Pannetier, G., Ann. Chim., (1974) 221

17. Contour, J.P., Pannetier, G., Bull. Soc. Chim. France, (1969) 2658

18. Figueras, F., Mencier, B., Bacaud, R., Urbain, H., C. R. Acad. Sci., 270 C (1970) 769

19. Hermann, R.A., Adler, S.F., Goldstein, M.S., De Baum, R.M., J. Phys. Chem., 65 (1961) 2189

20. Cvetanovic, R.J., Amenomiya, Y., Catal. Rev., 6 (1972) 21

21. Clewley, J.D., Lynch, J.F., Flanagan, T.B., J. Catal., 36 (1975) 291

22. Christmann, K., Ertl, G., Pignet, T., Surf. Sci., 54 (1976) 365

23. Boudart, M., Alday, A.W., Vannice, M.A., J. Catal., 18 (1970) 46

24. Peri, J.B., J. Phys. Chem., 69 (1965) 211

25. Okkerse, C., in: "Physical and chemical aspects of adsorbents and catalysts", B.G. Linsen, ed. Academic Press, London / New York (1970), p. 257

26. Sweet, G., Rideal, E., Actes 2ième Congr. Int. Catal., Paris 1960, Tome I, p. 175

27. Fassaert, D.J.M., van der Avoird, A., Surf. Sci., 55 (1976) 313.

Chapter V

Conversion of hexane and heptane over alumina supported Pt - Ir catalysts

V.1 Introduction

Our interest in the Pt - Ir system was initiated by its growing importance in hydrocarbon reforming. Patents on this subject claim an improvement of catalyst activity, selectivity and stability when iridium is added to the traditional Pt/γ-Al_2O_3 reforming catalyst (1-4). It seemed therefore interesting to investigate the behaviour of supported platinum/iridium catalysts when converting hydrocarbons in a hydrogen atmosphere. In view of the patents cited above, γ-alumina seemed to be the best catalyst-support for this purpose.

Out of the three parameters of interest (activity, selectivity and stability), selectivity is the one which is investigated most readily. Moreover, when investigating the selectivity behaviour of various catalysts, one obtains qualitative information about activity and stability as well. Though the selectivity generally depends on reaction temperature, most experiments have been carried out at about 650 K.

Preliminary experiments with hexane showed an important production of methylcyclopentane to take place, but no cyclohexane or benzene was formed. Since aromatics are very

important because of their high octane number, we chose heptane as a starting material for most of our experiments, because this hydrocarbon is easily dehydrocylcisized via 1,6-ring-closure. Indeed, a fair amount of toluene is formed when we convert heptane over platinum-rich catalysts, together with ethyl-cyclopentane and methylcyclohexane.

In view of the aim of the reforming process, i.e. increasing the octane number of a naphta, desired products are branched alkanes, cycloalkanes (and cyclo-alkenes), and aromatics. Hydrogenolysis and formation of a carbonaceous deposit , however, should be suppressed, though a limited degree of coking may favourably influence the selectivity of the catalyst. Excessive coke formation is one of the most important cost factors in reforming catalysis,since it makes regular reactivation of the catalyst necessary. Moreover, high hydrogen pressures are required, which implies expensive reaction equipment and a low yield of aromatics. If one would be able to develop a catalyst which suffers little or not from coking, the reforming process could be carried out at lower hydrogen pressures, resulting in a higher selectivity for the formation of aromatics (5). It will be clear that comparison of initial selectivity with steady state selectivity may provide useful information about this feature.

In the apparatus designed by us, hydrocarbon conversion is carried out at atmospheric pressure. Experimental details are discussed in section V.2.1. The results of the hydrocarbon conversion experiments are reported in section V.3. In the discussion (section V.4) an interpretation of these results is given, in connection with the theoretical phase diagram and the TPD-results. Some attention is given to the influence of chlorine, introduced into the catalyst system during catalyst preparation. The influence of coke-formation will be discussed in some detail.

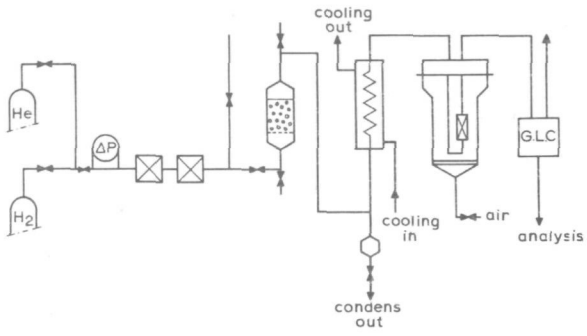

V.1 Flow apparatus for hydrocarbon conversion (see text)

For the conversion of hydrocarbons over platinum metals, various mechanisms have been proposed, which are reviewed by Clarke and Rooney (15). For hydrocarbons having at least five carbon atoms, there are two important mechanisms, which may act simultaneously.

The first, proposed by Anderson and Avery (20) under the term "bond-shift" involves an unsaturated intermediate product polyadsorbed at 1-3 (scheme 1). Once this intermediate has been formed, it may lead, by rearrangement under the effect of hydrogen, to an isomerization or a hydrogenolysis.

The second mechanism, proposed by Barron et al.(21) involves a cyclopentane intermediate, probably adsorbed on a single platinum atom (scheme 2). Hydrocarbon molecules containing six or more carbon atoms can form cyclic products via a 1-6 ring closure mechanism, similar to the 1-5 ring closure described above. According to Clarke and Rooney (15) carbided surfaces show a preference for 1-6 ring closure.

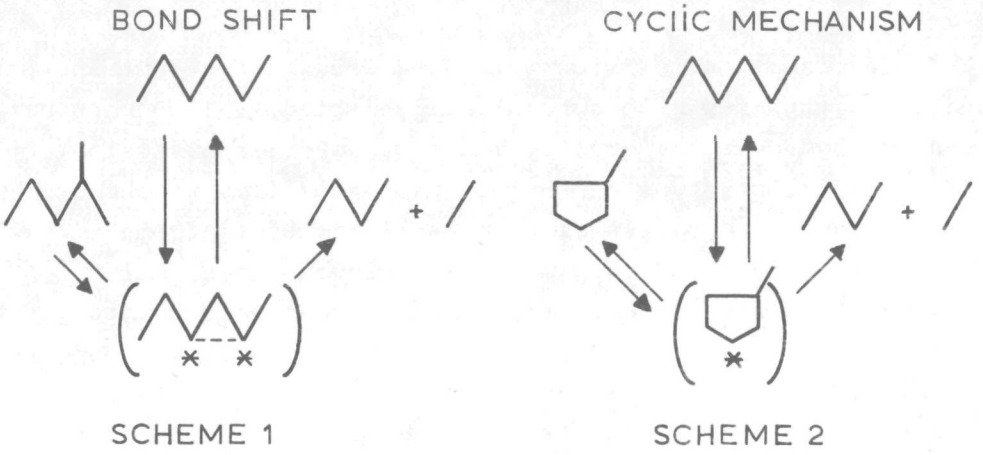

When these schemes are valid, the bond-shift mechanism would require a dual site, whereas the cyclic mechanism proceeds via a single site. Clarke and Rooney (15), however, propose a single site bond-shift mechanism (vinyl-shift). On this basis, Clarke (16) presents the following scheme of possible reactions and the type of sites on which they may take place:

- alkane isomerization (cyclic or bond-shift, both may lead to hydrogenolysis as well), and aromatization: single site
- alkane hydrogenolysis and surface carbiding: dual site
- self-poisoning with graphitic products and total alkane hydrogenolysis (towards methane): sites consisting of three or more metal atoms.

V.2 Experimental

V.2.1 Apparatus and procedure

Hydrocarbon conversion reactions were carried out in the apparatus depicted schematically in fig. V.1. A constant flow of hydrogen, metered by means of a Porter precision flow controller, type WCD - 1000, is freed from traces of oxygen over a copper on alumina catalyst (R3-11 from B.A.S.F.), and dried over molecular sieves Linde, Union Carbide type 3A. Subsequently, the hydrogen passes through the evaporator (fig. V.2), where it is saturated at room temperature with the vapour of the hydrocarbon to be converted. In the condensor, the gas-mixture is cooled to a pre-chosen temperature, as to achieve a hydrogen/hydrocarbon ratio of about 17. The reactor consists of a u-shaped stainless steel tube (4 mm internal diameter), in which the position of the catalyst bed is fixed by means of quartz-wool. A uniform temperature can be obtained making use of a fluid bed oven, filled with aerosil particles of 0.4 mm diameter. When a constant flow of air in the oven is maintained, and a constant potential governs the heating current, the temperature remains constant to within 1 K. The uniformity of the temperature is better than 0.1 K.

Samples of the mixture of reaction products are taken by means of a six-way sampling valve, and analyzed by means of gas/liquid chromatography. The column is a 3 meter silanized stainless steel tube of 3 mm internal diameter, filled with 25% squalane on chromosorb W.AW (100 - 120 mesh). The column is thermostated at 325 $\pm$ 0.5 K. The flow of the carrier gas (He) is maintained at 0.67 cm^3 (NTP) s^{-1}. Under these conditions, the reaction product with the longest retention time is toluene (4700 s), so that the whole

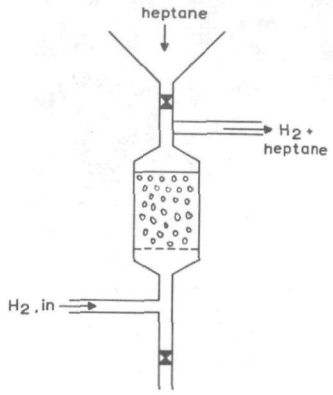

V.2 Evaporator, in which the hydrogen flow is saturated with hydrocarbon vapour

analysis takes about 1½ hrs. All possible reaction products can be separated over the gc-column, except for 2,2- and 2,4-dimethylpentane.

The detection part of the gas chromatograph consists of a flame ionistation detector, connected with a Hewlett - Packard electrometer model 5704 A. The signal thus obtained is registered on a chart recorder (Yokogawa, type 3051), and integrated by a digital integrator (Infotronics, CRS - 204).

Temperature measurement takes place in the condensor and in the reactor by means of chromel/alumel thermocouples, and in the fluid bed of the reactor oven by a Pt-100 platinum resistance thermometer. There is no detectable difference (< 0.1 K) between the temperature of the oven and the temperature in the reactor.

In most experiments the reactor temperature was 650 K. The value of W/F was chosen as to yield conditions for differential reactor behaviour. The regime for differential

behaviour was tested by varying both W (the weight of the catalyst) and F (the flow of reactants). Most experiments were carried out with $W/F = 77$ kg s mole^{-1}. Some of the samples had too high an activity as to behave differentially under these conditions. Those samples gave complete conversion to methane, and were not considered to be useful reforming catalysts. The samples can be reduced in situ in a hydrogen flow.

V.2.2 Materials

Hydrogen and helium are of high purity quality. The hydrogen is further purified over a palladium diffusion unit, operated at 580 K. Further purification over the Cu/Al_2O_3 catalyst is, in fact, not necessary, except when hydrogen is incidentally mixed with helium, which may contain traces of oxygen.

Heptane was purchased from Aldrich Europe, Belgium (lot no. 0A 032827), and was of "99+%" quality. It was purified by evaporation at room temperature, followed by condensation at 273 K. After this purification, the only impurity that could be detected was methylcyclohexane (ca. 0.1%). The hexane used was of spectroscopic quality (Merck, "für die Spectroscopie", Lot no. 4085084). It was subjected to the same purification as described for heptane. Afterwards, only 3 methylpentane (0.5%) could be detected as an impurity. Other hydrocarbons, used for establishing the retention volumes of possible reaction products, were of reagent grade purity.

For most catalysts, γ-alumina (AKZO, 0003P, $S_{BET} = 248$ m^2 g^{-1}) was used as a support, and only incidentally α-alumina (Rhône-Progil, SCS 9, $S_{BET} = 24$ m^2 g^{-1}). In the following, alumina is γ-alumina, unless otherwise

stated. See for materials used in catalyst preparation section IV.2.2. A number of catalysts were prepared by adsorption of H_2PtCl_6 and/or H_2IrCl_6 from aqueous solution on the alumina surface, followed by drying at 380 K and calcination in air at 800 K. Most catalysts, however, were prepared by the impregnation technique, described in section IV.3.1.2.

V.3 Description and results of hydrocarbon conversion experiments

V.3.1 Introduction

The hydrocarbon conversion experiments can be classified with regard to the type of catalyst used, and the hydrocarbon of which the conversion has been studied. In doing so, we arrive at the following scheme:

1) hexane conversion over catalysts, prepared via adsorption of H_2PtCl_6 and/or H_2IrCl6 on γ-alumina (type-1 catalysts)
2) conversion of heptane over impregnated α-alumina (type-2)
3) hexane conversion over impregnated γ-alumina catalysts with a high metal load (2.4 - 4.7 weight %, type-3)
4) heptane and, incidentally, hexane conversion over impregnated γ-alumina catalysts with a low metal content (type-4)

When impregnating γ-alumina, additional chlorine was added in the form of about 3 cm^3 of concentrated HCl. During the preparation of the impregnated α-alumina catalyst, no hydrogen chloride was added.

V.3.2 Gas chromatography and definitions of selectivities

As has been stated in section V.2.1, nearly all reaction products can be separated on our gas chromatographic column. The retention times of both reactants (hexane and heptane) have been determined experimentally, together with those of ten of the possible reaction products (methane, ethane, propane, butane, pentane, 2-methyl pentane, 3-methyl pentane, 2-methyl hexane, 3-methyl hexane, and toluene). The retention times t_x thus measured can be converted into values of the dimensionless parameter I_x, making use of the equation:

$$I_x = 100 \{i + \log (t_x/t_i) / \log (t_{i+1}/t_i)\} \qquad (V.1)$$

where t_i = the retention time of the alkane with i carbon atoms, t_{i+1} is the analogon for i+1 carbon atoms; $t_i < t_x < t_{i+1}$.
The computed I_x values agreed to within 1% with those reported by Schupp and Lewis for squalane columns (6). It was therefore considered a sound assumption that the retention times of the other possible reaction products can be computed on the basis of the reported I_x - values. In this way, all peaks in the chromatogram could be identified (fig. V.3).

The principle underlying the flame ionisation technique implies that the signal obtained is roughly proportional to the number of carbon atoms in the molecule. Making use of the correction factors reported by Dietz (7), the integrated peak surfaces can be converted to mole fractions of hydrocarbons in the product mixture. Since there are eighteen different hydrocarbons in the product mixture obtained when heptane is converted over γ-alumina supported Pt - Ir catalysts, it is not considered useful to report

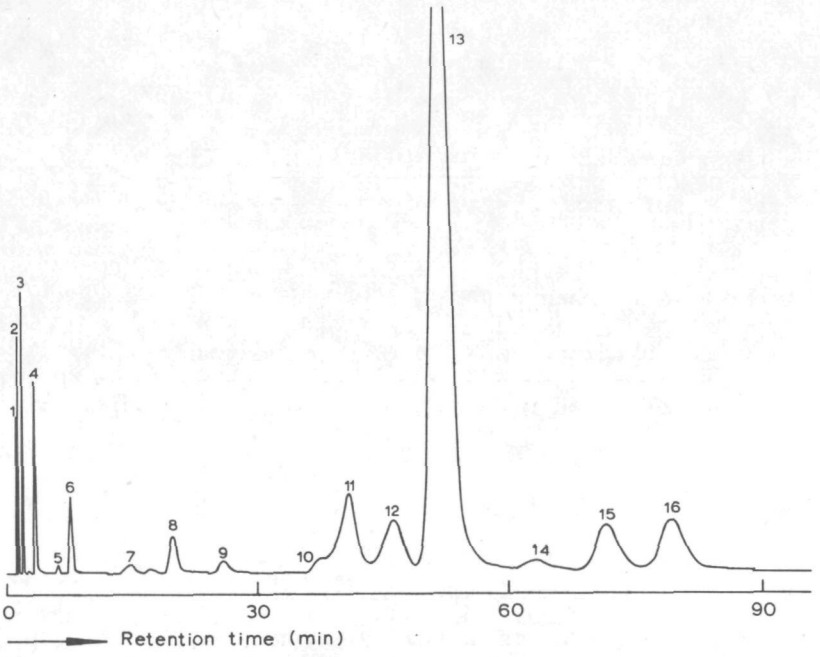

V.3 Chromatogram of a heptane conversion product mixture.
1: methane; 2: ethane; 3: propane; 4: butane; 5: methylbutane; 6: pentane; 7: 2-methylpentane; 8: hexane; 9: 2,2-dimethylpentane; 10: 2,3-dimethylpentane; 11: 3-methylhexane; 12: 3-ethylpentane; 13: heptane; 14: methylcyclohexane; 15: ethylcyclopentane; 16: toluene

detailed product distributions. Instead, when discussing catalyst behaviour, use will be made of four different "selectivities", computed according to the following equations:

Hydrogenolysis selectivity

$$S_h = \frac{\text{total of hydrocarbons having less than 7 C-atoms}}{\text{total of converted heptane}} \times 100 \qquad (V.2)$$

Isomerization selectivity

$$S_i = \frac{\text{total of branched alkanes with 7 C-atoms}}{\text{total of products with 7 C-atoms}} \times 100 \quad (V.3)$$

Cyclization selectivity

$$S_c = \frac{\text{cyclic hydrocarbons, aromatics excluded}}{\text{total of products with 7 C-atoms}} \times 100 \quad (V.4)$$

Aromatization selectivity

$$S_a = \frac{\text{aromatics}}{\text{total of products with 7 C-atoms}} \times 100 \quad (V.5)$$

The above definitions apply for the conversion of heptane. For hexane conversion, "7 C-atoms" should be replaced by "6 C-atoms", and "heptane" by "hexane".
Additionally, the selectivity S_{nd} for non-destructive reactions is defined by

$$S_{nd} = S_i + S_c + S_a \quad (V.6)$$

so that

$$S_{nd} + S_h = 100 \quad (V.7)$$

Moreover, when studying heptane conversion the following product concentration ratios will appear to be useful:

$$C_{5,6} = \frac{[\text{ethylcyclopentane}]}{[\text{methylcyclohexane}] + [\text{toluene}]} \qquad (V.8)$$

$$i_{5,6} = \frac{[\text{ethylpentane}]}{[\text{2-methyl hexane}] + [\text{3-methyl hexane}]} \qquad (V.9)$$

$$h_{3+4} = \frac{[\text{butane}] + [\text{propane}]}{[\text{hydrogenolysis products}]} \qquad (V.10)$$

Furthermore, the conversion, ξ, is defined in the usual way:

$$\xi = \frac{\text{amount of hydrocarbon converted in the reactor}}{\text{amount of hydrocarbon in the feed of the reactor}} \qquad (V.11)$$

The reported values of ξ are steady state conversions. During a period varying from 24 to 300 hrs, depending on the iridium content of the sample, the activity of the catalyst decreases. The steady state is supposed to be reached if the activity is constant to within experimental error for at least 24 hrs. (c.f. section V.3.9).

V.3.3 Hexane conversion over type-1 catalysts

The hexane conversion performances of some of the type-1 catalysts were tested under the following conditions: reactor temperature = 650 $\pm$ 2 K, total pressure = 10 N m^{-2}, H_2 / hexane ratio = 17 , hydrogen flow = 100 $\pm$ 1 mm^3 (NTP) s^{-1}.

Table V.1

code	M	$Ir_{\%}$	ξ	S_{nd}	S_{meth}
A_1	2.36	19	8.5	0	67
A_2	1.86	48	11	0	64
A_3	1.41	65	6.5	0	72

Table V.1

Product distribution of hexane conversion at 650 K over catalysts, obtained by adsorption of metal salts on γ-Al_2O_3 (type-1)

M = metal load in weight %

Ir gives the iridium content in atom % of the total metal load

S_{meth} = (moles of methane formed)/(total moles of carbon converted)

The results are collected in table V.1. It is seen that, in spite of the rather low conversion, all three catalysts show exclusively hydrogenolysis activity, methane being the preponderant reaction product. At a lower reaction temperature (600 K), other reaction parameters remaining unchanged, the conversion shows a slight decrease, but the relative product distribution is the same.

In X-ray diffraction, the catalysts appeared to contain pure platinum, pure iridium, and one or two alloy phases.

Presumably, when deposited via this adsorption method, the metal particles formed are more or less in thermodynamic equilibrium. Consequently, monophasic solid solutions cannot be obtained in this way, as the phase diagram shows a large

miscibility gap (chapter III). Therefore, type-1 samples were not considered appropriate to study bimetallic Pt - Ir reforming catalysts, and were not investigated further.

V.3.4 Hexane conversion over type-2 catalysts

In order to investigate in how far hydroxyl groups and/or Lewis-acid sites play a role in reforming, some experiments were performed with α-alumina instead of γ-alumina as a carrier. α-Alumina has a very low BET surface area (24 $m^2\ g^{-1}$), and no hydroxyl groups on its surface. This is the reason for its high degree of inertness in catalysis. Possible carrier effects have been reduced further by preparing α-alumina supported catalysts having a high metal load.

Table V.2

code	$M_{\%}$	$Ir_{\%}$	ξ	S_i	S_c	S_a	S_{meth}
W9	16.3	0	10	57	26	0	-
W6	5.6	32	100	0	0	0	100
W5	12.8	70	100	0	0	0	100
W10	5.8	100	100	0	0	0	100

Table V.2
Product distributions of hexane conversion at 650 K over impregnated Pt-Ir α-alumina catalysts (type-2)
For explanation of symbols: see table V.1 and section V.3.2

Hexane conversion was carried out under the same conditions as described in section V.3.3. The results are presented in table V.2. The activity and selectivity of α-alumina supported platinum are very similar to the activity and selectivity obtained with platinum/γ-alumina as a catalyst (section V.3.5 and V.3.6). Addition of iridium makes the conversion increase considerably. As a consequence, the reactor was not operated under differential conditions any more. Methane was the only reaction product over iridium containing type-2 samples.

These results will be discussed in section V.4, in comparison with the performance of the γ-alumina supported samples.

V.3.5 Hexane conversion over type-3 catalysts

As demonstrated in section V.3.3 our catalysts obtained by adsorption of Pt and Ir metal salts at the surface of γ-alumina were no good reforming catalysts. Therefore, we prepared a new series of samples by the impregnation technique described in section IV.3.1.2. Contour et al.(8) propose an interesting mechanism for the interaction of iridium with η-alumina in the case that chloride ions are present in the solution during the impregnation. For this reason, the impregnation was carried out in the presence of excess of chloride ions, by adding 3 cm^3 of concentrated HCl to the solution.

The first series thus prepared had a rather high metal load (table V.3). As a consequence, the mean metal particle size, as determined from X-ray line broadening, was rather large for this series (50 $\pm$ 5 nm). Nevertheless, all bimetallic samples contained only one alloy phase.

The hexane conversion over these catalysts shows an

interesting pattern of product distributions (table V.3,

Table V.3

code	$M_{\%}$	$Ir_{\%}$	ξ	S_i	S_c	S_a	S_h
W 8	3.82	0	44	31	5	0	64
W 4	4.72	11	44	32.6	13.6	0	53.8
W 3	2.36	19	20	45.5	21.5	0	33.0
W 2	3.72	48	12	47.8	25.2	0	27.0
W 7	4.12	100	8	39.6	0	0	60.4

Table V.3
Product distribution of hexane conversion at 650 K over impregnated Pt - Ir / γ-Al_2O_3 catalysts with relatively high metal load (type-3)

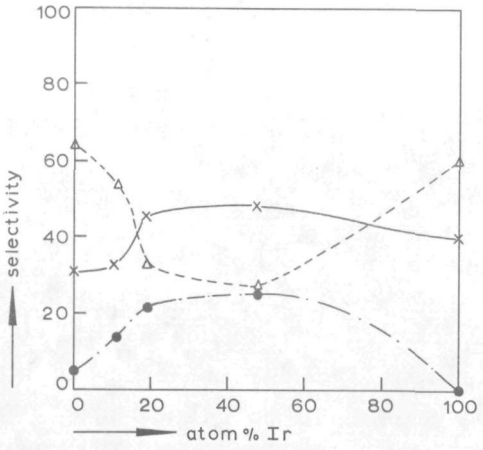

V.4 Hexane conversion over type- 3 catalysts.
X isomerization selectivity, S_i
Δ hydrogenolysis selectivity, S_h
● cyclization selectivity, S_c

fig. V.4). In contrast with the α-alumina supported samples, the catalysts on γ-alumina show an increase in both isomerization and cyclization selectivity when the iridium content increases from 0% to 50%. When more than 50% iridium is present, the catalysts exhibit a higher hydrogenolysis selectivity, though the conversion decreases with increasing iridium content. Again, hydrogenolysis appears to be an iridium propensity. When supported on γ-alumina, iridium shows a much higher isomerization selectivity and a much lower overall activity than the α-alumina supported sample.

V.3.6 Hexane conversion over type-4 catalysts

Type-4 catalysts are identical with type-3, except for the lower metal content. If there is an effect of the supported γ-alumina on the catalytic conversion of hydrocarbons, it is expected to be more pronounced for the type-4 series.

As a result of the lower metal content, metal crystallites in type-4 samples have smaller mean diameters than found in type-3 ($\bar{d}_w$, from X-ray line-broadening, is 15 nm, against 30 nm for type-3).Moreover, the presence of very small particles ($d < 2$ nm) on the former type of catalysts should not be excluded. Those bimetallic samples of the type-4 series that have been investigated by X-ray diffraction showed one metallic phase only, indicating complete mixing of the constituent metals, at least, in those particles which are large enough to be detectable by X-ray diffraction.

The results of the conversion of hexane over three of these catalysts are presented in table V.4. Fig. V.5 clearly demonstrates that the effect of adding iridium to plati-

num strongly depends on the resulting alloy composition. Comparison with type-3 catalysts shows that, the lower the metal content, the lower the hydrogenolysis selectivity, even when the conversion is as high as 50.

Table V.4

code	$M_{\%}$	$Ir_{\%}$	ξ	S_i	S_c	S_a	S_h
W 13	1.70	0	15	31	50	0	19
W 12	1.75	4	50	60	16.4	0	23.5
W 14	1.80	8	6	14	67	0	19

Table V.4

Product distributions of hexane conversion at 650 K over impregnated Pt - Ir / γ-Al_2O_3 catalysts with relatively low metal load (type-4)

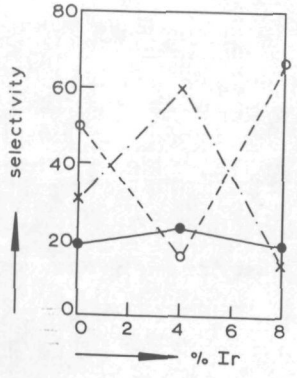

V.5 Hexane conversion over type- 4 catalysts
× isomerization selectivity, S_i
○ cyclization selectivity S_c
● hydrogenolysis selectivity, S_h

V.3.7 Conversion of heptane over type-4 catalysts

Though two of the three type-4 catalysts, that have been tested in hexane conversion, showed a remarkably high selectivity for cyclic reaction products, no aromatics (i.e. benzene) could be detected in the product mixture. In fact, the only cyclic product was methylcyclopentane, indicating that 1,6-ring closure of hexane does not occur on these catalysts under the reaction conditions applied here (section V.3.3). However, a group of French workers (9) reports a remarkable production of toluene when converting heptane over α-alumina supported Pt - Ir catalysts, their reaction conditions being comparable with ours. It seemed worthwhile to test heptane conversion over our type-4 catalysts as well. The results, presented in table V.5 and Fig. V.6 indeed show a considerable production of toluene when conversion of heptane is carried out over platinum-rich samples (of course, toluene is the only aromatic product of heptane conversion). The H_2/heptane ratio was 17; the other conditions were still the same as for hexane conversion over type-1 catalysts (section V.3.3) and over type-2 and type-3 catalysts.

S_a = 21 for the supported platinum sample, and S_a = 0 for iridium / γ-Al_2O_3. The decrease in selectivity to aromatics is almost linear in iridium content, though there is a small but significant dip near an iridium content of 25%.

We note that the pure iridium sample is much less active than the platinum-rich ones, but shows a considerable isomerization selectivity, whereas the more active type-2 and type-3 iridium catalysts have pronounced hydrogenolysis activity. Furthermore, we observe that the shapes of the S_i - curve and the S_c - curve are mirror-symmetrically related to each other: a maximum in the S_i - curve is

Table V.5

code	$M_{\%}$	$Ir_{\%}$	ξ	S_i	S_c	S_a	S_h
W 13	1.70	0	30.0	40.0	20.0	21.0	19.0
W 12	1.74	4	22.0	44.6	18.5	19.8	17.0
W 14	1.80	8	10.0	35.9	25.8	16.4	21.9
W 15	1.80	10	10.5	36.4	24.9	17.6	21.9
W 20	1.65	23	11.1	67.6	11.3	12.3	8.8
W 27	1.70	27	9.7	39.2	32.1	9.2	19.5
W 22	1.63	30	14.0	31.8	34.1	15.0	19.1
W 24	1.60	47	8.0	44.1	31.0	11.7	13.2
W 23	1.60	73	8.6	53.8	24.1	7.6	13.5
W 25	1.71	100	1.0	70.7	0	0	29.3

Table V.5

Product distributions of heptane conversion at 650 K over impregnated Pt-Ir / γ-Al_2O_3 catalysts with relatively low metal load (type-4)

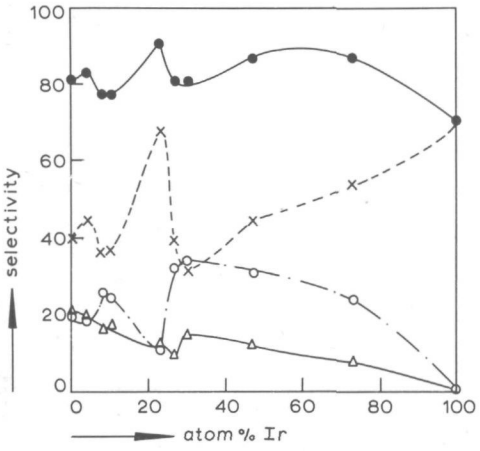

V.6 Heptane conversion over type-4 catalysts
Δ aromatization selectivity, S_a
O cyclization selectivity, S_c
X isomerization selectivity, S_i
● selectivity for non-destructive reactions, S_{nd}

associated with a minimum in the S_c - curve at the same catalyst composition, and vice versa. In the region 30% to 100% Ir range the iridium character of the catalyst (high isomerization selectivity, no cyclization) increases almost linearly with iridium content. In the region 0 - 30% Ir, both the S_i- and the S_c curve show a complex shape, 5%, 10%, 25% and 30% iridium being crucial alloy compositions.

As for type-3 catalysts, the catalyst activity declines with iridium content, the effect being more pronounced for type-4 catalysts.

V.3.8 Influence of reaction temperature on heptane conversion

With three of the type-4 samples, heptane conversion has been carried out at higher temperatures. The results are collected in table V.6. Comparison with table V.5 reveals some interesting trends. In all cases, the conversion increases with increasing temperature. Nevertheless, the selectivity for non-destructive reactions remains virtually constant. All samples show a remarkable increase in toluene production, at the expense of S_i and S_c. It is interesting to note that at temperatures above 650 K, toluene is also formed over γ-alumina supported iridium, though at 650 K this sample does not show any cyclization activity. How these phenomena can be reconciled with current ideas with regard to the mechanisms of hydrocarbon conversion over platinum metal catalysts will be discussed in section V.4.4.

V.3.9 Change in catalyst activity with time; coke deposition

All our catalysts are subjected to in situ reduction in a hydrogen flow (100 mm^3 (NTP) s^{-1}) at 650 K for 16 hrs., after calcination in air at 770 K. Subsequently, the hydrogen/hydrocarbon mixture is fed to the reactor, which is still at 650 K. During the first few days, catalyst activity, characterized by the conversion, ξ, attained under the conditions described in section V.3.3, is not constant. The change in catalyst activity with time is depicted in fig. V.7 for various type-4 samples. It is seen in this figure that platinum-rich samples show a slow but prolonged deactivation. During this deactivation period, the material

Table V.6

code	T_K	ξ	S_i	S_c	S_a	S_h
W 13	748	84.3	23.2	3.8	47.2	25.8
W 13	773	81.7	14.9	3.3	66.8	15.0
W 20	733	73.5	43.9	3.4	37.0	15.7
W 20	773	77.6	10.2	0.7	62.2	26.9
W 25	743	6.5	48.0	0	29.0	23.0
W 25	758	6.6	43.2	0	33.5	23.3

Table V.6

Product distributions of heptane conversion over some type-4 catalysts at temperatures above 650 K

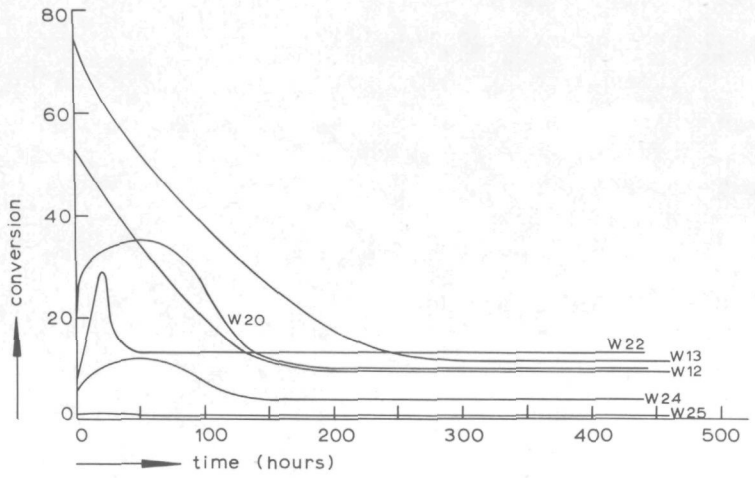

V.7 Catalyst activity as a function of time for various type-4 Pt-Ir /γ-Al_2O_3 catalysts. Total metal load: 1.7 weight %
W 13: 100% pt ; W 12 : 4% Ir ;
W 20: 23% Ir ; W 22 : 30% Ir ;
W 24: 47% Ir ; W 25 : 100% Ir

balance over the reactor shows a hydrocarbon deficit, indicating that some kind of carboneaceous deposit is formed on the catalyst. Platinum-rich samples which have been used in the reactor have a dark-grey colour, and show a "loss on ignition" (loss in weight as a result of heating in air for 1 hr. at 770 K) of about 5 weight % (10% for Pt/γ-Al_2O_3).

Iridium-rich samples have an initial conversion which is much lower than that of platinum-rich samples having the same total metal content (1.7 weight %). The activity of the former group increases, passes through a maximum, and decreases somewhat, until a steady state activity is reached. This steady state activity decreases with increasing iridium content. The iridium-rich samples form little or no coke deposit, and their loss on ignition is less than

one weight %. Used samples are only slightly darker in colour than fresh catalysts. This difference in colour may be due to the formation of metal particles during the reduction. The implications of these phenomena will be discussed in section V.4.4.

V.4 Discussion

V.4.1 Introduction

In the foregoing sections, the point was stressed already that both the type of alumina and the metal load may have an influence on the catalytic performance. Especially a possible interpretation in terms of a "carrier effect" asks for our attention.

Furthermore, we will concentrate on our results with our type-4 catalysts, because of their rich selectivity pattern, including the production of aromatics, and the considerable selectivity of iridium-rich samples for non-destructive reactions.

V.4.2 Effect of the support

When comparing the product distribution of hexane conversion over platinum catalysts of types 2, 3 and 4 (table V.7), a clearcut carrier effect cannot be distinguished. It is true that S_c is rather low for sample W 8, (γ-Al_2O_3), but this might be due to the high conversion. Supported iridium, however, shows a marked effect of both the metal load and the carrier (table V.7). Over the α-alumina supported sample (W 10), all hexane is converted into methane. This is in agreement with the "hydrogenolysis character" of iridium, which has been reported by several authors (9-12). It will be clear that we have no differen-

Table V.7

code	sup	$M_{\%}$	$Ir_{\%}$	C_6/C_7	ξ	S_i	S_c	S_a	S_h	S_m
W 9	α	16.3	0	C_6	10	57	26	0	17	-
W 8	γ	3.82	0	C_6	44	31	5	0	64	-
W 13	γ	1.70	0	C_6	15	31	50	0	19	-
W 13	γ	1.70	0	C_7	30	40	20	21	19	-
W 10	α	5.8	100	C_6	100	-	-	-	100	100
W 7	γ	4.12	100	C_6	8	40	0	0	60	-
W 25	γ	1.71	100	C_7	1	71	0	0	29	-

Table V.7

Influence of the metal content of the catalyst and the type of alumina used as support on the product distributions of hexane and heptane conversion at 650 K

sup = type of alumina used as support

C_6/C_7 = type of hydrocarbon converted

C_6 = hexane, C_7 = heptane

S_m = selectivity towards methane

tial reaction conditions in this case, since the conversion, ξ, is 100. Fréty et al. (9) report S_h to be about 90 when heptane is converted over Ir/α-Al_2O_3 under differential conditions.

The γ-alumina supported iridium samples, however, show a considerable isomerization selectivity. This effect is stronger for the catalyst with the lower metal content.

In chapter IV we have already mentioned the possible incorporation of iridium in the alumina lattice as Ir (III) (8). In fact, part of the iridium of our type-4 catalyst W 25 appeared to be soluble in a concentrated aqueous hydrogen chloride solution, indicating the presence of non-reduced iridium.

The influence chorine has on catalyst selectivity is well-known for alumina-supported platinum. Goble and Lawrance(14) report an enhancement of the isomerization activity, exhibited by alumina supported platinum, when chlorine is added to the support. The effect is dependent on the type of alumina: bayerite (β-alumina) > pseudo-boehmite (α-alumina). This supports the views, defended by Leclère et al. (8), that platinum can be incorporated in alumina via the same mechanism as they describe for the formation of their Ir (III) complex, in which chloride ions and surface hydroxyl-groups are essential.
The γ-alumina used by us was not subjected to a heat treatment prior to the catalyst preparation, so it contained many surface hydroxyl groups.

We assume that the isomerization selectivity of γ-alumina supported iridium is enhanced as a result of the formation of octahedrically surrounded Ir(III) complexes, oxygen, hydroxyl, and chloride ions being the most important ligands. The interaction of the metal ion with the support takes place at an electronegative (Lewis acid) site on the

alumina surface. Isomerization of a hydrocarbon molecule may take place via a cyclic intermediate, followed by selective hydrogenolysis of one of the C-C bonds, or via a bond shift mechanism. The absence of cyclic products at 650 K may point to the bond shift mechanism to be operative in the isomerization; the carbonium ion bond shift mechanism proposed by Rooney and Clarke (15) is the most probable one for isomerization over iridium-in-interaction-with-γ-alumina.

The question remains why the selectivity of our supported platinum samples is much less influenced by the nature of the support than that of iridium. Betizeau et al. (13), who used a method of catalyst preparation very similar to ours, report only marginal differences in activity in benzene hydrogenation and cyclopentane hydrogenolysis between Pt/α-Al_2O_3 and Pt/γ-Al_2O_3. So, unlike iridium, the hydrogenolysis activity is more or less independent of the kind of alumina.

The platinum of our sample W 13 appeared to be (at least partly) soluble in a concentrated hydrogen chloride solution, indicating that platinum can interact with the support under the conditions applied. Presumably, the steady state selectivity of supported platinum catalysts is mainly governed by the formation of a carbonaceous deposit on them. Hence, the effect of the support is much less pronounced than in the case of iridium. Initial selectivities for hydrogenolysis do show a carrier effect for platinum that is comparable with the one found for iridium steady state selectivities: S_h (initial): Pt/α-Al_2O_3 > Pt/γ-Al_2O_3 (type-3) > Pt/γ-Al_2O_3(type-4).

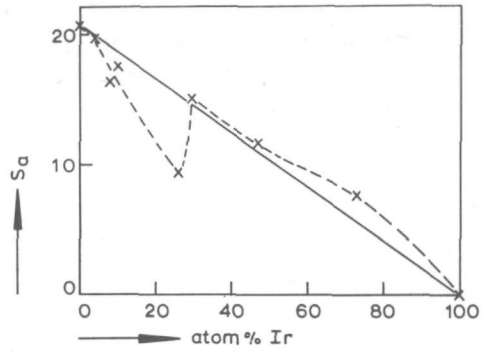

V.8 Aromatization selectivity in heptane conversion over type-4 catalysts.
Solid line: theoretical curve for single site reaction, synergistic effects, and surface enrichment being absent.
Dashed line: experimental curve

V.4.3 The influence of alloy composition on catalytic reforming

Now that we have arrived at a first qualitative insight in the behaviour of type-4 iridium and platinum catalysts, we can subject fig. V.6 to a closer examination.

Only platinum-containing samples show production of toluene at 650 K. According to Clarke (16), dehydrocyclisation of hexane to benzene proceeds via a single site mechanism. We assume that the same applies for conversion of heptane into toluene. The almost linear decline of S_a with increasing iridium content (fig. V.8) strongly suggests that the surface composition is about equal to the bulk composition of the alloy. Betizeau et al. (13) arrive at the same conclusion for their Pt - Re alloys.

The small dip in the curve near 25% Ir may be partly due to scatter in the experimental observations; however, the deviation from the straight line of six selectivity units considerably exceeds the estimated experimental

error (± 2). Other explanations may be: 1) a relative enrichment of the surface near 25% iridium, Ir having no aromatization activity, together with a relative surface enrichment in platinum for alloys with overall compositions near 50% iridium, or, 2) some kind of electronic effect in the region near 25% Ir. In view of the remarkable behaviour of the S_i and the S_c curve in the same region, the latter possibility seems to be the most probable one.

The anti-parallelism, shown by the S_i curve and the S_c curve suggests the products of these two groups to be formed via processes which compete with each other. This may be a competition between two mechanisms (bond shift or cyclic), or both reactions proceed via the cyclic mechanism and the competition is between desorption and hydrogenolysis of a C-C bond before desorption, the first leading to cyclic products, the latter to heptane isomers.

On alloying platinum with iridium, three different effects may play a role in the catalytic activity and selectivity of the resulting alloy:

- a geometric effect: new sites are created, which contain one or more iridium atoms
- an electronic effect: platinum and iridium may interact, and as a result their electronic structures changed markedly
- a cleaning effect: as has been observed in our TPD experiments, iridium can reduce drastically the carbon contamination on surrounding platinum sites (section IV.5.6).

When these three effects act simultaneously, a complex behaviour like the one depicted in fig. V.6 may result

Combination of a geometric effect and the cleaning effect may result in curve-shapes like the dotted lines in fig. V.9 and V.10. Initially, when little amounts of

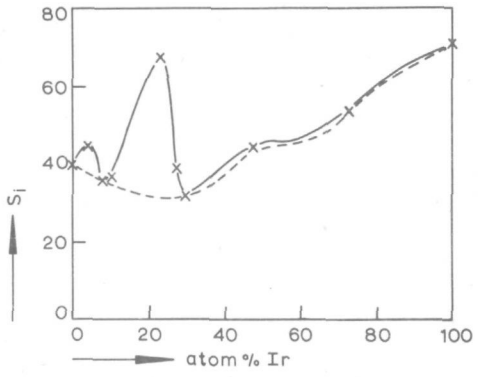

V.9 Isomerization selectivity in heptane conversion over type-4 catalysts.
Dashed line: theoretical curve, if only the "cleaning" effect and the geometric effect would play a role (see text).
Solid line: experimental curve

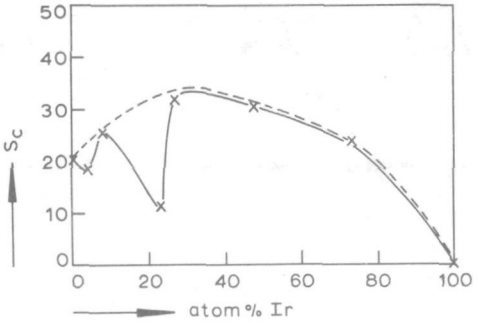

V.10 As fig V.9, for the cyclization selectivity

iridium are added to platinum, the former metal mainly acts in removing surface carbon, thus enhancing the 1,5-ring closure mechanism (15), and slowing down 1,6-ring closure and isomerization. This is in agreement with our observations not discussed above, i.e. the initial selectivities shown by fresh $Pt/\gamma\text{-}Al_2O_3$ catalysts: S_i (initial) < S_i (steady state), S_a (initial) < S_a (steady state), and S_c (initial) > S_c (steady state). When the iridium content is higher, the geometric effect becomes predominant, resulting in an increase in isomerization, and a decrease in cyclization selectivity.

As to an electronic effect, we recall the thermodynamic arguments, presented in chapter III, which point to strong mutual interaction between Pt and Ir near the composition $Pt_{0.75}\ Ir_{0.25}$. Apparently, this interaction is associated with an electronic effect, favouring isomerization at the expense of cyclization. Due to the interaction between platinum and iridium atoms, the electronic energy at the Fermi-level of the alloy is lowered. As a consequence, the chemisorbed hydrocarbon is more carbonium-ion like than on pure platinum, so that isomerization is favoured over cyclization. This would also explain the dip in the S_a - curve near the composition $Pt_{0.75}\ Ir_{0.25}$.

The existence of a platinum-iridium interaction is also consistent with a weakening of hydrogen chemisorption on the alloy of this composition, as we observed in our TPD experiments (c.f., e.g., table IV.2); the hydrogen desorbing at temperatures above 300 K is electronegatively chemisorbed (17), and hence the chemisorptive bond is weaker on an alloy that is more electronegative than its constituents.

One may wonder why this electronic effect is detected only within a narrow composition region around 25% Ir. The answer is that the mobility of the metal atoms is very limited at temperatures up to 800 K, so that the required

ordering only takes place between the spinodal points in the G(x) - x diagram (fig. III.7, see also ref. (18)).

On superimposing the electronic effect on the dotted curves in figs. V.9 and V.10, we obtain the curves determined experimentally. The small relative maximum in fig. V.9, and the dito minimum in fig. V.10, near 5% Ir can also be accounted for by an electronic effect, since we know that at lower temperatures there is a minimum in the G(x) curve near x = 0.05 as well (fig. III.7). The third minimum in the G(x)-curve near x = 0.98 may be associated with a more complex behaviour of the S_i and S_c curves in the composition region $0.90 < x < 1.00$ than has been depicted in figs. V.9 and V.10. As in this composition region no catalytic conversion was measured, the best we can do is connecting the points at x = 0.73 with those at x = 1.00 by smooth curves.

The picture of the dependence of the hexane conversion over type-3 catalysts on alloy composition (fig. V.4) does not show the complex behaviour as found for heptane conversion over type-4 (fig. V.6).

Several reasons may be given for this difference

- due to the higher metal load on type-3 samples, the interaction iridium-support is lower, resulting in a flatter S_i-curve
- the use of hexane as a reactant excludes the possibility of 1,6-ring closure under the conditions employed, causing a lower cyclization selectivity than found for heptane conversion
- only five different alloy compositions have been investigated in the type-3 series, so that no detailed picture could be constructed.

The latter reason may be the most important one, since the observed selectivities do not exclude the possibility that

the type-3 catalysts show a behaviour which is similar to the one found for type-4 (fig. V.11).

V.4.4 Deactivation of the catalyst

The initial decrease in catalytic activity, like we observed for our platinum-rich samples, is traditionally ascribed to coke-formation on the surface of the catalyst. Our observation, that iridium containing catalysts deactivate less, and need less time to reach a steady state conversion than pure platinum catalysts, seems to support this view, for iridium is resistant against surface carbiding and reduces carbon contamination on neighbouring platinum sites. Rooney and Clarke (15) observe a parallelism between the rate of surface carbiding and the selectivity towards methane in hydrocarbon conversion. In their opinion the high yield of methane obtained when hexane is converted over iridium films points towards rapid surface carbiding of this metal.

In our opinion, however, the production of methane suggests an incidentally formed carbonaceous deposit to be easily hydrogenated. As reported by Nieuwenhuys et al.(19), iridium activates the hydrocarbon molecule more than platinum does. As a consequence, C-C and C-H bonds scission occurs more readily on iridium than on platinum. The resulting carbon deposit is strongly bound to the iridium surface. Surface carbiding of iridium is therefore more likely than formation of a graphitic coke deposit. Under high hydrogen pressures (1 bar), this surface carbide is reduced to methane, in contrast with the graphitic deposit. The presence of iridium atoms in the surface of platinum exhibits the formation of ordered carbonaceous overlayers (an effect similar to that caused by the presence of kinks

in a stepped platinum surface (22)). As a result, the iridium containing surface can be cleaned more easily by hydrogen. The observations of Rooney and Clarke may still be valid when the total pressure is low (10^2 N m^{-2}) as in their experiments, but do not apply to our case.

The initial increase in activity of the iridium-rich samples suggests that these catalysts are activated by hydrocarbon molecules. It should be noted that these samples have a lower activity than the platinum-rich samples. Over catalyst W 25 (1.7% Ir/γ-Al_2O_3), only isomeric products are formed initially. The activated catalyst, however, also has ethylcyclopentane in its heptane conversion product mixture. Presumably, the activated catalyst contains sites which are less electronegative than those on the non-activated sample. In view of the nature of the Ir(III) sites (8), this may be due to exchange of chlorine ligands with hydrocarbon molecules, e.g. alkenes, formed in the hydrocarbon conversion reaction.

V.5 Summary and concluding remarks

Hexane and heptane conversion over Pt, Pt-Ir and Ir catalysts of various types have been investigated. Expecially the behaviour of iridium appeared to be strongly dependent on the type of the support. This can be explained in terms of formation of iridium (III) surface aluminate, which can take place on γ-alumina, and not on α-alumina.

Alloys of platinum and iridium show three effects which act simultaneously:

- geometric effect (creation of new sites)
- electronic effect (change in character of the metal atoms)
- cleaning effect (removal of surface carbon by iridium in the presence of hydrogen)

The most spectacular changes in selectivity are due to an electronic effect. The observations strongly support the phase diagram proposed in postulate no. 3 (section III.3).

The changes in catalytic activity of the platinum-rich samples can be ascribed to surface carbiding. On the iridium-rich samples, a second mechanism is probably operative, presumably associated with ligand exchange on the Ir(III) sites.

Concluding, we may state that

- the heptane conversion experiments strongly indicate that surface enrichment in the Pt-Ir system plays a minor role
- mutual interaction exists between Pt and Ir atoms in the region near 25% Ir, as expected on a thermodynamic basis and observed in TPD experiments (chapter IV), and confirmed by the selectivity behaviour of Pt-Ir alloys in heptane conversion
- interaction of iridium with γ-alumina in the presence of chlorine has been established convincingly.

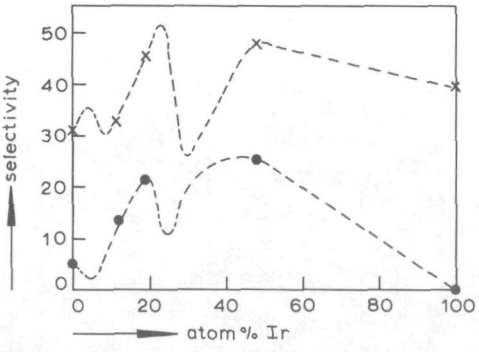

V.11 Experimental points of fig. V.4. The dashed lines show that the experimental points do not exclude a behaviour line the one depicted in fig. V.6

References

1. U.S. Patent 3,953,368
Exxon Research & Engineering Co.

2. U.S. Patent 3,867,280
Exxon Research & Engineering Co.

3. U.S. Patent 3,839,194
Esso Research & Engineering Co.

4. U.S. Patent 3,886,061
Cie. française de Raffinage

5. Sinfelt, J.H., Plat. Met. Rev., 20 (1976) 114

6. Schupp, O.E., Lewis, J.S.,
"Gas Chromatographic Data Compilation"
A.S.T.M., April 1971, p. 503

7. Dietz, W.A., J. Chromatogr., (1967) 68

8. Leclère, C., Contour, J.P., Pannetier, G.,
Ann. Chim., (1974) 221

9. Tournayan, L., Charcosset, H., Fréty, R.,
Preprint 5ième Congr. Ibero-Mexicain de Catalyse,
Lisbon (1976)

10. Brunelle, J.P., Montarnal, R.E., Sugier, A.A.,
Preprints 6th Int. Congr. Catal., London (1976),
paper B 24

11. Ramaswamy, A.V., Ratnasamy, P., Sivasanker, S.,
Preprints 6th Int. Congr. Catal., London (1976),
paper B 25

12. Gray, T.J., Masse, N.G., Oswin, H.G.,
Actes 2ième Congr. Int. Catal., Paris, Technip (1961)
2, 1697

13. Bétizeau, C., Leclercq, G., Maurel, R., Bolivar, C.,
Charcosset, H., Fréty, R., Toumayan, L.,
J. Catal., 45 (1976) 179

14. Goble, A.G., Lawrance, P.A.,
Proc. 3rd Int. Congr. Catal., Amsterdam (1964)
North-Holland, Amsterdam (1965), p. 320

15. Clarke, J.K.A., Rooney, J.J., Advan. Catal., 25 (1976)
125

16. Clarke, J.K.A., Chem. Revs., 75 (1975) 291

17. Nieuwenhuys, B.E., Surf. Sci., 59 (1976) 430

18. Swalin, R.A., "Thermodynamics of Solids", 2nd ed.
John Wiley & Sons, New York (1972)

19. Nieuwenhuys, B.E., Hagen, D.I., Rovida, G.,
Somorjai, G.A., Surf. Sci., 59 (1976) 155

20. Anderson, J.R., Avery, N.R., J. Catal., 5 (1966) 446

21. Barren, Y., Maire, G., Mulller, J.M., Gault, F.G.,
J. Catal., 5 (1966) 428

22. Baron, K., Blakeley, D.W., Somorjai, G.A.,
Surf. Sci., 41 (1974) 45

Chapter VI

Comparison of the results with literature data; general discussion

VI.1 Introduction

TPD-experiments (chapter IV) revealed the existence of several types of hydrogen adsorption on platinum, iridium, and platinum-iridium alloy surfaces. The results can be used in calculating the enthalpy and the entropy of each type of adsorption, and the order in coverage of the desorption reaction indicates if the adsorption is, for instance, dissociative or molecular in nature. Moreover, the effect of a contaminant can be investigated by deliberate poisoning the catalyst, carrier effects can be studied by comparing the TPD-spectra of supported catalysts with those of non-supported metal powders.
Further insight can be obtained when the TPD results are compared with the available literature, dealing with hydrogen adsorption on platinum and iridium surfaces. This will be done in the following sections.

On Pt Kulifay-powders, we observed hydrogen desorption peaks at 123, 186, 223, 323, 376 and 500 K. The enthalpies of adsorption derived from them are collected in table VI.1. The peak at 123 K has first order desorption characteristics. We ascribed it to weakly adsorbed hydrogen molecules with limited mobility on the surface. The 186 K - peak shows pseudo first order behaviour, and appears to be

associated with the presence of dissolved hydrogen. The desorption is assumed to take place via a mechanism which involves combination of a surface hydrogen atom with a subsurface hydrogen atom. If this type of desorption takes place via a carbided surface, the peak maximum shifts to 223 K.

All peaks observed at temperatures above 300 K exhibit second order desorption kinetics, and the adsorption entropies point to very limited mobility of the adsorbed species. We believe all peaks to be associated with dissociative adsorption. Anticipating on what will be discussed in section VI.2.3, we ascribe the different enthalpies of adsorption to different sites in the platinum surface (different crystal planes exposed, and the presence of steps and kinks).

The H_2/Ir TPD-spectra are very similar to those recorded for the H_2/Pt - system (peak maxima at 123, 186, 334, 389 and 500 K), and they are interpreted in the same way. However, the analogue of the 223 K - peak is lacking in the H_2/Ir spectrum. This is consistent with the phenomenon observed by us, that carbon contamination on an iridium surface can be easily removed by hydrogen.

VI.2 Enthalpies of hydrogen adsorption

VI.2.1 Adsorption enthalpies of hydrogen on platinum, as determined by calorimetry and derived from isotherms

Many investigators have determined the enthalpy of adsorption of hydrogen on platinum, most of them using a calorimetric method, or deriving isosteric heats from adsorption-equilibrium data. A survey of the available

literature on this subject is given by Cerny et al. (1). The reported enthalpies of adsorption range from 40 KJ $mole^{-1}$ to 250 kJ $mole^{-1}$. As shown in fig. VI.1 there are regions of enthalpy values where most of the reported enthalpies are concentrated. The enthalpies derived by us from TPD data (table VI.1, ref. g) are at least not in contradiction with the values reported in fig. VI.1, none of them lying in a region where no calorimetric or isosteric enthalpies have been reported.

VI.2.2 Comparison of our results with literature published TPD-spectra

Various authors have reported enthalpies of hydrogen adsorption on platinum which they derived from (peak maxima in) TPD-spectra. Some of these enthalpies are collected in table VI.1. Several investigators observed only one, two or three peaks in their TPD-spectra (table VI.1, ref. a-e). In some cases, this is due to the limited temperature region covered in their experiments, but, especially in flash desorption experiments, poor resolution of peaks may be the reason why only one or two peaks are observed (ref. a and b in table VI.1).

Tsuchiya et al. (d) report four peaks, but they computed the corresponding heat of adsorption for only one of them. Whereas we found two peaks in between 350 K and 550 K, associated with ΔH-values of 63 and 87 kJ $mole^{-1}$, respectively, Scholten and Konvalinka (f) found only one peak in that temperature region, with a corresponding adsorption enthalpy of 78 KJ $mole^{-1}$. Since their experimental conditions were very similar to ours, we believe this difference to be inherent in the respective samples. This will be discussed further in section VI.2.3. The low temper-

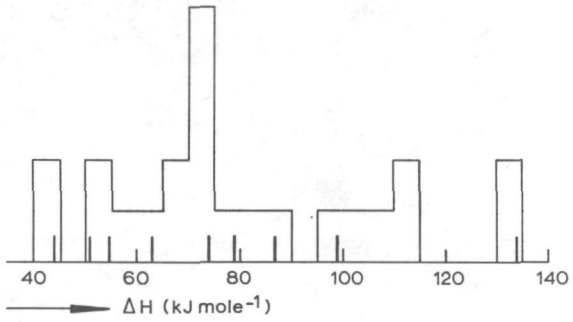

VI.1 Scheme, showing the number of times various hydrogen adsorption enthalpies on platinum are reported in literature. The reported values are detemined calorimetrically, or derived from isotherms. The bars indicate enthalpy values which have been derived by us from TPD spectra.

Table VI.1

Ref.	Sample	H (kJ mole^{-1})						
a	Filament						96	
b	Ribbon			42		70		
c	Pt-black			42			96	
d	Pt-black			50				
e	Polycrist film		33	50		88		
f	Pt-black		23	51		78	104	135
g	Pt-Kulifay	11	32	51	63	87		
g	Pt / SiO_2	11	32	44	55	74		
g	Pt/γ-Al_2O_3	11	32				109	135
g	Pt / C	11	32	51	63	79		

References:

a) Wiesendanger, H.D.U., J.Catal., 2 (1963) 538
b) Nishiyama, Y., Wise, H., J. Catal. 32 (1974) 50
c) Kubokawa, Y., Takashima, S., Toyama, O., J. Phys. Chem., 68 (1964) 1244
d) Tsuchiya, S., Amenomiya, Y., Cvetanovic, R.J., J. Catal., 19 (1970) 245
e) Stephan, J.J., Ponec, V., Sachtler, W.M.H., J. Catal., 37 (1975) 81
f) Scholten, J.J.F., Konvalinka, J.A., unpublished results
g) This thesis

Table VI.1 Enthalpies of hydrogen adsorption on platinum, derived from TPD-spectra, as reported by various authors, and compared with our results

ature peaks in ref. (f) agree well with those obtained with our Kulifay-powders. The adsorption enthalpies which Konvalinka and Scholten derived from their high-temperature desorption peaks are very similar to those we obtained with our γ-alumina supported samples (the only samples that we investigated at temperatures above 700 K).

As many authors, when discussing hydrogen adsorption on platinum, refer to the work published by Tsuchiy et al. (table VI.1, ref. d), it is important to examine in how far our results can be reconciled with those of Tsuchiya c.s. The latter authors worked with a platinum black of low surface area (S_{BET} = 0.125 m^2 g^{-1}). They do not mention how the sample was pretreated.
The BET surface area was determined from CO_2 adsorption, so contamination of the sample with carbon seems very likely. The heating rate was twice the rate we employed (0.52 K s^{-1} and 0.25 K s^{-1}, resp.). Moreover, in the temperature region below room temperature, the heating rate was still higher, especially at very low temperatures. We therefore conclude, a priori, that the peaks will have their maxima at higher temperatures than the corresponding peaks in our TPD-spectra had.

Tsuchiya et al. report four peaks, having their maximum at 173 K (α), 253 K (β), 363 K (γ) and 573 K (δ). In view of their experimental conditions, we identify the δ-peak with the one observed by us with Pt Kulifay-powders at 123 K, their β-peak with ours at 223 K (dissolved hydrogen desorbing via a carbon contaminated platinum surface) (section IV.5.5), the γ-peak with one of those at 323 K and at 376 K, respectively, and the δ-peak with our peak at 500 K. The authors cited report their α-peak to be associated with an activated adsorption, the activation energy of adsorption being about 12 kJ $mole^{-1}$. This supports our

view, that we are dealing here with chemisorbed hydrogen, not with physisorption.

For their γ-peak, Tsuchiya and coworkers report an activation energy of desorption of 50 kJ $mole^{-1}$, and an activation energy of adsorption of 1.7 kJ $mole^{-1}$, indicating an enthalpy of adsorption of ca. 48 kJ $mole^{-1}$, which is in reasonable agreement with the value of 51 kJ $mole^{-1}$, determined by us for our 323 K-peak. Since the assumption of negligible readsorption made by Tsuchya et al. is not valid, they probably measured the enthalpy of adsorption, rather than the activation energy of desorption, and hence, the agreement with our results is even better. However, according to lit. d, the γ-peak shows first order desorption kinetics, whereas we found second order. First order kinetics was arrived at on the basis of isothermal desorption at 294 K. As pointed out in chapter IV, subsurface hydrogen may recombine with surface (γ) hydrogen via a process that is first order in coverage, the rate of which is limited by the rate of diffusion of dissolved hydrogen from the bulk to the surface. At higher temperatures, the normal second order desorption process predominates. This explains why the isothermal desorption at 294 K is first order, while the desorption peak in the TPD-spectrum has second order characteristics.

The above interpretation is consistent with the variation of the amounts of β-, γ-, and δ-hydrogen with adsorption time at 294 K (reported in ref. d). The amount of β-hydrogen decreases, whereas the amounts of γ- and δ-hydrogen increase, the sum of the three remaining constant. At 294 K, β-hydrogen desorbs, and readsorbs as γ- or δ-hydrogen. Meanwhile, dissolved hydrogen migrates to the subsurface, to form β-hydrogen with a surface hydrogen atom. Since this diffusion of dissolved atoms is supposed to be

slow (3), the amounts of γ- and δ-hydrogen increase, at the expense of β.

Concluding, we may state that our experimental results confirm those reported by other authors, especially those of Tsuchiya et al. Moreover, our interpretation of H_2/Pt TPD-spectra is confirmed by experimental details, reported by the Canadian workers.

VI.2.3 Enthalpies of hydrogen adsorption on platinum single crystal surfaces

Several authors report enthalpies of hydrogen adsorption on well-defined platinum crystal planes (2-5). It should be noted that adsorption experiments with well-defined single crystal planes are carried out at very low hydrogen pressures ($\lesssim 10^{-4}$ Torr.) As a consequence, certain types of hydrogen adsorption are not formed. E.g., for the type of hydrogen adsorption, responsible for the I.R. band at 2060 cm^{-1} (section VI.3), a hydrogen pressure of at least 0.1 Torr is required (11).
According to Lu and Rye (2), adsorption on the (111)-plane is second order. In flash desorption, these authors observe only one peak, having its maximum at about 330 K for high hydrogen coverages. The temperature of the peak maximum shifts to higher values with decreasing coverage. A plot of $\ln (n_o T_M^2)$ versus $1/T_M$ (n_o being the number of hydrogen atoms, initially adsorbed per unit of surface area) yields a straight line, from the slope of which a desorption activation energy of 73 kJ $mole^{-1}$ is obtained.

Christmann et al. (14) observed two peak maxima in flash desorption spectra for H_2/Pt (111). For the one near 330 K they derived, using $\ln (n_o T_M^2)$ versus $1/T_M$, a value of 39 kJ $mole^{-1}$, and about 27 kJ $mole^{-1}$ for the one near 220 K,

both types of adsorption being atomic. Isotherms obtained on the basis of work function changes confirm the value of 39 kJ $mole^{-1}$ for ΔH, when the coverage, $0.1 < \theta < 0.5$, dropping to 29 kJ $mole^{-1}$ for $\theta \approx 0.8$. On imperfect (111)-planes, however, ΔH may be as high as 70 kJ $mole^{-1}$ at low coverages. On a stepped (111) surface, Christmann and Ertl (5) found the initial adsorption enthalpy to be about 50 kJ $mole^{-1}$.

Plots of ln ($n_o T_M^2$) versus $1/T_M$ constructed from flash desorption spectra for H_2/Pt(100) yield ΔH = 62 kJ $mole^{-1}$, whereas a line shape analysis leads to a value for ΔH of 67 kJ $mole^{-1}$ (3).

Lu and Rye (2), however, report the existence of at least five peaks in the H_2/Pt (100) TPD-spectrum, which can be divided into two groups: one group around 250 K, and the other around 430 K, associated with adsorption enthalpies near 54 kJ $mole^{-1}$ and near 113 kJ $mole^{-1}$, respectively. The spectra for the (110)-plane are composed of two poorly resolved peaks (2): one occurring at $\sim$ 260 K ($\sim$ 60 kJ $mole^{-1}$), and the second at $\sim$ 350 K ($\sim$ 80 kJ $mole^{-1}$)

The results of hydrogen adsorption experiments with platinum single crystal surfaces can be summarized as follows. The (111)-planes have very low adsorption enthalpies, unless the surface contains steps; (100)-planes show either a simple desorption behaviour, and an adsorption enthalpy of about 67 kJ $mole^{-1}$, or a complex behaviour and enthalpies around 54 and 113 kJ $mole^{-1}$. The (110)-plane is reported to have adsorption enthalpies near 60 and 80 kJ $mole^{-1}$. The experiments of Netzer and Kneringer with the (100)-plane of platinum confirm our hypothesis of the solubility of hydrogen in this metal.

Comparison of these results with table VI.1 reveals that stepped (111) surfaces probably preponderate on all

samples. Kulifay-powders may contain also (100)-planes in the surface, responsible for an extra peak, associated with an adsorption enthalpy of 63 kJ $mole^{-1}$. This would explain the different desorption spectra for Pt-blacks and Kulifay-powders. The complex and little pronounced spectra of our γ-alumina supported sample, together with the important peaks at elevated temperatures, suggest the occurrence of (imperfect) (100)-planes on this sample as well (c.f. fig. IV.11) though also on this sample the platinum surface will mainly consist of (stepped) (111) planes. If this is to be ascribed to a short distance support effect, metal particles with a small diameter are to be present. This would be consistent with the rapid desorption of dissolved hydrogen, discussed in section IV.5.7

VI.2.4 Literature on TPD of hydrogen from iridium

There is little information from literature on TPD experiments with the H_2/Ir-system. Contour and Pannetier (6) observed two peaks in a H_2/Ir- γ-Al_2O_3 TPD-spectrum, one at about 380 K, and the second at about 1020 K. The former is not found by them on non-supported iridium, and the authors ascribe it to desorption from iridium in interaction with the support. The enthalpies of adsorption are determined to be 43 and 113 kJ $mole^{-1}$, respectively. Mimeault and Hansen (7) observed two peaks in the hydrogen flash desorption spectrum of an iridium filament, at 280 K and at 480 K. Both peaks are ascribed to dissociative adsorption. For the one at 480 K, an initial adsorption enthalpy of 100 kJ $mole^{-1}$ is obtained from a second order Arrhenius-plot. When starting desorption at 77 K and applying a heating rate of 0.17 K S^{-1}, Escard et al. (8) obtain three peaks in the H_2-from-unsupported-iridium spectrum (T_M= 207,

298, and 773 K, resp.), and four in the H_2/36% Ir-η-Al_2O_3 spectrum (T_M = 223, 323, 393 and 773 K, resp.). The extra peak is ascribed to iridium in electronic interaction with the support. The reported adsorption enthalpies are 25, 33, and 105 kJ $mole^{-1}$ for the unsupported sample, and 27, 38, 44, and 105 kJ $mole^{-1}$ for the η-alumina supported one.

It is not clear how the data from lit. (8) can be reconciled with ours (table IV.2 and IV.3).According to Escard et al., the poor resolution of their desorption peaks would reveal the heat of adsorption to be coverage dependent. In our opinion, however, in view of the tailing shown by their adsorption peaks, the poor resolution may be due to diffusion retardation. Thus readsorption cannot be neglected, as assumed by the authors of lit. (8). Moreover, the positions of the peak maxima may be influenced by the diffusion phenomenon. This would explain why the supported sample has all peak maxima at higher temperatures than the non-supported one.

Therefore, a further comparison of our results with literature data is not considered useful. We just note that the interaction of iridium with the support gives rise to an extra peak in the hydrogen desorption spectrum, as has been confirmed by us (section IV.5.7).

VI.2.5 Conclusions

Comparison of our H_2/Pt TPD results with the available literature on this subject reveals that:

- there is good agreement with TPD-spectra, reported in literature
- experiments with well-defined platinum crystal planes account for the existence of a series of adsorption enthalpies for dissociatively adsorbed hydrogen

- the predominant surface plane in polycrystalline or supported samples appears to be a stepped (111) surface
- γ-alumina supported samples and Kulifay-powders may have (imperfect) (100)-planes in the surface as well.

The results obtained with the platinum samples give confidence in the data obtained for iridium, and hence we may state:

- enthalpies of hydrogen adsorption on iridium are only slightly higher than those of adsorption on comparable platinum sites
- the scarcely available literature, dealing with H_2/Ir TPD is unreliable.

VI.3 The infrared active adsorbed hydrogen

Both on platinum (9-12) and on iridium (13) at least one type of adsorbed hydrogen is active. All investigators investigating the H_2/Pt system report two I.R. absorption bands at ca. 2120 and at ca. 2060 cm^{-1}, resp. However, their opinions about the interpretation differ considerably. Eischens and Pliskin (9) ascribe both infrared bands to atomic hydrogen, their band at 2120 cm^{-1} being associated with weak adsorption, and the one at 2060 cm^{-1} with a strongly adsorbed species. Eley et al. (10) found their 2120 cm^{-1} band to be enhanced by a treatment with oxygen, whereas the 2040 cm^{-1} band is removed by this treatment. They propose that infrared active hydrogen adsorption takes place on platinum oxide patches, and they suggest the 2040 cm^{-1} band to result from adsorbed hydrogen bounded to adjacent surface OH-groups.

Primet et al. (11), however, ascribe the 2040 cm^{-1} band to a Pt-CO species, the CO being formed via dissociative adsorption of CO_2 from the alumina support. In

contrast with previous investigators, they found an isotope shift only for the 2120 cm^{-1} band when hydrogen was replaced by deuterium, the band at 2040 cm^{-1} remaining unchanged.

Dixon et al. (12) report hydrogen bands on alumina-supported platinum at 2120 cm^{-1} and at 2060 cm^{-1}, and corresponding deuterium bands at 1520 and 1480 cm^{-1}. Both species are reversibly adsorbed at room temperature. Since Dixon et al. combined their infrared experiments with detailed adsorption studies (14), we can try to determine on the basis of the adsorption characteristics, which of the types of adsorbed hydrogen observed by us in TPD is I.R. active.

In ref. (14) five types of hydrogen adsorption on platinum are reported.

Type I is reversibly adsorbed at 77 K, and, consequently, is not observed in our TPD-spectra.

Type II is irreversibly adsorbed at 77 K on surfaces which have not been exposed to hydrogen previously. Type II represents hydrogen that desorbs in our experiments at 123 K, and probably also the atomically bound hydrogen, responsible for the peaks at 323 K and 376 K.

Type III is bound reversibly at room temperature, and causes the I.R. band at 2060 cm^{-1}. Type IV, associated with the 2120 cm^{-1} band, is also reversibly adsorbed at room temperature, and can be adsorbed at 77 K if the platinum surface has been previously exposed to hydrogen at 295 K or at a higher temperature. We conclude therefore that type IV is identical with our peak at 186 K (dissolved hydrogen). We believe the infrared active species to be a hydrogen atom adsorbed on top of a platinum atom, the latter being surrounded by subsurface hydrogen atoms. The presence of these subsurface hydrogen atoms causes a weakening of the metal - metal bonds, so that the bond between the

platinum atom and the surface hydrogen atom becomes very hydride-like in nature, which is confirmed by the frequency of the infrared band. When subsurface hydrogen is absent, the bridged and centered positions (fig. III.10) are the preferred sites for adsorption, and hence the hydrogen atom shares its electron with several surface platinum atoms, and the species is no longer infrared active (11). Since type III can be removed by a pretreatment of the sample in oxygen, we believe this type of hydrogen to be associated with the 224 K - peak which we observed for carbon contaminated samples. The electronegative character of the carbon atom causes a weakening of the Pt-H bond, resulting in a shift of the I.R.-band to a lower frequency ($2120 \rightarrow 2060\ cm^{-1}$). The carbon atoms block the interstitial sites, thus causing a higher activation energy of desorption of the dissolved hydrogen via the mechanism described in section IV.5.3. The result is a shift of the TPD peak maximum from 186 K to 224 K.

Dixon's type V hydrogen is adsorbed at 295 K, not at 77 K, and is a prerequisite for adsorption of type IV. Therefore, it surely is partly composed of dissolved hydrogen, and probably spillover hydrogen as well, as type V adsorption is strongly enhanced by preadsorption of water (14).

Infrared investigations of the H_2/Ir- γ-Al_2O_3 system reveals the existence of two bands, at $2120\ cm^{-1}$ and $2050\ cm^{-1}$, respectively (13). The first one is associated with reversible adsorption at room temperature. The second one can be removed by pumping at room temperature during 15 minutes. Analogous to the H_2/Pt system, the $2120\ cm^{-1}$ band has to be ascribed to an Ir-H stretching mode, influenced by the presence of subsurface hydrogen. The authors of ref. (13) do not exclude an influence of the support to

be responsible for the band at 2050 cm^{-1}. Since the band at 2050 cm^{-1} is only a small shoulder, the possibility of a surface carbide being responsible for the 2050 cm^{-1} band should not a priori be ruled out.
As discussed in section V.4.4, the iridium surface is readily carbided. Presumably, the surface carbide is not reduced under the conditions employed by Bozon - Verduraz et al. (13) (300 Torr H_2, static adsorption).

VI.4 The platinum - iridium system in reforming catalysis

Apart from the patent literature, only a few papers have been published dealing with the reforming behaviour of bimetallic platinum - iridium catalysts. Usually, patents are not restricted to specific alloy compositions. The inventors prefer to formulate patents which claim the whole composition range, although in most examples the iridium content is 25% of the metal load, or less (see ref. 1-4 of chapter V). In view of our results with heptane conversion over Pt-Ir / γ-Al_2O_3 catalysts (section V.3.7), this is the composition region where good reforming catalysts are found: a low value of S_h, and reasonably high aromatization activity. Often, addition of chlorine is proposed in order to reduce the hydrogenolysis activity, and to improve the yield of isomerization products (see, e.g., ref (15)). This effect has been confirmed by our experiments and we ascribed it to the formation of Ir(III) complexes and the creation of electronegative sites. A similar effect has been reported for sulfur (16), deliberately deposited on a Pt/Al_2O_3 and on a $Pt-Ir/Al_2O_3$ catalyst. Since the electronegativity values for sulfur and carbon are about the same, it is not surprising that the formation of a carbided surface has the same effect on selectivity as a sulfur deposit has. So, surface carbiding to a certain extent is

advantageous for catalyst selectivity, but excessive coking reduces the catalyst activity, and should therefore be avoided. The selectivity towards coking can be diminished by adding a third metal, like thallium or indium (15). Karpinsky and Clarke (17) propose tin as a third constituent in Pt-Re catalysts.

Apart from the thermodynamic data cited in chapter III, little evidence is found in literature for strong intermetallic interaction in the Pt-Ir system. Tournayan et al. (18) report a platinum-like behaviour for iridium contents up to 70%, when heptane is converted over α-alumina supported Pt-Ir catalysts. However, X-ray diffraction experiments reveal the existence of more than one metallic phase in these catalysts, indicating limited mixing of both metals. Ramaswamy et al. (16) mention neither the composition of their bimetallic Pt-Ir catalyst, nor the type of alumina used as a support. On the basis of the product distribution we expect the iridium content to be about 50%. As our results indicate, no synergistic effect is to be expected in this composition region, so that the resulting selectivities are merely a weighted average of those of the pure constituents.

When discussing the activity of various Pt-Re catalysts in H_2/D_2 - exchange and hydrogenation of benzene, Bétizeau et al. (19) arrive at the following conclusion: "possibly there is an electronic structure intermediate between platinum and iridium which is more favourable to both reactions". Though we did not test our catalysts in reaction with benzene, we believe that our results may provide support for this statement.

Kropotova et al. (20) report on liquid phase hydrogenation of organic molecules over Raney platinum-iridium catalysts (solid solutions in all compositions). The apparent activation energy for the dehydrogenation of

acetone is 38 kJ mole^{-1} over all catalysts, except for the catalyst Pt-75 Ir (25% Ir), which reduces the activation energy to 8 kJ mole^{-1}. This result strongly suggests intermetallic interaction between platinum and iridium near the composition 75% Pt, 25% Ir.

VI.5 Conclusions

The adsorption of hydrogen on iridium and platinum exhibits virtually the same characteristics. Hydrogen appears to dissolve in both metals. Platinum and iridium differ markedly in their behaviour towards carbon. Whereas platinum is apt to be covered with a graphitic layer under reforming conditions, the iridium surface is only carbided. As a consequence, the carbon contamination on an iridium surface can be removed by hydrogen. The carbonaceous layer on platinum makes a treatment in oxygen necessary for reactivation of a conventional Pt/γ-Al_2O_3 reforming catalyst.

The hydrogenolysis activity of iridium can be attenuated by addition of an electronegative element (chlorine, sulfur, carbon). Chlorine has a dual effect, as it enables iridium to form an Ir(III) complex in the surface of γ-alumina. This complex has a considerable isomerization selectivity, as compared with metallic iridium.

An important isomerization selectivity is also shown by Pt-Ir alloys in the composition region near 25% Ir, due to the strong intermetallic interaction between platinum and iridium in this composition region.

For preparing a good reforming catalyst, the following points are important

- use of an alumina which contains surface hydroxyl groups (e.g. γ-alumina)

- addition of chlorine
- a Pt/Ir ratio $\geq$ 3
- use of a catalyst preparation method that yields a solid solution of both metals (e.g. impregnation)

The catalyst thus obtained will exhibit
- a higher steady state activity
- a better selectivity for non-destructive reactions
- a better stability against coke-formation

than the conventional Pt reforming catalyst.

References

1. Cerny , S., Smutek, M., Buzek, F., J. Catal., 38 (1975) 245

2. Lu, K.E., Rye, R.R., Surf. Sci., 45 (1974) 677

3. Netzer, F.P., Kneringer, G., Surf.Sci. 51 (1975) 526

4. Christmann, K., Ertl, G., Pignet, T., Surf.Sci., 54 (1976) 365

5. Christmann, K., Ertl, G., Surf. Sci., 60 (1976) 365

6. Contour, J.P., Pannetier, G., Bull. Soc. Chim. France, (1969) 2658

7. Mimeault, V.J., Hansen, R.S., J.Chem.Phys., 45(1966)2240

8. Escard, J., Leclère, C., Contour, J.P., J. Catal., 29 (1973) 31

9. Pliskin, W.A., Eischens, R.P., Z. Physik. Chem., 24 (1960) 11

10. Eley, D.D., Moran, D.M., Rochester, C.H., Trans. Faraday Soc., 64 (1968) 2168

11. Primet, M., Basset, J.M., Mathieu, M.V., Prettre, M., J. Catal., 28 (1973) 368

12. Dixon, L.T., Barth, R., Gryder, J.W., J. Catal., 37 (1975) 368

13. Bozon - Verduraz, F., Contour, J.P., Pannetier, G., C.R. Acad. Sci., Ser.C., (1969) 1436

14. Dixon, L.T., Barth, R., Kokes, R.J., Gryder, J.W., J. Catal., 37 (1975) 376

15. British Patent 1,364,744
Société français des produits pour catalyse

16. Ramaswamy, A.V., Ratnasamy, P., Sivasanker, S., Leonard, A.J.,
Preprints 6th. Int.Congr.Catal., London (1976),paper B25

17. Karpinsky, Z., Clarke, J.K.A.,
J. Chem. Soc., Faraday Trans. I., 71 (1975) 893

18. Tournayan, L., Charcosset, R., Fréty, R.,
Preprints 5ième Congr. Ibero-Mexicain de Catalyse, Lisbon (1976)

19. Bétizeau, C., Leclerq, G., Maurel,R., Bolivar, C., Charcosset, H., Fréty, R., Tournayan, L.,
J. Catal., 45 (1976) 179

20. Kropotova, N.V., Semenova, A.D., Vovchenko, G.D.,
Russ. J. Phys. Chem., 49 (1975) 843

Summary

Bimetallic γ-alumina supported platinum-iridium catalysts are known to be good reforming catalysts. Patents claim that Pt - Ir catalysts have a higher activity and a better stability and selectivity than the traditional $Pt/\gamma\text{-}Al_2O_3$ catalyst.

The aim of the research program on which is reported in this thesis was to find out why and how $Pt/\gamma\text{-}Al_2O_3$ are improved on addition of iridium. Keeping this aim in mind, we investigated the performance of platinum-iridium catalysts of various compositions and deposited on various supports (SiO_2, $\alpha\text{-}Al_2O_3$, $\gamma\text{-}Al_2O_3$) in temperature programmed desorption (TPD) experiments with hydrogen. Moreover, the samples were tested in hydrocarbon conversion reactions, mainly heptane reforming over γ-alumina supported Pt - Ir catalysts.

Among the numerous TPD analysis methods described in literature, only the one proposed by Cvetanovic et al. can be used for the analysis of TPD-spectra obtained with a flow apparatus as used by us. Their method was extended by us with the equations for second order desorption kinetics. Furthermore, we corrected the mathematical expressions for temperature of the adsorption entropy. Moreover, we derived linear equations describing various types of desorption peaks, and hence, apart from a visual line shape analysis, a mathematical analysis method has become available.

The procedure for the analysis of TPD-spectra developed by us could be applied successfully for our experiments with hydrogen desorption from iridium, platinum, and their alloys. On all these samples, seven types of hydrogen adsorption appeared to be present, five of them being irreversibly adsorbed at room temperature. All these five types of

adsorption are dissociative, and almost immobile. On platinum, the adsorption enthalpies vary from 44 to 135 kJ $mole^{-1}$. On iridium, adsorption enthalpies of the analogous adsorption types are about 5 kJ $mole^{-1}$ higher. Different types of adsorption are associated with different adsorption sites: different crystal planes may be exposed, and these planes may contain steps and kinks. The metal surfaces appear to consist mainly of stepped (111) surface planes.

As already mentioned, the hydrogen adsorption enthalpy on iridium is only slightly higher than on platinum. However, hydrogen chemisorption on alloys containing about 25% iridium is weaker than hydrogen chemisorption on platinum. This is in agreement with the phase diagram, postulated by us on the basis of literature data: thermodynamic data, extrapolated to lower temperatures, suggest the formation of a compound with a composition near $Pt_{0.75}Ir_{0.25}$.

One of the two remaining types of hydrogen adsorption has been ascribed to molecular chemisorption, the enthalpy of which is equal for all samples: 11 kJ $mole^{-1}$.

The hydrogen desorbing in a peak with its maximum at 186 K is associated with dissolution of hydrogen in Pt and Ir. A carbon deposit on platinum makes this peak shift to 223 K. Iridium appears to be much less sensitive to carbon contamination, which is in agreement with observations in Auger Electron Spectroscopy (AES).

Heptane conversion has been carried out at 650 K, and a H_2/C_7 ratio of 17. Under these conditions, the main products are toluene, methylcyclohexane and ethylcyclopentane, iso-C_7 species, and hydrogenolysis products. Iridium catalysts show a high hydrogenolysis selectivity. In the presence of Cl^-, an Ir(III) complex can be formed in the

surface of γ-alumina; this comples exhibits a high isomerization selectivity. Alloys containing about 25% iridium also show a high isomerization selectivity, which is consistent with the probable compound formation near this composition.

On the basis of the results presented above, we conclude that TPD-results obtained with a flow apparatus may provide useful information about the adsorption behaviour of a catalyst. TPD-experiments with the Pt - Ir system, together with test reactions and a literature study, shows that interesting reforming catalysts are obtained when solid solutions containing about 25% iridium, are formed on the surface of an alumina which contains hydroxyl-groups, and in the presence of chloride ions. The resulting favourable catalytic properties are mainly due to

- strong mutual interaction of platinum and iridium in the composition region in question
- interaction of iridium with the support
- resistance of iridium against coke formation.

This book contains a survey of the available literature on the kinetics of Temperature Programmed Desorption (TPD). An extension is given to pseudo-equilibrium first and second order desorption. Application of this theoretical model is demonstrated in the analysis of experimental results with hydrogen desorption from platinum, iridium, and platinum-iridium alloys.
The selectivity behaviour shown by platinum-iridium alloys in heptane conversion reactions exhibits a remarkable parallellism with the phase-diagram, derived from thermodynamic data. Other important topics are coke formation on the alloy surface, and absorption of hydrogen in the bulk of (supported) alloy particles.

This publication provides a basis for application of TPD in the study of heterogeneous catalysts for technical use. Moreover, it emphasizes the role of synergistic effects in bimetallic catalysts. It is, therefore, of great value for anyone working in the field of heterogeneous noble metal catalysis, especially petrochemists, investigators interested in chemisorption, and people working in the field of catalyst design.

J.C. Rasser was born in a suburb of Leiden, the Netherlands. After obtaining his Master's Degree in Chemical Engineering at Delft University of Technology, he continued his studies with Professor Scholten at the same University. The present studies were carried out in Professor Scholtens' group. At present, the author is working at Proctor & Gamble ETC, Strombeek-Bever, Belgium.

DELFT UNIVERSITY PRESS

771215